CRYSTAL STRUCTURES OF N-ACETYLMANNOSAMINE KINASE: INSIGHTS INTO ACTIVITY, MUTATIONAL MODIFICATIONS AND INHIBITION

Dissertation zur Erlangung des akademischen Grades des

Doktors der Naturwissenschaften (Dr. rer. nat.)

eingereicht im Fachbereich Biologie, Chemie, Pharmazie

der Freien Universität Berlin

vorgelegt von

LONG DUC NGUYEN

aus Hanoi (Vietnam)

2011

Die Arbeit wurde vom Oktober 2008 bis September 2011

im Institut für Biochemie und Molekularbiologie

Campus Benjamin Franklin

Charité – Universitätsmedizin Berlin

Arnimallee 22, 14195 Berlin-Dahlem

unter der Leitung von PD Dr. Hua Fan

angefertigt.

1. Gutachter: PD Dr. Hua Fan

2. Gutachter: Prof. Dr. Volker Haucke

Disputation am 14.12.2011

Acknowledgement

"Silent gratitude isn't much use to anyone." -G.B. Stern

In this sense I would like to use this space to fill it with my gratitude for all the people who have helped me over the years to finish this work. There are a lot more people outside of this working atmosphere, who has supported and inspired me like my family, relatives and friends. My silent gratitude will be with them, but for the people involved in this project, I am more than happy to thank them here. I would like to thank:

Prof. Dr. Werner Reutter - for the opportunity to do research, the optimistic view on outcomes and the subtle reminders on things that matter.

PD Dr. Hua Fan - for supervising and editing my work, for her close view on results and her commitment for correct scientific work.

Prof. Dr. Stephan Hinderlich - for constructive ideas and suggestions on the topic, his patience and friendliness in explaining difficult problems.

Dr. Maria Kontou - for her generosity in sharing scientific knowledge and biochemical insights.

Prof. Dr. Volker Haucke - for his willingness to grade this work as the 2nd supervisor

Prof. Dr. Wolfram Saenger - for offering the opportunity to cooperate with his group

Jacobo Martinez-Font and **Sebastien Moniot** for the fruitful cooperation, pleasant discussions and basic understanding of crystallography.

Colleagues in the lab: **Dr. Felista Tansi, Dr. Jing Hu, Yujing Yao, Susanne Thamm, Christiane Kilian, Anne Massah**

Students in the lab: **Robin Wratil, Shun Wang, Yuwen Gu, Heike Helgert, Steffen Doerr, Andrea Niederwieser**

Other colaborators: **Stefan Reinke, Detlef Grunow, Markus Berger, Veronique Blanchard, Stefan Reinke, Eva Tauberger, Dr. Reinhold Zimmer**

Other people in the institute: **Felisitas Kern, Uwe Schöneberger, Christiane Ossadnik, Seynel Gün, Katrin Büttner**

Die Sonnenfeld Stiftung for financial support and a special thank to **Prof. Dr. Hansjürgen von Villiez** for his steady personal encouragement and enriching insights.

Roland und Elfriede Schauer-Stiftung for supporting the end phase of my work financially. Special thank to the inspiration of **Prof. Dr. Roland Schauer** and his passion and continuous contribution on the field of sialic acid.

Table of contents

Abbreviations

3-O-Me-GlcNAc	3-O-Methyl-N-acetylglucosamine
6-O-Ac-ManNAc	6-O-Acetyl-N-acetylmannosamine
APS	Ammoniumperoxodisulfate (w/v)
DMAB	4-Dimethylaminobenzaldehyd
DMEM	Dulbecco's modified eagle medium
EDTA	Ethylenediaminetetraacetic acid
GABA	γ-Aminobutyric acid
GalNAc	N-Acetylgalactosamine
GlcNAc	N-Acetylglucosamine
GlcNCyc	N-Cyclopropanoylglucosamine
GlcNHex	N-Hexanoylglucosamine
GlcNProp	N-Propanoylglucosamine
GST	Glutathione-S-transferase
IPTG	Isopropyl-ß-D-thiogalactopyranoside
LDH	Lactate dehydrogenase
ManNAc	N-Acetylmannosamine
ManNBut	N-Butanoylmannosamine
ManNBz	N-Benzoylmannosamine
ManNiBut	N-Isobutanoylmannosamine
ManNPh	N-Phenoylmannosamine
ManNProp	N-Propanoylmannosamine
MEM	Minimum essential medium
NaDoc	Sodium deoxycholate
Neu5,9Ac_2	5-N-9-O-Acetylneuraminic acid
Neu5Ac	5-N-Acetylneuraminic acid
Neu5Ac9Lt	5-N-Acetyl-9-O-Lactylneuraminc acid
Neu5Gc	5-N-Glycolylneuraminic acid
PBS	Phosphate buffered saline
PEP	Phosphoenolpyruvic acid
PK	Pyruvate kinase
PMSF	Phenylmethylsulfonylfluoride
ROK	Repressor open reading frame kinase
RPMI	Roswell Park memorial institute 1640 medium
RT	Room temperature
Sia	Sialic acid
SDS	Sodiumdodecylsulfate
ST3Gal5	ST3 beta-galactoside alpha-2,3-sialyltransferase 5
ST8Sia1	ST8 alpha-N-acetyl-neuraminide alpha-2,8-sialyltransferase 1
TEMED	Tetramethylendiamine
TEV	Tobacco Etch virus
Tris	Tris(hydroxymethyl)aminomethane

Zusammenfassung (Deutsch)

Die humane ManNAc Kinase (hMNK) ist eine funktionelle Domäne des bifunktionellen Enzyms UDP-GlcNAc-2-Epimerase/ManNAc-Kinase (GNE). Die GNE ist das Schlüsselenzym der Biosynthese von Sialinsäure, dem häufigsten terminalen Zucker auf Glykanstrukturen. Das Ziel der Arbeit war es, die hMNK Kristallstruktur zu charakterisieren, wichtige Mutationen des Enzyms zu analysieren und die Grundlage für neuartige Inhibitoren der hMNK und Sialinsäurebiosynthese zu entwickeln.

In der Arbeit wurde gezeigt, dass aktive hMNK in einem prokaryotischen System exprimiert werden kann. Die gereinigte hMNK ist in Lösung ein Homodimer von 70 kDa mit spezifischer Aktivität für ManNAc. Für Kristallisationsversuche wurde die Aufreinigung der hMNK mit dem 6-His-Tag optimiert. In einem kurzen Reinigungsverfahren über zwei Schritte, Ni-NTA-Chromatographie gefolgt von FPLC-Gelfiltration, konnten mehr als 25 mg hMNK pro Liter *E.Coli* Kultur erhalten werden.

Zusätzlich zu der beschriebenen Apo-Kristallstuktur der hMNK, konnten drei neue Strukturen: MNK/ManNAc (1,65 Å), MNK/ManNAc/ADP (1,80 Å) und MNK/ManNAc-6-P/ADP (2,40 Å) Komplex analysiert werden. Das aktive Zentrum der hMNK ist in einem dichten Netzwerk von polaren und unpolaren Wechselwirkungen koordiniert. Nach der Bindung von ManNAc verändert die hMNK ihre Konformation von einer offenen zu einer geschlossenen, was die Bindung und Reaktion mit ATP ermöglicht. Die Aminosäure D517 ist das katalytische Zentrum des Enzyms und polarisiert das O6-Atom von ManNAc für den Transfer des γ-Phosphat von ATP. Zwei Ionen sind essentiell für das Enzym, nämlich Mg^{2+} für die ATP-Koordination und Zn^{2+} für ManNAc Bindung.

Mit den neuen Strukturinformationen konnten hMNK Mutationen, die die autosomal rezessive neuromuskuläre Erbkrankheit, Hereditary Inclusion Body Myopathy (HIBM), verursachen, neu bewertet werden. Die Aktivität und Spezifität der gereinigten hMNK HIBM Mutanten wurden analysiert und korrelieren mit den Erkenntnissen aus der Kristallstruktur. CD-Messungen zeigten ähnliche Veränderung in der Sekundarstruktur für alle Mutanten. Die Neigung dieser Mutanten verstärkt zu aggregieren, besonders bei höheren Konzentrationen, wurde als ein Grund für HIBM angenommen und stellt ein Hindernis für Kristallisationsversuche dar.

Um funktionale und in Zellen wirkende Inhibitoren für die Sialinsäure Biosynthese zu finden, wurden potentielle hMNK Inhibitoren *in vitro* und in etablierten Zell-Assays getestet. Die verwendeten GlcNAc-Derivate (GlcNProp, GlcNCyc und GlcNPent) sind jedoch keine starken Inhibitoren der hMNK *in vitro* und haben daher begrenzte Wirkung in Zellen. Durch Inhibitionsmodellierung der hMNK Kristallstruktur, wurde postuliert, dass eine einfache Modifikation am C6 von ManNAc ein potenter kompetitiver Inhibitor darstellen kann. 6-O-Ac-ManNAc wurde chemisch synthetisiert und zeigte sich als der bisher beste kompetitive hMNK-Inhibitor (Ki = 1,4 mm). Er kann als Leitstruktur für weitere Optimierungen verwendet werden.

Abstract (English)

Human ManNAc kinase (hMNK) is a functional domain of the bifunctional enzyme UDP-GlcNAc-2-epimerase/ManNAc-kinase (GNE). GNE is the key enzyme in the biosynthesis of sialic acid, the most abundant terminal sugar on glycan chains. The goal was to characterize the hMNK crystal structure, analyze important mutations of the MNK as well as create a basis to develop novel inhibitors of the hMNK and, as a consequence, of the sialic acid biosynthesis.

In this work it has been shown that active hMNK can be expressed in a prokaryotic system. The purified hMNK was characterized to be a 70 kDa homodimer in solution with specific ManNAc Kinase activity. To facilitate the crystallization process, the expression using the 6-His-tag was optimized for large-scale purification. In a rapid two-step purification procedure using a Ni-NTA chromatography followed by FPLC gel filtration, more than 25 mg hMNK per liter *E.coli* culture could be obtained.

Crystallization revealed, in addition to the previously described apo-structure, three novel structures: the MNK/ManNAc complex (1.65 Å), MNK/ManNAc/ADP (1.80 Å) and MNK/ManNAc-6-P/ADP (2.40 Å). The active center of the hMNK is highly coordinated in a network of polar and non-polar interactions. Upon ManNAc binding the hMNK exert a conformational change from an open conformation to a close conformation facilitating the binding and reaction with ATP. The amino acid D517 is found to be the catalytic center of the enzyme polarizing the O6 of the ManNAc and allowing the transfer of the γ-phosphate of ATP. Two ions are found to be essential for this enzyme, namely Mg^{2+} for ATP coordination, and Zn^{2+} for ManNAc binding.

Using novel information about the active center, hMNK mutations, which causes the autosomal recessive neuromuscular disease hereditary inclusion body myopathy (HIBM), was reassessed. Activity and specificity data were confirmed with purified hMNK HIBM mutants and correlated with the insights from the crystal structure. CD measurements revealed a similar change in secondary content for all the mutants. The strong propensity of hMNK to form aggregation at higher concentrations was seen as a potential underlying condition for HIBM and a hindrance to obtain workable protein crystals.

As an attempt to find functional sialic acid biosynthesis inhibitors for cellular assays, potential hMNK inhibitors were tested *in vitro* and in newly established cellular assays. The applied GlcNAc derivates (GlcNProp, GlcNCyc, and GlcNPent) were no strong inhibitors of the hMNK *in vitro* and therefore has very limited effects in cells. Applying inhibitor modeling on the given hMNK crystal structure, a simple modification at C6 of ManNAc was postulated to generate a potent competitive inhibitor. 6-O-Ac-ManNAc was chemically synthesized and found be the best competitive hMNK inhibitor so far (K_i = 1.4 mM), and may be used as a lead structure for further inhibitor design.

1. Introduction

Cells are surrounded by a plasma membrane, which acts as a barrier to their environment and protect the cell and its intracellular components. Through the structure and character of the plasma membrane cells keep their integrity and interact with other cells and their surroundings. Membranes are involved in the exchange of metabolites, transfer of signals, cell movement and replication. The lipid bilayer of membranes contains lipids and proteins, mostly glycosylated, which help them fulfill the diverse functions needed. Those glycoconjugates are in direct contact with the cell's surrounding. The terminal element in the glycan chains are usually N-acetylneuraminic acids, also called sialic acids. They play a diverse biological role in higher animals and have been the subject for decades of research [1].

1.1. History of sialic acids

Why sialic acids are also called neuraminic acids? In the midst 1930s this sugar was isolated from submaxillary mucin by Gunnar Blix leading to the name "sialic acid" from saliva-derived acidic compound [2]. Almost at the same time, Ernst Klenk isolated it from neuronal cells of the brain and termed it "neuraminic acid" [3]. Later Klenk's neuraminic acid was found to be the same compound as Blix' "sialic acid" and the nomenclature was clarified in 1957 [4]. Nowadays the name "sialic acid" is referred to the collection of this sugar with all of its modifications while the individual sugars retain their "neuraminic acid" nomenclature (e.g. N-acetylneuraminic acid, Neu5Ac).

1.2. Structure of sialic acids

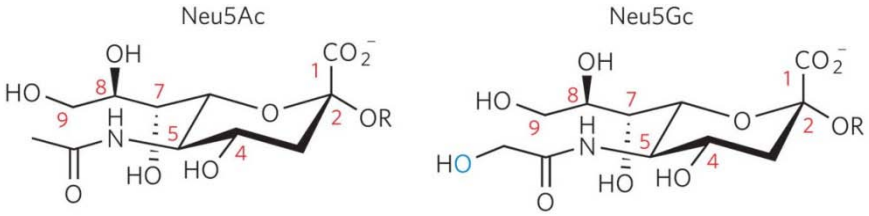

Figure 1.1: Two major sialic acids in mammalian cells[5]

Sialic acids are acidic terminal amino sugars of the oligosaccharide chains on glycoproteins and glycolipids. These sugars have 9 carbon groups with a carboxylated C2-position and an aminated C5-position. The carboxyl group makes this sugar negatively charged and acidic under physiological condition. The diversity of this sugar is due to the substitution of C5 amino group, as well as, the hydroxyl groups at C-4, C-7, C-8 and C-9. For the hydroxyl group substitutions of acetyl, lactonyl, sulfonyl, phosphonyl and methyl groups have been described. As modifications for the amino group acetyl and glycolyl groups are known [6]. There are more than 50 different sialic acid structures

known to exist in nature with N-acetylneuraminic acid (Neu5Ac) as the biosynthetic precursor of virtually all members of the sialic acid family [7]. They are modified in the trans-Golgi network after binding of Neu5Ac to oligosaccharides.

5-N-Glycolyneuraminic acid (Neu5Gc) has an additional oxygen atom in the N-glycolyl group of Neu5Ac. The human deficiency of Neu5Gc is explained by an inactivating mutation in the gene encoding CMP-N-acetylneuraminic acid hydroxylase, the rate-limiting enzyme in generating Neu5Gc in cells of other mammals. This deficiency also results in an excess of the precursor sialic acid N-acetylneuraminic acid (Neu5Ac) in humans [8].

In solution sialic acids form spontaneously the typical pyranose ring of hexoses between C-2 and C-6. In glycoconjugates, the α-conformation is predominant for this sugar. Only the activated CMP-Neu5Ac is a β-anomere [9].

1.3. Sources of sialic acids

Sialic acids are essential component of glycoconjugates of deuterostomia. Its expression is dependent on the species, location and ontogeny. In human tissues for examples three types of sialic acids exists. Neu5Ac, Neu5,9Ac_2, Neu5Ac9Lt can be found at different concentrations and locations. Neu5Gc is only expressed in fetal tissues and certain tumors [10, 11].

In other organism the expression of sialic acid is rather rare. Protosomes usually do not have sialic acids. However, certain bacteria and lower eukaryotes do express sialic acids [7]. In bacteria they are not terminal sugars but rather components of the polysaccharide mostly function as a protection barrier for host immune response. In certain insects, e.g. *Drosophila melanogaster*, the expression of sialic acid can be found in different developmental stages [12] and even fungi may have sialic acids [13]. In plants and yeast the amount of sialic acid detected is five orders of magnitude less than mammalian tissue [14].

1.4. Glycoconjugates

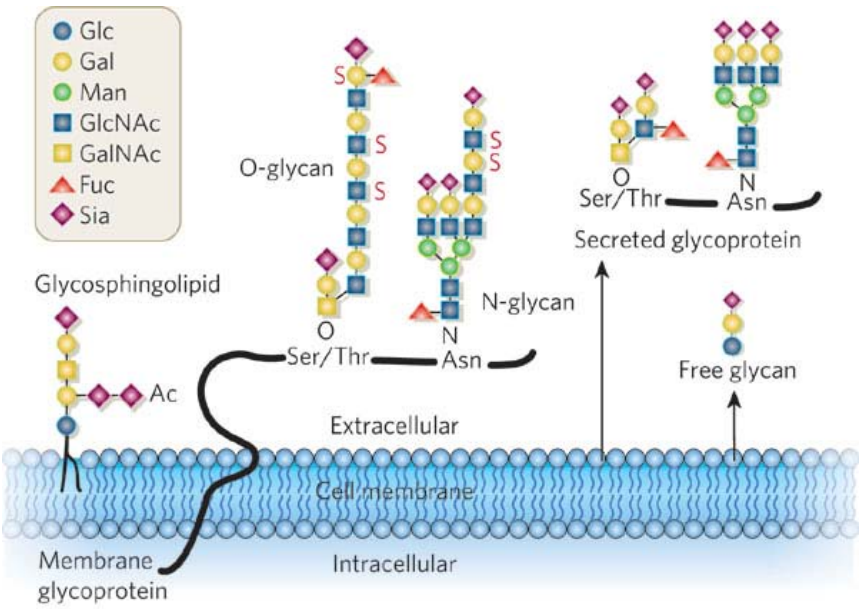

Figure 1.2: Sialic acids on cell-surface and secreted molecules [5]
Sia–sialic acid, Fuc-fucose, GalNAc-N-acetylgalactosamine, GlcNAc-N-acetylglucosamine, Man-mannose, Gal-galactose, Glc-glucose

In vertebrates sialic acids exist as terminal sugars on N- and O-glycans of glycoproteins and on glycolipids as ganglioside. N-Glycans are N-linked to asparagine (Asn) in the consensus sequence Asn-X-Ser/Thr and consists of a common core structure with two N-acetylglucosamine (GlcNAc) and three mannose residues (Figure 1.2). There are three main types of N-glycan structures: the high-mannose structure, with more conjugated mannose from the core; the complex structure, with additional galactose, N-acetylgalactosamine (GalNAc), fucose and sialic acid residues; and a hybrid form with character of both variants [15]. Sialic acids are connected via α2,3-, α2,6-, and α2,8-glycosidic linkages to the underlying sugar residue. A special form of sialylation is polysialylation, which is mostly found on neural cell adhesion molecules (NCAM). This α2,8 conjugate can be up to 200 sialic acids in length [16].

O-Glycans are linked via GalNAc on a serine or threonine residue of glycoproteins. There is no consensus sequence known for the O-glycosidic binding and the core structures of O-glycans are a lot more diverse [17]. The terminal linkage to sialic acid, however, is α2,3- or α2,6- as in N-glycans.

Sialylated glycolipids are called gangliosides. They are found predominantly in the grey matter of the brain. The glycosidic linkage of sialic acids on gangliosides can be α2,3-, α2,6-, and α2,8-.

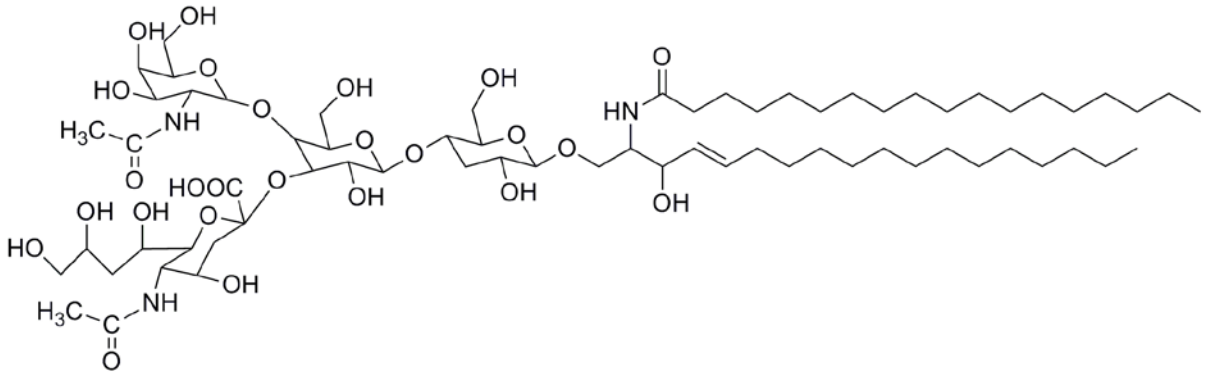

Figure 1.3: Chemical structure of GM2 ganglioside

1.5. Biological functions of sialic acid

Sialylation of glycoproteins and glycolipids is crucial for a myriad of biological functions. Because sialic acid is ubiquitously expressed as terminal components on eukaryotic cell surfaces it is involved in virtually all interaction processes of cells with their matrix or with other cells [5, 18-20]. One can classify their functions in three main groups. First, due to their diverse structure sialoconjugates offer recognition sites for certain interaction partners [5]. Then, because of their terminal position and their negative charge sialic acid can also mask active binding determinations [21]. And third, as an element of the glycan structure they are directly involved in the stability and functionality of defined glycoproteins [22].

1.5.1. Sialoconjugates as recognition sites

Cell-cell and cell-matrix interactions are basic processes of directed cell movement during ontogenesis, tissue formation during organogenesis, inflammation reactions, malignant cell growth or metastasis. Due to their terminal position on cell surfaces, sialic acid is directly involved in these processes. Specific sialic acid binding proteins mediates these interactions. Out of those the most studied families are selectins and siglecs.

Selectins are involved in the interaction of leukocytes with endothelia cells. They mediate the so called “rolling”, initiating the entrance of leukocytes in activated endothelial tissue. Selectins are expressed as L-selectins on leukocytes or as activated P-and E-selectins on endothelia. They bind in a Ca^{2+}-dependent manner structures containing sialyl-Lewis^x residues. L-Selectins bind preferably 6’-sulfo-sialyl-Lewis^x [23].

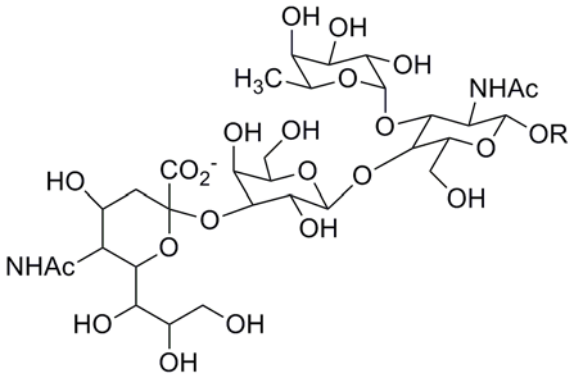

Figure 1.4: Chemical structure of sialyl-Lewis^x

Siglecs, termed for sialic-acid-recognizing Ig-superfamily lectins, are the biggest family of sialic acid binding lectins. They possess a N-terminal domain, which is structurally similar to variable domains of immunoglobulins (Igs), variable numbers of C2-like Ig domains (1-16), a transmembrane area, and a cytoplasmic tail [24]. In humans about 11 different members of this family have been discovered. Most of them are expressed on cells of the immune system. Research on individual Siglecs is still ongoing. The most important members, however, have been intensively studied. Sialoadhesin (Siglec-1) is exclusively expressed on macrophages and regulate their interaction with other cells via the binding of α2,3 linked sialic acids [25]. CD22 (Siglec-2) is involved in the homophilic interaction of B-cells and binds selectively α2,6 sialic acid residues [26]. MAG (Siglec-4), myelin-associated glycoprotein, is the most highly conserved siglec; it is specifically expressed in glial cells and recognizes gangliosides, ensuring long-term stability of myelin [27].

A second category of siglecs is the CD33-related siglecs (CD33rSiglecs), which is characterized by general homology to one another, the presence of tyrosine-based signaling motives, and rapid evolution. They are involved in recognizing sialic acids as self, and thus inhibiting responses of the immune system. It has been suggested that they are also involved in the recognition of pathogens expressing sialic acids [28].

Not only endogenous sialic acid binding proteins use sialic acid as binding partner, also pathogens use this pathway to infect the host cell. Viruses for example possess hemagglutinin, whose binding is mediated by recognition of sialic acids. The well-researched hemagglutinin of the influenza A virus is such an example, whose specificity is strictly dependent on the sialylation type of the host cell [29]. Through cross reactions of viruses, animal influenza viruses can adapt to the sialylation pattern of human cells leading to seasonal influenza epidemic, e.g. bird and swine flu.

Bacterial adhesins mediate the binding of the pathogen to the host cell. Bacteria types expressed distinct adhesins, making them selective for certain host and tissue infection. The *Helicobacter pylori*

for examples possess two adhesins selective for gangliosides or glycoproteins [30]. The adhesin of *E.coli* K99 binds specifically Neu5Gc, which is widely expressed in pig intestine, the host of *E.coli* K99 [31]. In many cases, toxins of the pathogen bind to sialic acid residues and get internalized via endocytosis: e.g. the binding of botulinum and tetanus neurotoxins to gangliosides [32].

1.5.2. Sialic acid masking antigenic determinants

Given their negative charge and hydrophilicity at terminal position, sialic acids provide a protection shield around cells. The negative charge on human erythrocytes and other cell types provides charge repulsion, preventing unwanted interactions of cells in the blood circulation. The luminal surface of vascular endothelium is likely for the same reason heavily sialylated [33].

In glycoconjugates, sialic acid can also recruit other factors to protect its surface. Factor H for example is a soluble glycoprotein, which regulates the alternative pathway of the complement system. By binding to host cell glycan structures, which is not present on pathogen's cell surfaces, it protects host cells from the complement activation. Several pathogens successfully cover their own surfaces with host cell sialic acid, recruit factor H and therefore evade the immunological response[34]. *Trypanosoma cruzi*, the cause of Chagas disease, for examples binds to glycoconjugates on the surface of host cells. Using its own neuraminidase and sialyltransferase it recruits host glycan structures on its surface and masks own antigenic structures [35].

Embryonic cells are also covered by a thick sialic acid layer, which protects them from mother's immune system. Embryonic stem cells, on the other hand, only have a weak sialylation, which increases after differentiation. Therefore, it has been postulated that the complement system is used as a possible mechanism for the organism to regulate cell death in embryogenesis [36].

The overall general increase in sialic content of tumor cells might also protect them from alternative pathway complement activation by recruiting factor H. Conversely maybe also a reason why tumor cells secrete factor H themselves [37].

1.5.3. Influence of sialic acid on stability and functionality of glycoproteins

The presence of sialic acid is important for the biological function of several glycoproteins. For examples the desialylation of somatostatin receptors causes a conformational change, which leads to a significant decrease of ligand binding [38]. Also nucleoporin p62 (NUP62) demonstrate a reduced activity without sialylation [39]. In our lab similar observations have been made with the GABA transporter (GAT1), where reduced sialic acid expression correlate with GABA uptake in a dose dependent manner [40].

In many cases sialic acid protect proteins from degradation, possibly due to the steric inhibition of proteolytic activity. The acetylcholine receptor is in this case a very prominent representative. Erythropoietin with low sialic expression is also less active due to its reduced half-life in the serum [41]. The circulation of blood cells is also regulated by the sialic acid concentration. Erythrocytes and thrombocytes gradually lose their terminal sialic acid or sialic acid containing structures are then detected by macrophages and eliminated [42]. The same can be observed with other serum proteins and antigen-antibody complexes. They are detected by hepatocyte asialoglycoprotein receptors on Kupffer cells and cleared [43].

1.6. Biological implications of sialic acid in diseases

Given their ubiquitous biological implications the role of sialic acid in human health and disease is huge. Investigations in all areas of the medical curriculum are ongoing. Extensive attention has been paid in the field of infectious diseases (e.g. influenza), neuroscience and oncology.

1.6.1. Infectious diseases

As already mentioned, sialic acid is involved in several infectious diseases. Maybe the best- known example is the binding of influenza A virus to airway epithelium. Special attention has been paid to the recent avian flu [33]. This infection, however, is only possible if the hemagglutinin components of the virus undergo specific mutations, switching from recognizing α2,3-linked sialic acid, which is predominant in birds' intestinal epithelium, to α2,6-linked sialic acid, more enriched on human upper airway epithelium [44]. In fact, such a direct transmission is rare. The virus is more likely to take the path from wild birds to poultry then eventually to domesticated mammals such as the pig, which is a putative "mixing vessel" as both α2,3- and α2,6-linked sialic acids can be found on the swine epithelium [29]. Severe or even lethal human avian flu infection is probably due to the fact that a high dose of virus was inhaled which reach the lower airways, where α2,3-linked sialic acids are present in human.

Many other pathogens are successful at expressing sialic acid on their surfaces, recruiting factor H and enhancing intercellular survival and immunogenicity. [45, 46].

1.6.2. Neuroscience

The brain is the organ with the highest concentration of sialic acid predominantly in gangliosides. The biosynthesis of polysialic acids facilitates sprouting and plasticity [47]. Ganglioside recognition by myelin-associated glycoprotein (Siglec-4) also plays a pivotal role in mediating myelin stability and in inhibiting neural sprouting after injury [48]. Sialidase injections enhance axon outgrowth *in vivo*, possibly due to the resulting reduced level of ganglioside ligands for Siglec-4 [49].

Immune reactivity against sialic-acid-containing nervous system molecules often results in severe pathology. Guillian-Barré syndrome, an acute peripheral neuropathy, for example, is triggered by *Campylobacter jejuni*, which synthesizes sialylated mimics of gangliosides on its lipooligosaccharides [50].

1.6.3. Oncology

Altered glycosylation is a general feature of cancer cells. Common phenotypic chances in malignancy are due to a dramatic transformation of cellular glycosylation [51, 52], Altered cell surface glycoconjugates, be it adhesion or antiadhesion molecules, contribute to the complex interaction of tumor cells with themselves and their environment during invasion and metastasis. Glycoconjugates secreted by a tumor interacts with other cell types and facilitate its own progression. Finally, changes in glycosylation of cell surface molecules can also modulate intrinsic functional characteristics contributing to the malignancy of tumor growth.

With respect to the terminal sugars on glycoconjugates, there are distinct changes in sialylation associated with malignant transformation in tumor cells. In tumor cells the concentration of surface Neu5Ac is increased and intimately connected with disturbed cell adhesion, invasiveness, and metastasis [53-55]. The increased sialic acid concentration serves to protect tumor cells from the alternative complement pathway [56].

Secreted carcinoma mucins bearing unusual forms of sialylation, e.g. Lewis X/A, can be detected in the blood stream of cancer patients and are used as diagnostic and prognostic tools [57].The sialylated forms of these mucins are resistant to clearance by liver receptors [58]

In many cases the overexpression of sialic acid in tumor cells is directly associated with a higher metastasis potential [59, 60]. This phenomenon is likely a result of stronger interaction between circulating tumor cells with selectins on platelets, leukocytes and endothelium, and thereby facilitating metastasis [61].

Parallel to that there is an accumulation of non-human Neu5Gc on tumors [11]. It has been suggested that the increased antibody production against these Neu5Gc-containing epitopes may result in a weakening of the immune response, which in term is beneficial for the tumor cell [62].

1.7. Biosynthesis of sialic acid

UPD-GlcNAc is an activated amino sugar and plays a central role in the synthesis of glycoconjugates (N-glycans, O-glycans, glycolipids, O-GlcNAc). Through various catalytic steps UDP-GlcNAc is generated from fructose-6-phosphate and can reach cellular concentrations of up to 100 – 200 µM.

The de novo-biosynthesis of sialic acid is often depicted to start with the irreversible transformation of UDP-GlcNAc to ManNAc and consequently to ManNAc-6-phosphate. These two steps are catalyzed by the bifunctional enzyme UDP-GlcNAc-2-Epimerase /ManNAc-Kinase (GNE) [63]. Subsequently, ManNAc-6-phosphate reacts with phospho*enol*pyruvate (PEP) in a condensation reaction to Neu5Ac-9-phosphate catalyzed by the Neu5Ac-9-phosphate-synthease followed by dephosphorylation to Neu5Ac-9-phosphate. All these steps occur in the cytosol.

Unlike other monosaccharides, the activation of Neu5Ac happens in the nucleus. Free Neu5Ac is condensed with CTP to CMP-Neu5Ac and pyrophosphate by CMP-Neu5Ac-synthease. While sialic acid in glycoconjugates is always α-linked, the linkage of CMP-Neu5Ac is β [9, 64] . This may ensure that CMP-Neu5Ac be protected from α-specific sialidases. CMP-Neu5Ac is then released into the Golgi apparatus through an CMP/CMP-Neu5Ac antiport [65]. In the *trans*-Golgi network Neu5Ac is then transferred via specific sialyl-transferases under release of CMP on N-glycans, O-glycans or gangliosides [66].

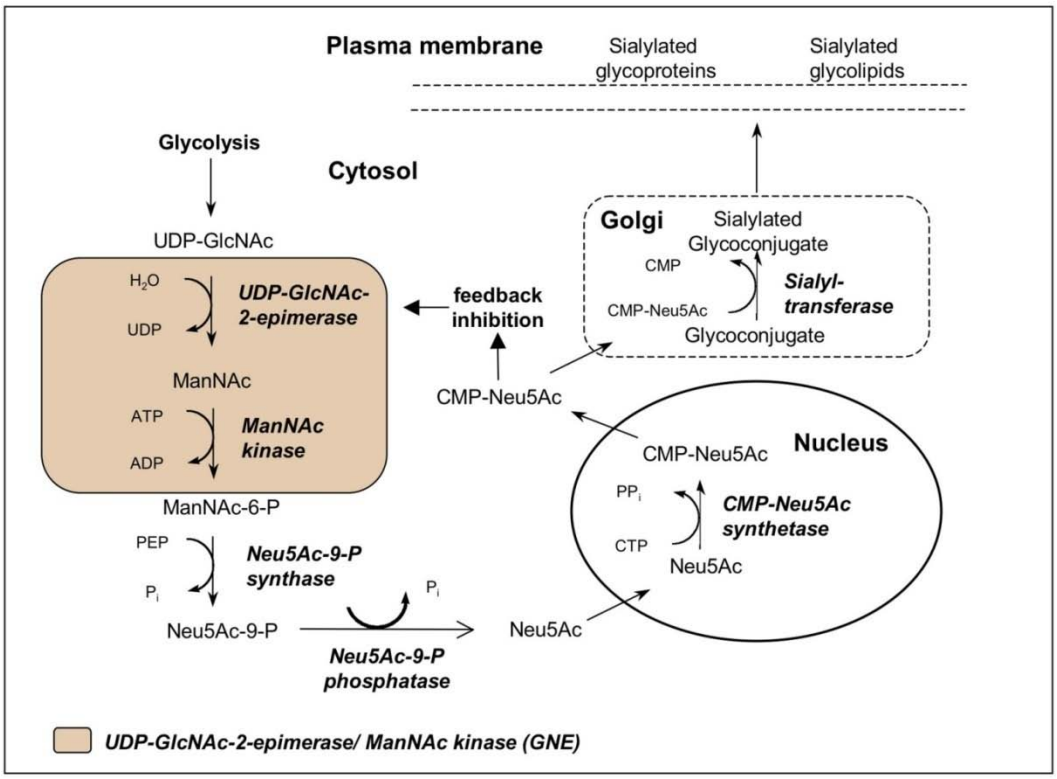

Figure 1.5: Schematic of sialic acid biosynthesis

1.8. UDP-GlcNAc-2-epimerase/ManNAc-kinase (GNE)

With the irreversible conversion of UDP-GlcNAc to ManNAc and consequently to ManNAc-6-phosphate, GNE is depicted as the bottle neck for sialic acid biosynthesis [67]. And in fact studies have shown that the reduction of GNE activity can lead to decrease cell surface sialylation [68, 69]. GNE is a highly conserved protein found throughout the animal species. Its highest expression is found in the liver and placenta of living organism. Historically, the UDP-GlcNAc-2-epimerase was first discovered by Cardini und Leloir (1957), its specific activity, however, was first correctly described by Comb and Roseman (1958)[70, 71]. The ManNAc Kinase activity was discovered by Ghosh and Roseman (1961) as well as Warren and Felsenfeld (1961) at the same time [72, 73]. Later it has been established that the subcellular localization and the tissue distribution of this two enzymes are identical [74]. Finally, Stäsche et al. (1997) and Hinderlich et al. (1997) could demonstrate that these two activities are expressed on a single polypeptide as a bifunctional enzyme [63, 75]. Through site-directed mutagenesis the 2-epimerase activity was established to be in the N-terminus of the enzyme and the kinase activity on the C-terminus [76].

1.8.1. GNE regulation

Due to its central role in the expression of sialic acid residues on the cell surface this enzyme underlies extensive regulation [69]. The strongest regulation is the feedback inhibition by CMP-Neu5Ac [77]. A point mutation abolishing this feedback inhibition leads to the hereditary genetic disease called sialuria, where patients excrete increased level of sialic acid and the intermediate acetamidoglucal in the urine [78]. The GNE is also regulated by oligomerization. Biophysical methods have revealed that GNE exists as both a tetramer and a dimer. Whereas the tetrameric form exhibits both epimerase and kinase activity, the dimer shows kinase activity only. The stabilization of the tetrameric form is ensured by physiological concentrations of UDP-GlcNAc [79]. Another form of regulation is through phosphorylation of GNE by protein kinase C (PKC). GNE has eight conversed motifs for PKC, several isoforms of PKC interact with GNE and upregulate enzyme activity upon phosphorylation [80]. On the genetic level GNE expression is regulated epigenetically. Downregulation of GNE mRNA expression is achieved by methylation of its promoter region as observed in Morris hepatoma [81] and HIV-infected lymphocytes [82].

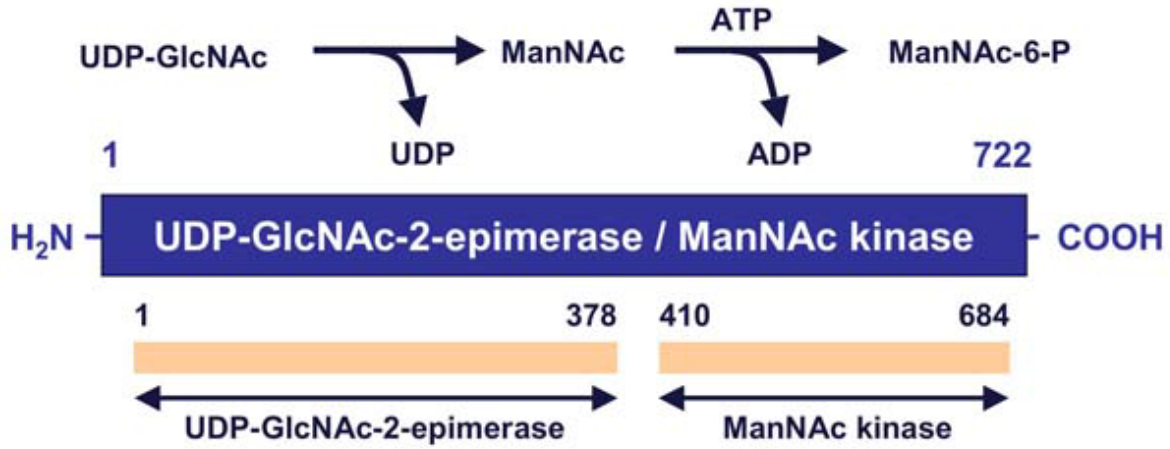

Figure 1.6: Schematic display of UDP-GlcNAc-2-epimerase/ManNAc kinase primary structure

1.8.2. GNE and sialuria

Several diseases are associated with the dysregulation of the GNE. As described, the allosteric feedback inhibition of GNE is defective in a human disease called sialuria. Patients having this disease experience developmental disorders and liver hypertrophy. The common symptom is the increased excretion of sialic acids and metabolites in their urine [83]. Sialuria is an autosomal dominant disorder caused by a missense mutation in one of the two arginine amino acids at position 263 (R263L) or at position 266 (R266Q) [84, 85]. This mutation prevents the binding of CMP-Neu5Ac, and thus disables the inhibitory effects of CMP-Neu5Ac on GNE activity.

1.8.3. GNE and hereditary inclusion body myopathy (HIMB)

Another disorder caused by missense mutations of the GNE is called hereditary inclusion body myopathy (HIBM). HIMB, also called h-IBM or IBM2, is an autosomal recessive neuromuscular disorder most common in the Persian-Jewish population with adult-onset, slowly progressive distal and proximal muscle weakness. The muscle pathology includes cytoplasmic rimmed vacuoles and cytoplasmic or nuclear filamentous inclusions. The clinical course of HIBM is relentless leading to progressive muscle weakness without involvement of the ocular, pharyngeal and respiratory muscles. A unique feature of this myopathy is the sparing of the quadriceps muscles allowing affected individuals to be able to walk and stand until very advanced stages. The genetic reason for this disease is an autosomal recessive inheritance of missense mutations in the GNE. Over the last decades over 60 GNE mutations associated with HIBM has been described in patients from different ethnic backgrounds. The effect of GNE mutations on the enzymatic properties of both the epimerase domain and kinase domain were assessed in various studies [86-88] revealing that these mutations lead to a decrease in enzyme activity of both domains. Moreover, mutations in one domain also

affect the activity of the other domain, suggesting that there is an interplay or structural connection between these domains and that these mutations impair this structural connection.

Other experiments revealed that the mechanism of pathology is not that of a typical autosomal recessive disorder with low enzyme activity of the gene product. Rather the total functional spectrum of the enzyme together with the activity of other enzymes in metabolically interconnected pathways are responsible for the pathology.

There are several hypotheses to why a single point mutation of the GNE could lead to a myopathy disease phenotype. First, the decreased enzyme activity of GNE leads to hyposialylation of glycoproteins important for muscle regeneration. Yet, cultured muscle cells from patients with HIBM mutations showed variable sialylation ranging from decreased to normal [87-89]. Hinderlich et al. also demonstrated normal membrane bound sialic acid levels in lymphoblastoid lines with the M712T mutation [90]. However, since HIBM is an adult onset disease, the effects of sialic acid deficiency may appear gradually. Because there is residual GNE enzymatic activity left, some glycoconjugates, like N-linked, might be more readily sialylated than others, like O-linked or PSA. Therefore, a shortage in sialic acid would affect the later to a greater extend leaving for example PSA-NCAM and α-dystroglycan inadequately glycosylated contributing to the pathology of HIBM.

Other groups favor the idea to look at the GNE as a multifunctional enzyme. Besides its enzymatic activity, GNE interacts with other proteins. Mutations of the gene could create structural changes in the protein leading to impaired cooperation with important interaction partners. As described before, interaction partners of the GNE have been found to be important in a myriad of processes, including apoptosis [91], cytoskeleton organization, protein degradation [92] and muscle functions [93]. The question why these phenomena are muscle cell specific can be fathomed with the tissue specific expression of different isoforms of the GNE (GNE2 and GNE3) [94]

1.8.4. GNE and alternative functions

While it is undeniable that GNE control the flux into the sialic acid biosynthetic pathway though conversion of UDP-GlcNAc to ManNAc [63] and has been characterized as the key determinant in the surface display of sialoglycans [69], there is still a lot to discover about its biological activity in health and disease. Accumulating evidences suggest that healthy cells maintain a higher level of GNE then required for sialic acid production and raised the possibility that GNE may serve multiple functions within the cell. This hypothesis has been reinforced by the fact that HIBM patients as described have approximately normal levels of sialic acid while *in vitro* studies demonstrated a reduced activity for this enzyme. The apparent disconnection between *in vitro* results and sialic acid production in HIBM patients can be resolved by considering the excess of GNE in the cells, which enable them to

maintain a basal level after CMP-Neu5Ac-mediated feedback inhibition. These considerations supply a mechanistic explanation for the nearly normal level of sialic acid found in HIBM patients but leave the biochemical basis of cellular abnormalities unanswered. Suggesting that there may be other mechanism involved in the disease process. In addition, the presence of GNE in the nucleus, where it is not required for ManNAc or ManNAc-6-P production, raises the intriguing possibility that this protein regulates gene expression. And indeed evidence has been presented that GNE expression correlates with the expression of ST3Gal5 and ST8Sia1 resulting in downstream bioactivity changes of its ganglioside substrates GM3 and GD3 and complex biological changes, including proliferation and apoptosis [91].

One recent report also established the relationship between neurite outgrowth and GNE expression, which is independent from sialic acid biosynthesis, suggesting an alternative function of this enzyme [95].

Protein-protein interaction could be verified for GNE and collapsin response mediator protein-1 (CRMP-1) [92]. CRMP-1 is mainly expressed within the nervous system, but also in a variety of lung tumors with high invasive potential. The interaction of GNE and CRMP-1 might therefore be interesting for the progression of cancer and nervous system biology. It has also been postulated that the interaction of GNE and CRMP-1 may play a role in the onset or progression of HIBM due to CRMP-1's involvement in cytoskeleton organization [96].

In the same work an interaction between GNE and promyelocytic leukemia zinc finger (PLZF) could also be detected. PLZF is a protein involved in the regulation of ubiquitinylation of proteins for degradation. Due to the abnormal accumulation of proteins in muscles of HIBM patients [97], it is possible to speculate that this interaction may play a role in the proper degradation of excess GNE.

And last but not least, a recent discovery about interaction of GNE with α-actinin 1, a usually non-muscle α-actinin form expressed in skeletal muscle tissue, opens novel avenues to think about GNE mediated processes in altering sarcomere functions [93].

1.8.5. GNE inhibitors

Judging from the key role the GNE plays in sialic acid biosynthesis and the need to elucidate its other functions a lot of efforts have been put in discovering a GNE inhibitor that is active in cell and living organism. Not only would this inhibitor be an indispensible tool for GNE and sialic acid research, it could also offer a novel approach to counterbalance the increased sialylation in tumors and metastatic cells.

The first inhibition of the GNE was observed using a cell-free system from rat liver homogenate. GlcNProp-6-phosphate as well as ManNProp-6-phosphate appears to be weak inhibitors of Neu5Ac biosynthesis [98]. Using the same system 3-O-Me-GlcNAc was detected to be a non-competitive inhibitor of the ManNAc kinase [99].

By use of saturation transfer difference NMR spectroscopy, the binding epitopes of UDP-GlcNAc and ManNAc to GNE could be characterized [100, 101]. Based on these results novel UDP-GlcNAc analogs could be synthesized [102]. Also novel UDP-glycal derivatives as transition state analogs were designed as GNE inhibitors [103]. Purified recombinant GNE allows the rapid and specific *in vitro* analysis of these new inhibitors [104]. However, since these inhibitors cannot penetrate the plasma membrane, they cannot be verified in a cellular system. Searching for a GNE inhibitor a lot of attention was paid on the 2-epimerase domain neglecting the other major part of this enzyme, the ManNAc kinase. Experiences from effective therapeutical kinase inhibitors, however, indicate that kinases can be very specifically targeted. And judging from the fact that an epimerization from GlcNAc-6-phosphate to ManNAc-6-phosphate cannot occur in mammals, due to the lack of a respective 2-epimerase, an inhibitor of the ManNAc kinase could be an equally valuable inhibitor for sialic acid biosynthesis as a 2-epimerase inhibitor.

GNE inhibitors and cellular assays

As for all inhibitors, cellular assays are a very important control for the efficacy of an inhibitor *in vitro*. In the case of the GNE following conditions applies.

First, previous inhibitors of the 2-epimerase domain, due to their bulky nature as substrate analogs, cannot efficiently enter cells. The plasma membrane prevents hydrophilic molecules from entering the cytosol. Since the GNE is a cytosolic protein, molecules must be membrane permeable to affect this enzyme. So the inhibitory effect which can be observed *in vitro* may not be reproduced in cells.

Second, GNE expression level in cells is high. Studies has shown that GNE is usually overexpressed and fulfill alternative functions in cells [91]. Due to this fact, the inhibitory effect of GNE inhibitor may vary for different cell types. Certain cells, therefore, requires a stronger inhibition of the GNE to significantly affect sialic acid expression. This difference has to be assessed with cellular assays of different cell lines.

Finally, there are also scavenger pathways providing cells with external sialic acid. Cells take up glycoproteins from their environment such as in the culture medium, break them down and recycle the available sugar residues. *In vivo*, sialic acid bound glycoproteins are also recycled in this way. This

effect could be observed in cells, where sialic acid biosynthesis has been genetically abolished. A complete knock out of this enzyme would not reduce sialic acid expression to zero [105].

Therefore, for the purpose of finding an efficient sialic acid inhibitor, cellular assays are required. To verify these assays previously characterized inhibitors of the MNK should be used to establish the experimental systems.

1.9. Goal of the work

This work focuses on the MNK domain of the GNE. The major goal is to solve high-resolution structures of this enzyme in complex with its ligands, e.g. ManNAc and ATP. These structures would offer fundamental information about the mode of action of this enzyme and reveal insights about the mechanism of similar sugar kinases. These structures may provide structural insight into the causes of HIBM and offer data for molecular modeling of an effective MNK inhibitor.

In order to achieve this goal different conditions have to be fulfilled:

First, a stable and efficient expression system for hMNK needs to be established. The enzyme needs to be active, specific and stably storable. Purified protein in milligram amount should be available for crystallization.

Second, high-resolution 3D structures of the ManNAc kinase should be obtain via X-ray crystallography. The goal is to obtain multiple structures in different active states in order to gain insights into the mechanistic character of this enzyme.

Third, in order to determine and understand structural changes in HIBM MNK mutants, these mutants need to be expressed, purified and characterized. Common characteristic traits of these mutants may reveal novel insights about HIBM.

Fourth, *in vitro* as well as cellular assays need to be designed, established and optimized for assessing potential MNK inhibitor. With known inhibitors these assays should be tested and their usefulness for further research as sialic acid inhibitors should be verified.

Finally, molecular modeling studies should be conducted to determine potential MNK inhibitors as effective inhibitors of the sialic acid biosynthesis.

2. Material and Methods

2.1. Materials

Unless otherwise indicated, vectors were purchased from Invitrogen (Netherland) or Amersham (Germany). Bacteria strains are from Invitrogen (Netherland). Insect cells (Sf9) come from GibcoBRL (USA). Mammalian cell lines originated from ATCC (USA). Chemicals, enzymes and other reagents were purchased from Sigma (Germany), Roth (Germany), Roche (Germany), Calbiochem (Germany), and GibcoBRL (USA).

MNK substrate and inhibitor

ManNAc and GlcNAc were purchased from Sigma (Germany). GlcNProp, GlcNCyc, GlcNHex, 3-O-Me-GlcNAc, ManNProp, ManNBut, ManNiBut, ManNPent, ManNBz, ManNPh were synthesized for previous experiments in this lab.

2.2. Equipments

Equipment	**Name**	**Company**
SDS-PAGE-System	Mini-Protean II	Biorad
Power Supply	Power-Pac 1000	Biorad
Thermo block	Thermomixer Compact	Eppendorf
Centrifuges	RC5-Superspeed	DuPont
	MultiFuge 1	Heraeus
	3-18K	Sigma
	Biofuge 13	Heraeus
Vortex	Genie 2	Scientific Instruments
Scale	1602 MP	Sartorius
PCR thermo cycler	Mastercycler	Eppendorf
pH meter	pH 211	HANNA Instruments
Vacuum concentrator	speedDry	Christ
FPLC	ÄKTApurifier	GE Healthcare
Photometer	Ultraspec500pro	Amersham Bioscience
	Multiscan GO	Thermo scientific
Microscope	Observer.Z1	Zeiss
FACS	FACScan	Becton Dickinson
CD spectrometer	J-720	JASCO
Incubator	Lab-Shake	Adolf Kühner
Sterile Bench	LaminAir	Holten

2.3. Protein biochemical methods

2.3.1. Determination of the protein concentration with the Bradford assay

The Coomassie dye forms a stable complex with proteins, which has an absorption maximum at 595 nm. To 10 µl of protein sample 1 ml of Bradford reagent (100 mg Coomassie G-250, 50 ml EtOH, 100 ml H_3PO_4 in 1000 ml H_2O) is added and incubated for 3 min at room temperature. The absorbance is measured at 595 nm. BSA at different concentrations is used as standard calibration. The assay is linear from 2 µg/ml to 120 µg/ml protein.

2.3.2. Determination of the protein concentration with the BCA assay

The peptide bonds in proteins reduce Cu^{2+} ions to Cu^{1+}, which then forms a stable chelate complex with two molecules of bicinchoninic acid. This complex has a maximum absorption at 562 nm. Compared to the Bradford assay, this method is less susceptible to detergents and has a broader linear range (10 µg/ml to 1400 µg/ml protein). To 20 µl of protein sample 200 µl of freshly prepared BCA reagent (reagent A and B in a ratio of 50:1 (Pierce, Rockford, USA)) is added and incubated at 37°C for 30 min. The absorption is subsequently measured at 570 nm. A calibration curve is determined using BSA at different concentrations.

2.3.3. Determination of the protein concentration with NANA Drop

The Protein A280 method is applicable to purified proteins that contain tryptophan, tyrosine and phenylalanine residues or cysteine-cysteine disulfide bonds and exhibit absorbance at 280 nm. This method uses the A280 absorbance value in combination with either the mass extinction coefficient or the molar extinction coefficient to calculate the concentration of purified proteins. After cleaning and blanking with buffer, 2 µl of the protein sample is loaded on the bottom pedestal and measured. The NanoDrop 2000/2000c Spectrophotometer automatically calculate the protein concentration based on an intrinsic standard. This quick method is recommended for purified proteins only, since lysate or crude protein extract may have other biomolecules like DNA and RNA which also absorb at the same wavelength.

2.3.4. SDS-Polyacrylamide Gel Electrophoresis

Sodium dodecyl sulphate (SDS) contains a 12-carbon hydrophobic chain and a polar sulfated head, which has strong denaturing character. The hydrophobic chain intercalates into hydrophobic parts of the protein and disrupts its tertiary structure. The sulphated head remains in contact with water, maintaining the solubility of the detergent-protein-complex. SDS coats proteins virtually uniformly with a layer of negative charge and make them migrate towards the anode when placed in an electric field. Therefore, there is a close relationship between mobility of the SDS-protein complex and protein mass.

Usually a discontinued gel electrophoresis system is used with two types of gels, the stacking gel and the resolving gel. The stacking gel is more acidic so that the twitter glycine ions are less anionic and more cationic. With the turn on of the electric field a strong local field between glycine cations and negatively charged chloride ions will be created in the stacking gel. This will result in faster movement of anionic proteins and a focusing of protein samples. In the resolving gel the pH value is increased making glycine ions more anionic. The local field is balanced and proteins can be separated according to their molecular mass in a constant external electric field.

Under denaturing conditions, protein samples are denatured in sample buffer for 5 min at 98°C. Under non-denaturing and non-reducing conditions this step will be skipped and the sample buffer does not contain DTT. The electrophoresis occurs then usually at 150 V for 60 min. Protein standards are purchased from Biorad, Germany.

Solution A

30% Acrylamid (w/w)

0,8% N,N-Methylenbisacrylamid (w/v)

Solution B

0.2% SDS (w/v)

1.5 M Tris-HCl, pH 8.8

Solution C

0.4% SDS (w/v)

0.5 M Tris-HCl, pH 6.8

Running buffer

25 mM Tris-HCl

192 mM Glycine

0.1% SDS (w/v)

5xSample buffer

0.3 M Tris-HCl, pH 6.8

50 % Glycerin (v/v)

15 % SDS (w/v)

0.015 % Bromophenol blue (w/v)

50 mM DTT (only in reducing sample buffer)

Resolving Gels

7,5% Gel: 2.25 ml A, 2.25 ml B, 4.5 ml H_2O, 100 µl 10% APS (w/v), 10 µl TEMED

10% Gel: 3.0 ml A, 2.25 ml B, 3.7 ml H_2O, 100 µl 10% APS (w/v), 10 µl TEMED

Stacking Gel

4% Gel: 0.4 ml A, 0.75 ml C, 1.85 ml H_2O, 24 µl 10% APS, 6 µl TEMED

Coomassie staining

Protein amounts higher than 0.5 µg in SDS-PAGE gels can be easily stained with Coomassie Blue G-250. This dye forms a complex with proteins and makes distinct protein bands visible. After electrophoresis gels are washed 3 times for 5 min. with 200 ml double distilled H_2O, then incubated for 1 h at room temperature with Bio-Safe™ Coomassie G-250 Stain (Bio-Rad Laboratories). After

washing the stained gel in 200 ml ddH_2O the background color will disappear, making stained protein bands clearly visible.

Silver staining

Protein amounts from 50 ng to 0,5 µg are visualized via silver staining. After electrophoresis gels are incubated 20 min at RT in fixing solution; subsequently washed 3x for 5 min in 50% ethanol. Then for exactly 60 s the gel is immersed in 25 ml of solution A, washed 3x shortly with ddH_2O; then incubated for 15 min in solution B and washed 3x again with ddH_2O. The protein bands should be visible after 1-5 min of reaction in solution C. This reaction is stopped by putting the gel in fixing solution for 20 min and stored in water.

Fixing solution	Solution B
40% Ethanol (v/v)	0.16% $AgNO_3$
10% Acetic acid (v/v)	0.08% Formaldehyde (v/v)
0.05% Formaldehyde (v/v)	Solution C
Solution A	5% Na_2CO_3
0.02% $Na_2S_2O_3$	0.0005% $Na_2S_2O_3$ (w/v)
	0.05% Formaldehyde

2.3.5. Western Blot

Directly after the gel electrophoresis, separated protein bands are transferred on a nitrocellulose membrane adapted from a method by Towbin et al. (1979)[106]. In a blot chamber, protein gel and membrane are put together so that the nitrocellulose membrane (Protan® Nitrocellulose Transfer Membrane; Schleicher & Schuell, Germany) is faced to the anode. The transfer takes place at constant current of 250 mA for 60 min at ice-cooled blot buffer (25 mM Tris, 160 mM glycine, 10% (v/v) EtOH).

To verify the transfer, the membrane is stained with Ponceau-solution (0.2% (w/v) Ponceau-Red, 3% (v/v) trichloracetic acid, 3% (w/v) sulfosalicylacid) for 1 min and destained with 1% acetic acid until protein bands are visible. Subsequent 2x washing in PBS + 0.1% Tween-20 will completely remove the dye.

The membrane is now ready for further staining with antibodies (AB) or lectins.

First, the membrane is incubated in 5% (w/v) milk powder in PBS for 30 min at room temperature to block unspecific binding sites. Subsequently, membranes are washed 2x with PBS-Tween for ca. 5 min and immerse in the primary antibody solution. Antibodies solutions are dissolved depending on

the purity of the AB in ratio of 1:2000 to 1:500 (v/v) AB to PBS. The incubation time also depends on the AB and can be 2 h at RT or overnight at 4°C. After this, the membrane will be washed again 2x with PBS-Tween and incubated 2 h at RT with the second antibody. This AB is usually attached to a peroxidase, which catalyzes the oxidation of H_2O_2. Unspecific binding has to be washed away with PBS-Tween again. Specific protein bands can be than stained and make visible with DAB substrate (Roche), a color reaction triggered by H_2O_2 radicals.

PBS (pH 7.4)	PBS-Tween (pH 7.4)
137 mM NaCl	137 mM NaCl
2.7 mM KCl	2.7 mM KCl
10 mM Na_2HPO_4	10 mM Na_2HPO_4
1.76 mM KH_2PO_4	1.76 mM KH_2PO_4
	0.1% Tween-20

2.3.6. Immunoprecipitation

This method is used to isolate a single target protein from a protein lysate. A specific antibody for this protein, which is coupled to a solid beat, is used to precipitate the protein of interest out of the solution.

For the coupling of polyclonal antibodies (pAb) to solid beats, 40 mg of Protein A Sepharose (GE Healthcare) is resuspended in 1 ml PBS for 10 min and then added to it 40 µl of the target pAb serum. This suspension is than rotated overnight at 4°C. For the coupling of monoclonal antibodies (mAb), 50 µl of Protein G Sepharose (GE Healthcare) is taken in 1 ml PBS and rotated with 200 µl of mAb supernatant overnight at 4°C. The suspension is than washed twice with 1 ml PBS and aliquot into 4 tubes; each containing 250 µl.

The cell lysates, which have been disrupted and centrifuged down, are now added to the tubes and incubated for at least 30 min at 4°C. Afterwards, the precipitate is washed twice with RIPA, twice with PREWASH and twice with PBS. The supernatant is discarded as completely as possible and 8 µl of 5xsample buffer is added to the precipitation. Target proteins and AB are than detached from the sepharose beads by denaturing at 98°C for 5 min and analyzed on SDS page.

RIPA (pH 7.4)	PREWASH (pH 7.2)
50 mM Tris-HCl	10 mM Tris-HCl
150 mM NaCl	1 M NaCl
1% Sodium deoxycholate	0.1% Triton X-100
1% Triton X-100	
0.1% SDS	

2.3.7. CD spectroscopy

Purified proteins in gel filtration buffer were used for CD measurement. The protein concentration was determined using BCA. CD spectra were recorded at 25°C in quartz cuvettes in the range of 195-240 nm in a Jasco J-720 spectropolarimeter equipped with a temperature control unit (Lauda, Königshofen, Germany). The secondary structures of the proteins were assessed using CDNN (Applied Photophysics) based on 33 reference spectra of soluble proteins. As result the normalized secondary structure predictions were presented. The melting temperatures of proteins are calculated based on thermal stability CD measurements at 222 nm.

2.4. Protein purification methods

2.4.1. Glutathione affinity chromatography

Glutathione-S-Transferase (GST) tagged fusion proteins can be purified using Glutathione Sepharose 4 Fast Flow (GS4FF) affinity chromatography (GE Healthcare). The binding capacity of GST on this column material is 10-12 mg/ml. For each liter of *E.coli* cell culture, therefore, 2 ml of this material is prepared on an Econo-Pac® Chromatography Columns (Biorad). The GS4FF beads are stored in 20% ethanol. This needs to be washed away with 2x5 ml GST wash buffer before the protein mixture can be added to the column. The proteins and beads are then incubated together for 1-12 h at 4°C to enable binding.

After proper binding took place, the column is washed 3x with GST wash buffer and eluted several times with 500 µl GST elution buffer. The collected fractions will be analyzed with SDS-PAGE to assess the quality of the eluted protein. Protein concentration is determined by the Bradford assay.

The column material can then be reused by cleaning with 5 ml 6 M Guanidiniumhydrochlorid, washing with 10 ml GST wash buffer and storing in 20% Ethanol at 4°C.

GST wash buffer (PBS pH 7.3)	GST elution buffer (pH 8.0)
140 mM NaCl	50 mM Tris-HCl
2.7 mM KCl	10 mM Glutathione
10 mM Na_2HPO_4	
1.8 mM K_2HPO_4	

Thrombin digestion of GST-fusion protein

The GST tag can be selectively cleaved off by the endopeptidase thrombin. This digestion can take place on column or after the GST-fusion is eluted from the column.

After protein elution 10 µl (1 U) thrombin protease (Amersham Pharmacia Biotech, UK) is incubated in 500 µl eluate for 16 h at 16-25°C.

For on column digestion, 100 µl (10 U) of thrombin is added directly to the GST column after the washing and incubated for 16 h at 16°C-25°C. 250 µl fractions will then be collected using GST wash buffer. Prior to size exclusion chromatography thrombin can be removed via a Benzamidine FF chromatography.

Batch scale analysis of GST-fusion protein

Expression of target protein can be checked in a small scale using this method. Bacteria pellets of 4 ml cultures under different expression conditions are resuspended in 300 µl lysis buffer (10 mM Na_3PO_4, 1 mM EDTA, 1 mM DTT, 1 mM DMSF, pH 7.5) and lysed via sonication. This lysis solution is then centrifuged at 18000 rpm for 30 min to sediment cell debris and unbroken cells. In the meanwhile, 30 µl of GSH sepharose column material for each sample is washed two times with GST wash buffer. 300 µl of the lysis supernatant is then added to each batch and incubated at 4°C for 1-12 h.

The batch samples are then washed 3x with GST wash buffer and eluted with 20 µl GST elution buffer. 15 µl of each elution solution is then separated with SDS-PAGE and stained with Coomassie blue. Expression of purified protein is then estimated from the intensity of the protein bands and from the measured protein concentration of the lysate.

2.4.2. Ni-NTA affinity chromatography

Recombinant His-tagged proteins can be purified using the Ni-NTA-agarose column (Qiagen). The binding capacity of this resin is up to 50 mg/ml. For each liter of *E.coli* culture, 1 ml of this material is used on a Econo-Pac® Chromatography Column (Biorad). The column is washed with 10 ml Ni-NTA wash buffer prior to addition of the protein mix. The column with the protein mixture can then be

rotated up to 1-12 h at 4°C, before it is thoroughly washed with 10 ml of Ni-NTA wash buffer. The bound His-tagged proteins are then eluted with Ni-NTA elution buffer containing 100 mM imidazol into different 500 µl fractions.

After this chromatography step imidazol needs to be removed via a PD10 column chromatography for storage, or the protein sample is collected and immediately loaded on a gel filtration column.

Ni-NTA wash buffer (pH 7.5)

50 mM Na_3PO_4

300 mM NaCl

20 mM Imidazol

PD10 buffer (pH 7.5)

10 mM Na_3PO_4

100 mM NaCl

1 mM EDTA

1 mM DTT

Ni-NTA elution buffer (pH 7.5)

50 mM Na_3PO_4

300 mM NaCl

100 mM Imidazol

For the use of the HisTrap FF 5 ml column (GE Healthcare, Germany), the wash buffer was 20 mM Tris-HCl, pH 8.0, 500 mM NaCl. The elution buffer was 20 mM Tris-HCl, pH 8.0, 500 mM NaCl, 500 mM Imidazol, which was added as a gradually up to 20% to elute His-tagged proteins from the column.

2.4.3. Size exclusion chromatography

The size exclusion chromatography, also called gel filtration, is usually the last step in the purification process of a protein, because it can really separate native protein from other aggregated or oxidized forms. For the separation of up to 2 ml of proteins between 10 kDa and 600 kDa the Superdex™ 200 10/300 GL is the column of choice. The Äkta Purifier UPC10 system is used to run this chromatography. Prior to sample injection, the column is washed and equilibrate with 2 column volume (CV) (50 ml) of gel filtration buffer (10 mM Tris-HCl, pH 8.0, 150 mM NaCl) . The elution takes place at the flow rate of 0.5 ml/min for 1 CV (25 ml) and fractions of 0.5 ml or 1 ml are collected. The molecular masses of the protein are determined by calibration of the column with FPLC protein standard (Biorad) consisting of thyroglobulin (670 kDa), γ-globulin (158 kDa), ovalbumin (44 kDa), myoglobin (17 kDa), and vitamin B12 (1.35 kDa).

For higher sample volumes the HiLoad 26/60 Superdex 200 pg column is used instead. The column volume of this column is 320 ml and the flow rate of elution is up to 5 ml/min. The optimal sample

volume is less than 13 ml and fraction size of 10 ml are collected. These columns are washed with 1 CV of degassed ddH_2O after use and stored in 1 CV of 20% ethanol.

2.5. DNA biochemical methods

2.5.1. Polymerase chain reaction

This method is commonly used to amplify a chosen DNA sequence *in vitro*. In the cloning process this method is used to amplify a certain DNA insert of choice or to analyze a clone insert. The basic components of a PCR are DNA template, specific primers for this template, heat-stable polymerase and dNTPs. Depending on the reaction, the $MgCl_2$ concentration needs to be adjusted as well as the heating cycle program.

PCR sample (50 µl total):

DNA Template 10-100 ng

Primers each 20 pmol

PCR Supermix by Invitrogen (Darmstadt) containing dNTPs each 200 µM, *Taq* DNA polymerase 1 U and buffer (20 mM Tris-HCl, pH 8.4, 50 mM KCl, 1.5 mM $MgCl_2$)

The thermo cycling condition is adjusted for different primer and contain a denaturation, an annealing and an elongation phase.

2.5.2. DNA purification

DNA solutions are purified from unwanted oligonucleotide primers, salt, enzymes, agarose gel, oil and detergent using Machery-Nagel NucleoSpin® Extract II columns according to their manual.

2.5.3. DNA concentration determination

The concentration of a DNA solution is determined by spectral photometric measurements at 260 nm using a 1:60 dilution of the DNA sample. The purity of the DNA probe can be deduced from the absorption at 280 nm. A pure DNA solution has an extinction ratio 260/280 of about 1.8.

2.5.4. Agarose gel electrophoresis

This method is used primarily to separate DNA fragments according to size. The running velocity is linear to the inverse proportional logarithm of the molecular mass. Plasmid DNA can exist in different forms: linear, coiled and supercoiled. According to their compact structures, coiled and supercoiled structures tend to move faster in the gel. Therefore, prior to gel separation plasmid DNA should be linearized with a specific restriction enzyme.

The electrophoresis separation takes place in 0.8-1.5% agarose gels in a horizontal position. Agarose powder is suspended in TAE buffer (40 mM Tris, 5 mM sodium acetate, 1 mM EDTA, pH 7.9) and

heated in a microwave for ca. 3 min until the gel is completely dissolved. The gel will then be left to cool down and polymerize in a gel chamber. DNA samples are then prepared with 6xDNA sample buffer (30% glycerin, 0.25% bromophenol blue). Depending on the sample pocket 10-50 µl of a sample can be placed in the gel. 5 µl of 1 kb DNA standard ladder (Gibco-BRL, USA) is used to compare the DNA size. The electrophoresis then takes place in 1xTAE buffer under a constant field of 0.5 V/cm^2 gel surface. The agarose gel is than soaked in ethidium bromide solution (0.5 g/l ethidium bromide in TAE-buffer) for 10 min and DNA bands are made visible under UV light at 254 nm.

2.5.5. DNA digestion with restriction endonuclease

Restriction endonucleases are enzymes that cut double-stranded DNA at specific nucleotide palindromic sequences (usually 4-8 bp) known as restriction sites. They create highly specific DNA sticky or blunt ends useful in cloning of certain DNA fragments. The reactions are carried out with 1-40 µg DNA and 1-40 U restriction enzymes in the appropriate buffer as given by the manufacturer. Depending on the activity of the enzymes the digestion is completed within hours at 37°C.

2.5.6. DNA ligation

The reconnection of DNA fragments via a ligase enzyme is called ligation. Usually this method is used to clone a certain insert, the DNA gene of choice, in an expression vector. The ligase forms a phosphodiester bond with adjacent 3'-hydroxyl and 5'-phosphate group. When insert and vector are digested with the same restriction enzymes (e.g. *Xho*I and *Nde*I), they may ligate together and form a new fusion DNA construct. This procedure is most successful when the molar ratio of insert to vector is at least 3:1 and when 1 µl of T4- DNA ligase (10 U, Fermentas) is used at 16°C overnight.

Ligation reaction (20 µl total):

1 µl T4-DNA-Ligase (10 U)

2 µl 10xligation buffer

1 µl Vector (100 ng)

5 µl DNA insert (500 ng)

11 µl ddH_2O

After the ligation is completed, usually 10 µl of this mixture is used for *E.coli* transformation.

2.5.7. Production of PCR blunt plasmids

Blunt vectors (Zero Blunt® PCR vectors) are used to clone blunt DNA fragments mostly PCR products into a bacterial plasmid. This is a way to preserve PCR products and to amplify these PCR fragments in *E.coli*. The pCR®-Blunt vector contains the lethal *E.coli* ccdB gene fused to the C-terminus of LacZα. Usually *E.coli* transformed with this vector are killed by the ccdB- LacZα fusion protein when plated.

The ligation of a blunt fragment disrupts the formation of this fusion gene, allowing transformed cells with insert to survive on Kanamycin selective plates.

According to the manual protocol 1 µl pCR®-Blunt vector is used with up to 5 µl of purified PCR products. 1 µl 10x ligation buffer (+ATP), 1 µl T4-DNA-ligase and ddH_2O are added to a total volume of 10 µl. The ligation reaction takes place at 16°C overnight.

2.5.8. Sequencing

All plasmid constructs used in this work are sequenced based on the Sanger dideoxy method according to the manufacturer's instructions of Thermo Sequenase Primer Cycle Sequencing Kit (Amersham Biosciences). A typical protocol involves the addition of 1 µl primer solution (2 pM) to up to 1.3 µg template DNA diluted in 12 µl ddH_2O. From this stock solution (total 13 µl) 3 µl is transferred into 4 tubes containing 3 µl of each sequencing reagent A, C, G or T. Beside a mixture of dNTPs (Deoxyribonucleotide) each of the reagents contains the respective ddATP, ddCTP, ddGTP, ddTTP (Dideoxyribonucleotide) which cause the interruption of polymerization at those sites.

In general the thermo cycling condition is as follow.

Initial step:	Denaturation	3 min 94°C
24 Cycles:	Denaturation	20 s 94°C
	Annealing	20 s 45-60°C
	Elongation	20 s 72°C

The reaction is stopped by adding 5 µl of stop solution and run for another 3 min. The products are then separated on a 6% acrylamide gel and analyzed in an automatic sequence analyzer (Licor 4000, MWG-Biotech)

Sequencing primers tagged with 3'-IRD700 or IRD800:

GST Seq Fw	5' - GCAAGCTACCTGAAATGCTG
GST Seq Rv	5' - GTATCACGAGGCCCT
His Seq Fw	5' - CCCAAGGGGTTATGCTAGTT
His Seq Rv	5' - ATACGACTCACTATAGGG

The sequencing experiments were carried out with the help of Katrin Büttner (Prof. B. Wittig's lab, FU Berlin).

2.5.9. Production of point mutations

For the production of point mutations the "Quikchange™ Site-Directed-Mutagenesis Kit" of Strategene (USA) is used. Defined primers as well as their reverse complement counterpart are used

as listed below for certain mutants. As template the pET28a-MNK construct was used. Temperature cycling is performed with PfuTurbo DNA polymerase (Strategene). Parental template DNA is then digested with *Dpn*I. The synthesized plasmids, containing the desired mutation, are transformed into supercompetent InvαF' *E.coli* cells (Invitrogen).

Mutagenesis primers for GNE point mutations (only forward primer shown):

D517A 5'- CCCTGTGTGGGTAGACAATGCTGGCAACTGTGCTGCCC

D517N 5'- CCCTGTGTGGGTAGACAATAATGGCAACTGTGCTGCCC

D517 mutants were kindly produced by Jacobo Martinez (Prof. W. Saenger's lab, FU Berlin).

2.6. Sialic acid analysis

2.6.1. Periodate-resorcinol assay

Based on Jourdian et al (1971)[107], this method is most frequently used to determine the sialic concentration of a solution.

A cell pellet, containing at least $2x10^6$ cells, is washed well with PBS to remove residual sialic acid in the medium. The pellet is then resuspended in 250 µl PBS. This suspension is then shock frozen with liquid nitrogen and thawed at 37°C for three times to ensure cell lysis. A sialic acid standard curve of 0, 50, 10, 150, 200, 250 µM in 250 µl volume is prepared together with the 250 µl cell samples. 5 µl of the periodic acid solution (400 mM) is added to each sample and the standard solution. The samples are then incubated 10-90 min on ice. If the concentration of conjugated sialic acid alone needs to be assessed, the excess of free sialic acid can be degraded by periodic acid by incubating at 37°C for 90 min.

Subsequently, 500 µl of freshly prepared resorcinol-Cu-solution will be added to each tube and mixed shortly. The samples are then boiled at 99°C for 15 min, left to cool down and extracted with *tert*-butyl alcohol. The sample will be vortexted and centrifuged for 5 min to sediment cell debris. The supernatant is poured into a cuvette and measured at 630 nm. The sialic acid concentrations of the samples are calculated with the sialic acid standard curve calibration.

Resorcinol-Cu-solution:

6% Resorcinol

2.5 mM $CuSO_4$

44% HCl

2.6.2. FACS analysis

Up to 1x10^6 cells are washed with PBS and then incubated in 100 µl of PBS containing 20 µg/ml FITC-labeled *Limax flavus* agglutinin (LFA) for 1 h at 4°C in the dark. Subsequently, cells are washed with PBS, resuspended in 500 µl PBS and analyzed by flow cytometry at 530 nm (Becton Dickinson FACScan).

2.6.3. Sialic acid glycan staining

Nitrocellulose membrane with the protein of target (e.g. GAT1-GFP) will be stained with MAA (DIG Glycan Differentiation Kit, Roche) to detect 2, 3-linked sialic acid. This specific lectin is conjugated with digoxigenin for immunological detection.

The procedure is described in details in the manufacturer protocol. In brief, the membrane is blocked in the provided blocking solution for 30 min at room temperature, then washed twice with TBS and once with Buffer 1. The membrane is then incubated in MAA solution (50 µl in 10 ml Buffer) at room temperature for 1 h and then washed 3x10 min with TBS. Subsequently, the anti-Digoxigenin-AP solution (10 µl in 10 ml TBS) is added to the membrane and incubated for 1 h at RT. Digoxigenin-AP is then washed away and the blot is than stained with freshly prepared NBT/BCIP solution (200 µl in 10 ml Buffer 2). Once bands are visible, the reaction can be stopped by rinsing the membrane with water several times. The sialic acid amount on the target protein can be quantified using Quantity One Software by Biorad.

TBS (p.H 7.5)	Buffer 1 (pH7.5)	Buffer 2 (pH7.5)
50 mM Tris-HCl	TBS	100 mM Tris-HCl
150 mM NaCl	1 mM $MgCl_2$	100 mM NaCl
	1 mM $MnCl_2$	50 mM $MgCl_2$
	1 mM $CaCl_2$	

2.7. Enzyme activity analysis

2.7.1. Coupled optical UDP-GlcNAc-2-epimerase assay by Warburg

This assay couples three enzymatic reactions leading to the oxidation of NADH, which can be photometrically quantified at 340 nm.

$$UDP - GlcNAc \xrightarrow{GNE} ManNAc + UDP$$

$$UDP + PEP \xrightarrow{PK} UTP + Pyruvate$$

$$Pyruvate + NADH \xrightarrow{LDH} Lactate + NAD^+$$

In a total reaction volume of 200 µl, 80 µl of the sample including GNE and inhibitors in PD10 buffer is preincubated for 20 min at 37°C. Then a 120 µl mixture containing 45 µl $MgCl_2$ (50 mM), 10 µl freshly prepared PEP (100 mM), 10 µl freshly prepared NADH (15 mM), 2.5 µl UDP-GlcNAc (100 mM) and 2 µl LDH/PK mix (2 U) in 200 mM sodium phosphate buffer (pH 7,5) is added. After the whole mixture is incubated at 37°C for 20 min, 800 µl EDTA (10 mM) is added to stop the reaction. The extinction is measured at 340 nm.

2.7.2. UDP-GlcNAc-2-epimerase activity assay via Morgan-Elson

This assay is based on the detection of produced ManNAc by formation of a stable chromogen of ManNAc with DMAB [108]. 100 µl of the GNE sample in PD10 buffer is mixed with 45 µl 50 mM $MgCl_2$ and 2.5 µl 100 mM UDP-GlcNAc followed by incubation for 20 min at 37°C. The reaction is stopped by heating the sample for 1 min at 99°C. The denatured proteins are separated via centrifugation at 13000 rpm for 2 min. 150 µl of the supernatant is added to 30 µl H_3BO_3 (800 mM, pH 9.1 in KOH) and incubated for 3 min at 99°C. Subsequently, 800 µl of DMBA solution (1% (w/v) DMAB, 1.25% (v/v) 10 m HCl in 100% acetic acid) is added and incubated for 30 min at 37°. The extinction is detectable at 578 nm.

2.7.3. UDP-GlcNAc-2-epimerase activity test via radiometric detection

In a reaction tube containing 100 µl GNE sample, 45 µl 200 mM sodium phosphate buffer (pH 7,5), 45 µl 50 mM $MgCl_2$ and 8 µl 10mM UDP-GlcNAc, 25nCi of ^{14}C-UDP-GlcNAc, is added and incubated for 30 min at 37°C. The reaction is then stopped with 350 µl EtOH (100%). 200 µl of this solution is used for paper chromatography (see below). The R_f for UDP-GlcNAc is 0.08 for ManNAc 0.55.

2.7.4. Coupled optical ManNAc kinase assay by Warburg

Similarly to the epimerase activity assay, the kinase activity is coupled with the oxidation of NADH in a multistep enzymatic reaction.

$$ManNAc + ATP \xrightarrow{GNE} ManNAc-6-P + ADP$$

$$ADP + PEP \xrightarrow{PK} ATP + Pyruvate$$

$$Pyruvate + NADH \xrightarrow{LDH} Lactate + NAD^+$$

In a 200 µl reaction volume, 80 µl GNE/MNK sample in gel filtration buffer with or without inhibitors is added to 120 µl of reaction solution containing 68 µl kinase buffer (200 mM Tris.HCl, 65 mM $MgCl_2$, pH 8.1), 20 µl ATP (100 mM), 10 µl ManNAc (100 µM), 10 µl PEP (10 mM), 10 µl NADH (15 mM) and 2 µl PK/LH mix (2 U). The sample is then incubated for 30 min at 37°C and stopped with 800 µl EDTA (10 mM). The extinction of NADH is then measured at 340 nm.

2.7.5. ManNAc kinase activity test via radiometric detection

The reaction mix containing 100 µl GNE/MNK diluted sample, 65 µl kinase buffer, 40 µl ATP (100 mM), 8 µl ManNAc and 50nCi ^{14}C-ManNAc, is incubated for 30 min at 37°C and stopped with 350 µl EtOH. 200 µl of the sample is used for paper chromatography. The R_f for ManNAc-6-phosphate is 0.11 for ManNAc 0.55.

2.7.6. Paper chromatography

Samples are added on a 2x48 cm Whatman 3 mm Chr-Chromatography paper and separated with 70% (v/v) 1-propanol in sodium acetate (100 mM, pH 5.0) for 15-20 h. The ^{14}C radioactivity (cpm) of the dried 2x4 cm Whatman pieces is measured via the 1900TR Liquid scintillation detector (Packard) with 6 ml Ultima X Gold LSC cocktail (Packard, Perkin Elmer).

2.7.7. Kinetic measurement

Enzyme activity for is measured at different substrate concentrations. The result is graphed on a double reciprocal plot (Lineweaver-burk plot). Reliable K_m and v_{max} values were determined by combining average results of 4 independent measurements.

2.7.8. Inhibition assays

Potential inhibitors in different concentrations are incubated with the enzyme and activity is measured as described. The inhibitory effects of those substances are expressed as reduced enzyme activity compared to control without inhibitor. Self-absorption of the inhibitor substrates at 340 nm has been deducted.

2.7.9. Preparation of 6-O-Ac-ManNAc

ManNAc (442 mg, 2 mmol) was dissolved in pyridine (10 ml). *O*-Acetylpropanon-oxime (207 mg, 1.8 mmol), 4 Å-molecular sieves (100 mg) and lipase AY30 (1.1 g) were added, and the suspension was stirred vigorously at 50 °C. After 5 days additional lipase AY30 (1.1 g) was added and the suspension stirred for additional two days at the same temperature. The lipase was removed by filtration and the precipitate was washed with MeOH (10 ml). After addition of toluene (15 ml) the solvents were removed by a rotary evaporator, this process was repeated with another 10 ml of toluene and the resulting crude product was purified by flash chromatography (silica gel, EtOAc:MeOH:H2O = 25:4:1) to yield 6-*O*-acetyl ManNAc (18 mg, 4%). This preparation was kindkly conducted by Dr. Reinhold Zimmer (Prof. H. Reißig's lab, FU Berlin).

2.8. Mammalian cell culture

Sterile media and equipments are essential for mammalian cell culture. Solutions and media are sterilized either by autoclaving at 121°C for 20 min or sterile filtration through a 0.22 µm filter.

2.8.1. Cell culture medium

DMEM

500 ml DMEM (PAN Biotech)

5 ml L-Glutamine (200 mM) (PAN Biotech)

5 ml Sodium pyruvate (100 mM) (PAN Biotech)

5 ml Penicillin/Streptomycin (10000 U/10 mg)/ml (PAN Biotech)

50 ml FCS (Perbio, Thermo Scientific)

RPMI

500 ml RPMI (PAN Biotech)

5 ml L-Glutamine (200 mM)

5 ml Sodium pyruvate (100 mM)

5 ml Penicillin/Streptomycin (10000 U/10 mg)/ml

50 ml FCS

α-MEM Eagle

500 ml α-MEM (Lonza, Verviers, Belgium)

5 ml L-Glutamine (200 mM)

5 ml Ribonucleosides

5 ml Penicillin/Streptomycin (10000 U/10 mg)/ml

50 ml FCS

2.8.2. Subculture of monolayer cell lines

Adherent cell lines are usually grown in a 100x20 mm Petri dish (BD Biosciences, Heidelberg) to a confluence of 80-100% before they are split into a new vessel. Depending on the cell lines 0.1% EDTA or Trypsin/EDTA 0.05/0.01% in PBS are used to detach the cells from the cell surface. 10^4-10^5 cells are then plated on a new Petri dish and evenly distributed on the dish surface with 10 ml of growth medium. Adherent cell lines are kept at 37°C in a 5% CO_2 atmosphere.

2.8.3. Subculture of suspension cell lines

Under normal conditions 10 ml of cell suspension is cultured in a 25 cm^2 flask (Corning Incorporated, Acton, USA) at 37°C in a 5% CO_2 atmosphere. According to the growth rates of the cell lines, cell suspensions are diluted in fresh growth medium each 3 to 4 days. The optimal subculture density is also cell line dependent and ranges between $1x10^5$ to $5x10^5$ cells/ml.

2.8.4. Freezing cells for storage

Well growing cells of one 10 cm Petri dish (about 80% confluence) or one 25 cm^2 flask are collected and stored in 10% DMSO/FCS (v/v) at –175°C in cryogenic vials (Nalgene).

Table 2.1. Cell culture conditions

Cell line	Cell type	ATCC®-No.	Growth medium	Dilution solution
CHO K1	Chinese Hamster Ovary	CCL-61	α-MEM	EDTA/PBS
HEK 293	Human Embryonic Kidney	CRL-1573	DMEM	EDTA/PBS
A-Zellen	Murine adenocarcinoma	N.A	DMEM	EDTA/PBS
Hekl	Human primary fibroblasts	N.A	DMEM	EDTA/PBS
MELA 2	Human Melanoma	N.A	DMEM	EDTA/PBS
SAOS 2	Human Osteosarcoma	HTB-85	DMEM	Trypsin/EDTA
LN 405	Human Astrocytoma	N.A	DMEM	Trypsin/EDTA
PANC-1	Human Pancreatic Carcinoma	CRL-1469	DMEM	Trypsin/EDTA
MCF 7	Human Breast Adenocarcinoma	HTB-22	RPMI	EDTA/PBS
HL 60	Human Promeolytic Leukemia	CCL-240	RPMI	Suspension
Jurkat	Human T-Lymphoma	TIB-152	RPMI	Suspension
U266	Human Myeloma	TIB-196	RPMI	Suspension
Raji	Burkitt's Lymphoma	CCL-86	RPMI	Suspension

The LN405 cell line was provided by the German Collection of Microorganisms and cell cultures (Braunschweig, Germany). A-Zellen were kindly provided by Dr. A. Klein (Charité Berlin). Hekl cells were provided by Dr. M. Kontou (Charité Berlin).

2.8.5. Cell treatment with potential GNE inhibitors

Substrates are diluted and sterile filtrated according to the concentrations needed. Cells are plate with an initial concentration of 10000 cells/ml to a total volume of 9.5 ml. After 2 h, when cells completely adhere, 500 µl of the substrate stock solution in PBS is added to the medium. The concentration of the stock solution is prepared to be 10x the final concentration in the medium.

2.8.6. Proliferation assay with AlamarBlue©

Chemical oxidation as a result cell proliferation can be measured with this assay. AlamarBlue© consists of an indicator dye, which changes color and fluorescence according to the oxidation reduction state of a solution. 180 µl of cell suspension (usually 10^4 cells/ml) is preincubated for 24 h

in a 96-well microplate and treated with 20 µl of sterile substrates for the indicated time. Subsequently, 20 µl of the AlamarBlue© solution is added, incubated for another 6 h and measured at 570 nm and 620 nm. As blanks, the same solutions are measured prior AlamarBlue© addition. The proliferation rates are calculated according to the method provided by AbD Serotec (Oxford, UK).

2.8.7. Cell counting assay

Cells are grown in standard medium for the time indicated; usually 3 days. All the cells are then detached and collected in PBS. About 50 µl of this suspension is then diluted in trypan blue dye to visualize viable and non-viable cells. Using a hemacytometer, a cell counting chamber, the number of cells is then manually counted under the microscope. Since each square is 0.1 mm^3 or 10^{-4} cm^3 (=10^{-4} ml), one cell count per square is equal to 10^4 cells per ml in the diluted solution.

2.8.8. GABA uptake assay

To determine the GABA uptake activity of GAT1 transfected cells, 180 µl of cell suspension (usually 10^4 cells/ml) is preincubated for at least 2 h in a 96-well microplate and treated with 20 µl of sterile substrates for the indicated time (usually 3 days). After cell are washed 2 times with GABA wash buffer (128 mM NaCl, 5.2 mM KCl, 2.1 mM $CaCl_2$, 2.9 mM $MgSO_4$, 5 mM dextrose, 10 mM Hepes, pH 7.4). Then 200 µl of ^{3}H-GABA wash buffer ($3.7x10^4$Bq) is added to the cells and incubated for 15 min at 37°C. The ^{3}H-GABA solution will then be removed and the cells washed 2x with 200 µl cold wash buffer. Cells are than lysed in 100 µl of 0.5% SDS (w/v) solution for at least 1 h at 4°C. 20 µl of the lysate is added to 6 ml of Ultima X Gold LSC cocktail (Packard, Perkin Elmer) and measured for 5 min in 1900TR Liquid scintillation detector (Packard). The other part of the lysate is used to determine the protein concentration via the BCA assay. All measurements are done in duplicate at least three times. Difference in the specific uptake activity is compared to control samples (100% uptake).

2.9. Insect cell culture

2.9.1. Sf9 cell culture

Sf9 cells from Invitrogen are cultured at 27°C as suspension cultures at 115 rpm (Multitron shaker, HAT-Infors, Switzerland). They can be stored in 90% FCS and 10% DMSO under liquid nitrogen for longer use. When needed frozen cells are thawed at RT and cultured in fresh medium.

Two times a week cells are counted and diluted to $2x10^6$ cells/ml with fresh medium. For protein production Sf9 cells are accustomed to serum free Sf900 medium.

Sf9-Medium:	Sf900-Medium: serum free Sf9 medium
1 l SF900 II medium (Invitrogen)	1 l SF900 II medium (Invitrogen)
10 ml L-Glutamine (200 mM)	10 ml L-Glutamine (200 mM)
100 ml FCS	

2.9.2. Virus amplification

In order to reproduce virus titer of a certain bacmid recombinant virus, 100 ml of Sf9 cell suspension ($0.5x10^6$ cells/ml) is infected with 5 ml of the initial virus stock and incubate at 27°C for 5 days. The supernatants is then harvested via centrifugation at 2000 rpm for 5 min and stored at 4°C.

2.9.3. Protein expression

Depend on the amount of cells needed for protein production, insect cells are cultured in Sf900 medium to $2x10^6$ cells/ml and transfected with MOI 1 of the virus titer. The transfected cells are then incubated at 27°C and harvested after 48 h via centrifugation at 2000 rpm for 5 min.

2.9.4. His-GNE expression

For the expression of the whole His-GNE, hGNE1 cDNA is cloned into the expression vector pFastBacHTa, The vectors are then transformed into *E.coli* DH10 BAC cells. Bacmid DNA is generated by homologous recombination in the DH10 cells, isolated and transfected into Sf9 cells. Bacmid virus amplification and protein expression thereafter depend on the harvesting conditions.

2.10. Bacteria cell culture

Bacteria (e.g. *Escherichia coli*) are usually cultured in a 37°C shaking incubator (225 rpm) in selective media, mostly LB-medium. Bacteria cultures can be stored at –80°C with 20% glycerin for many years. Stored cells can be defrozen and resuspended in medium for cultivation.

LB-Medium
10 g/l Peptone
5 g/l Yeast extract
10 g/l NaCl (as low salt only 5 g/l NaCl)
15 g/l Agar (only for LB plates)

SOC-Medium
20 g/l Peptone
5 g/l Yeast extract
0.5 g/l NaCl
4 g/l $MgCl_2$
0.186 g/l KCl
3.6 g/l Glucose

SOB-Medium
20 g/l Peptone
5 g/l Yeast extract
0.6 g/l NaCl
0.2 g/l KCl
10 mM $MgCl_2$
10 mM $MgSO_4$
Mg^{2+} solutions are added after autoclaving, before use.

Selective medium
LB-Medium or LB Agar plates
+ Ampicillin (50 mg/l) or
+ Chloramphenicol (25 mg/l) or
+ Kanamycin (50 mg/l) or

2.10.1. Preparation of competent *Escherichia coli*

Competent cells are cells more capable of taking up free DNA fragments. They allow desired plasmids to be incorporated and cells transformation to take place. Competent cells have permeable membranes, which can be generated via different methods. The method of choice in this lab is the exposure to a cold 100 mM $CaCl_2$ according to Dagert und Ehrlich 1979[109]. One culture of *E.coli* cells (Top10, BL21 RIL, InvαF) is cultured overnight in SOB medium. 2 ml of this culture is then added to 100 ml of SOB and further cultured until the suspension reaches an OD_{600} of 0.2-0.3. Cells are than centrifuged down at 4000 rpm for 10 min, resuspended in 20 ml cold $CaCl_2$, and put on ice for 30 min. Subsequently, *E.coli* cells are centrifuged down again and put in 1 ml of cold $CaCl_2$ for at least 1 h. Finally, these cells can be directly used for transformation or stored at –80°C with 20% glycerin.

2.10.2. Transformation of Plasmid-DNA in *Escherichia coli*

Transformation is the process of changing a bacteria's DNA by inserting a foreign DNA plasmid into the cell. To do so, 10 µl of the ligation mixture or ca. 100 ng plasmid DNA is added to 100 µl of competent cells and incubated for 30 min on ice. Depending on the cell lines, these cells are then heat-shocked for exactly 25-45 s in 42°C water bath and cooled down again for 2 min. Subsequently, 250 µl of pre-warmed SOC medium is added to the mixture and cells are left to recover in a shaking incubator for at least 1 h at 37°C. 50-200 µl of this culture is plated on pre-warmed LB Agar plates with selective medium and incubated overnight at 37°C.

2.10.3. Overnight culture production

An overnight culture is usually produced to amplify a certain clone for further applications. A clone of choice on the agar plate is picked and grown in selective medium at 37°C overnight till saturation. The overnight culture can then be used to prepare protein expression cultures or to isolate plasmid DNA.

2.10.4. Plasmid amplification in *Escherichia coli*

For plasmid amplification, plasmid constructs or vector are transformed into Top10 *E.coli* cells. Top10 *E.coli* strain has a high transformation efficiency (up to $1x10^9$ cfu/µg) and is ideal for cloning and plasmid propagation. Due to the intrinsic expression of Endonuclease I, non-specific DNA is digested for optimized downstream application of the target plasmid. The transformed Top10 cell line is then cultured overnight and pDNA will be isolated.

2.10.5. Plasmid DNA preparation

All plasmid purification methods are adapted from the alkaline extraction method of Birnhoim and Doly (1979)[110]. In the lab the buffer system of Machery-Nagel NucleoBond® Xtra Kit is used.

For a mini plasmid preparation (20-30 µg), 2 ml of *E.coli* overnight culture is collected and centrifuged for 10 min at 7000 rpm. The bacteria pellet is then completely resuspended in 200 µl RES buffer, where 100 mg/l RNAse is added. Subsequently, 200 µl of LYS buffer is added to the suspension and gently mixed by inverting the tubes 5 times. This alkaline NaOH/SDS solution lyses the cell and releases the plasmid DNA. The addition of 200 µl NEU buffer (acetic acid) neutralizes this solution and due to the high salt concentration in this solution, proteins and chromosomal DNA will be precipitated. This process takes place for 15 min on ice. The precipitation is then separated from the solution in two centrifugation steps, each for 15 min at 13000 rpm. After this, plasmid DNA is precipitated via 450 µl 2-propanol at –20°C for 30 min and collected in the pellet after centrifugation of 15 min at 13000 rpm. To desalt the DNA collection, the pellet is washed in 500 µl of ice-cold 70% EtOH. The precipitate is subsequently dried and dissolved in 20-50 µl of ddH_2O or TE buffer (10 mM Tris.HCl, pH 7.5, 1 mM EDTA). For storage samples should be stored in TE buffer at –20°C.

For the extraction of higher DNA amount, 50-200 ml overnight cultures are produced. The isolation is via the same principle with a Qiagen Maxi-preparation kit according to their user manual.

2.10.6. Expression of recombinant proteins in *Escherichia coli*

The overexpression of recombinant proteins for pGex-4T (Amersham Biosciences) and pET-28a (Novagen) constructs are based on the producer's manual. BL21 Star™ (DE3) pLysS and BL21 CodonPlus (DE3) RIL strains are used for protein expression. In general, clones from overnight cultures are seeded in a ratio of 1:100 in selection medium, grown at 37°C to an OD_{600} of 0.3-0.5 and

induced for protein expression with 0.3-1 mM of IPTG. The *E.coli* is then left to produce proteins, which will be harvest after an optimal incubation time.

2.11. Crystallization

Purified His-MNK were initially used for crystallization screening and subsequently used to optimize crystallization conditions. Purified MNK and ManNAc were gently mixed and incubated for 30 min on ice. The final mixture containing 15 mg/ml MNK and 2 mM ManNAc was used for further experiments. The crystallization experiments were conducted with Jacobo Martinez under the supervision of Dr. Sebastien Moniot in Prof. W. Saenger's and Prof. M. Wahl's lab (FU Berlin).

2.11.1. Crystallization screening

Crystallization screens I and II from Hampton Research (USA), JCSG from Jena Bioscience and PACT from Qiagen are used to look for initial crystallization conditions. The drops are set up by mixing equal volumes (1 µl) of protein and screen reservoir solution at 18 °C. Flat-bottomed multi-subwell plates (Greiner) are used to set up the sitting drop vapor-diffusion experiments that are incubated at 18 °C.

2.11.2. Crystal soaking

The soaking solutions are prepared by mixing 0.1 M sodium cacodylate pH 6.5, 50% PEG 300 and 20 mM ADP, ATP, or AMPPCP. Since calcium acetate addition resulted in precipitation, this was not used. The mother liquor is stepwise replaced by the soaking solution and the crystals are incubated for at least 30 minutes.

2.11.3. X-ray data collection and processing

The X-ray diffraction data are collected from single crystals at beam line BL 14.2 at BESSY, Berlin at 100°K and 0.918 Å wavelength. The data are integrated, reduced and scaled using XDS (Kabsch, 1993). The structures are solved by molecular replacement using MOLREP of the CCP4 program suite [111, 112]. A single monomer structure of the apo-form from MNK with pdb code 3EO3 is used as a search model [113]. Only one kinase monomer could be located in the asymmetric unit. This first solution is subjected to rigid-body refinement, followed by iterative cycles of TLS and restrained-maximum likelihood refinement, including isotropic temperature factor adjustment with REFMAC [114] and by manual rebuilding using COOT [115]. During this process, 5% randomly selected reflections have been used to calculate R_{free} to monitor bias during model building and refinement. Water molecules were added using COOT. Validation of the model is carried out using MOLPROBITY.

The refined structure of the MNK/ManNAc was used as a search model to solve the structures of the other two complexes (MNK/ManNAc/ADP and MNK/ManNAc/ATP).

3. Results

3.1. ManNAc kinase protein purification

For biochemical experiments, like *in vitro* inhibitory assays, as well as crystallizations attempts, pure MNK is required in mg amount. Therefore, the first step of this work is to establish a method to purify soluble native human MNK. The expression system of choice was *E.coli* since this is the most well-established and cost effective method to receive larger quantity of pure recombinant cytosolic proteins.

3.1.1. GST-MNK plasmid design and cloning

To express the MNK with a GST-tag at the N-terminus, expression vector, pGEX-4T2, was chosen. The pGEX vector is optimized for inducible GST-tagged recombinant protein expression in *E.coli*. It has an Ampicillin resistance gene and a thrombin cleavage site between the GST and the target protein. The elution conditions for GST-tagged fusion proteins are mild, thus minimizing the effects on antigenicity and reduced activity of target proteins. A schematic display of the GST-MNK fusion protein is given in figure 3.1.1.

Figure 3.1.1: Schematic display of recombinant GST-MNK fusion protein

Since the MNK domain is in the C-terminus of the GNE gene (Uniprot code Q9Y223). Primers were designed to excise different fragments of this domain at three different fragment lengths and to insert two specific endonuclease sites *Eco*RI/*Sal*I (Table 3.1.1). The PCR product was initially cloned into pCR Blunt vector and subsequently cloned into pGex-4T2 vector to express GST-MNK fusion protein. Having multiple constructs and protein lengths is advantageous for subsequent expression and crystallization attempts.

Table 3.1.1: MNK cloning primers for GST-fusion construct
Numbers in the primer name indicate the starting position of the amino acid on the GNE

Primer name	Sequence (5' -> 3')	Tm [°C]
For MNK 367	CAACTT G'AATTC TTCCAAGGATTTTGAAG (29)	61.0
For MNK 387	CAACTT G'AATTC AATTCTGCTTTCCTCC (28)	62.2
For MNK 407	GTAGTAG'AATTC CTCTAAGTGCCT TG (26)	61.6
Rev MNK 722	TATTAT G'TCGAC GGGTAGATCCTGCGTGC (29)	68.1

A-*Eco*RI site, A-*Sal*I, A-GNE sequence

As experimental procedure, the pGEX-4T2 vector was first amplified in Top10 *E.coli* according to the described method. The amplified vector was then double digested with *Eco*RI and *Sal*I overnight and purified via gel extraction. The goal was to have 10 µl (100 ng/µl) of completely digested and linearized pGEX-4T2 vectors for ligation. Since the vector is digested at two ends, the directionality of the insert is determined and re-ligation is minimal. Therefore, the linearized DNA does not need to be dephosphorylated.

PCR was performed with 30 cycles of 30 s 94°C denaturation, 30 s 55°C annealing and 150 s 68°C elongation using one forward primer (For MNK 367, For MNK 387, For MNK 407) together with the indicated reverse primer (Rev MNK 722). As template, human GNE1 DNA in a pUMVC3 vector (pUMVC3-hGNE1) was used (kindly provided by Prof. Hinderlich's lab). Expected MNK fragments after PCR are 1100 bp, 1040 bp and 980 bp (Figure 3.1.2A). At the 5'-terminus an *Eco*RI restriction site and in the 3'-terminus a *Sal*I restriction site were introduced. The GST-tag was introduced in the N-terminus. The stop codon of the vector after the multiple cloning site was used for this fusion protein. Therefore, the GST-MNK has an additional tail of 8 amino acids (PSTRAAAS) at the C-terminus (Figure 3.1.1). The whole GST-MNK fusion construct is therefore 593 aa, 574 aa, 554 aa long respectively. After thrombin digestion the MNK fragments would be 369 aa, 350 aa and 330 aa respectively

The PCR products were distinct DNA bands at the expected sizes around 1000 bp. No other unspecific bands were visible under this set up. At 10 pmol primers and 10 ng template DNA (pUMVC3-hGNE1) PCR product yield was highest (Figure 3.1.2B).

In order to easily amplify the PCR products, these fragments were isolated from the gel and cloned into a pCR Blunt vector (Figure 3.1.2C). Double digestion of the isolated plasmids of selected clones with *Eco*RI/*Sal*I demonstrated that the two endonuclease sites were correctly inserted. For all three fragments, the desired MNK insert at about 1000 bp could be obtained in the positive clones.

Both pGex-4T2 vector and pCR Blunt MNK plasmids (pCR-M1-3, pCR-M2-2, pCR-M3-6) were double digested with *Eco*RI/*Sal*I overnight. The MNK inserts were isolated and ligated with the linearized pGex-4T2 vector. After double digestion of selected clone plasmids with *Eco*RI/*Sal*I, a fragment about 1000 bp could be observed, indicating that all three MNK fragments were successfully cloned into pGex-4T2 vector (Figure 3.1.2D). The constructs were confirmed by sequencing to be correctly ligated in the right frame and orientation.

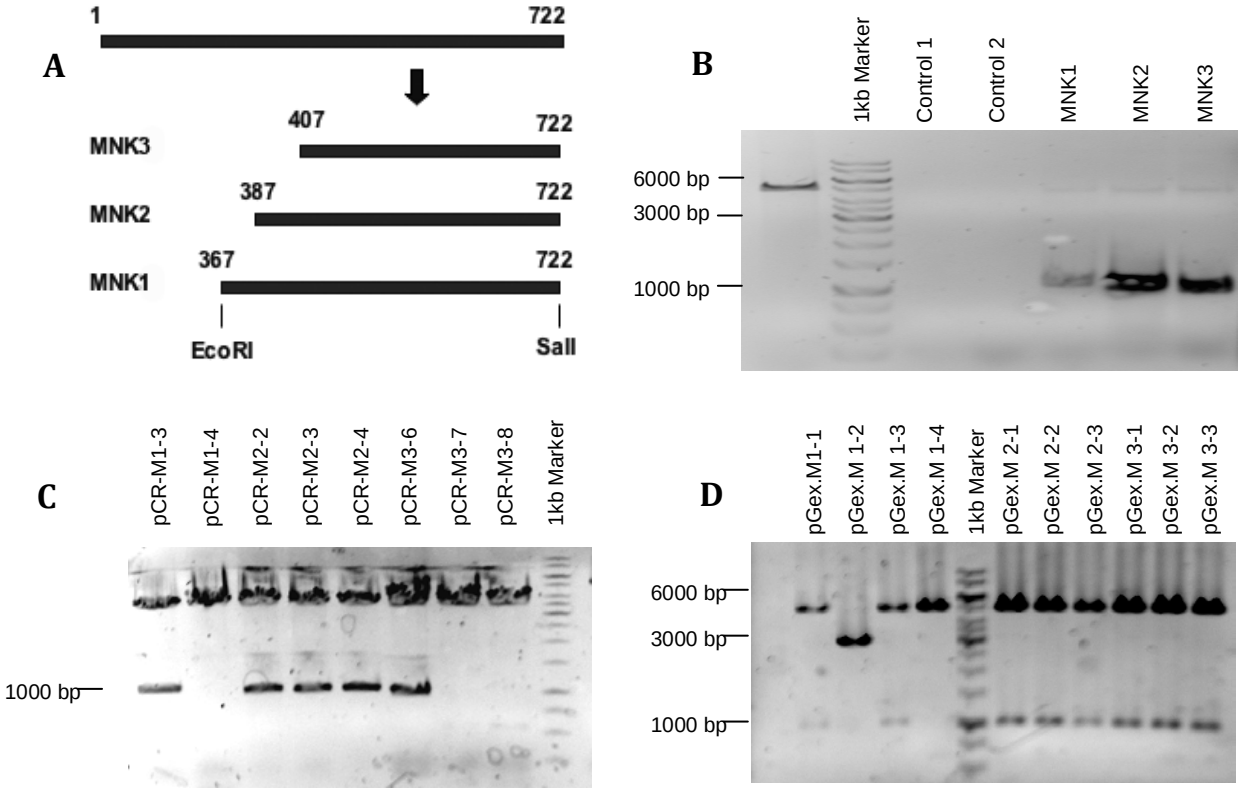

Figure 3.1.2: Cloning of the hMNK domain in pGex-4T2 vector
A. Schematic display of the different MNK protein fragments produced by the given primer pairs.
B. 1% Agarose gel of MNK PCR products, PGex-4T2 dd – double digested pGex-vector, control 1 - no template DNA, control 2 - no primer.
C. MNK PCR products cloned into pCR Blunt vector. Positive clones were double digested with *Eco*RI/*Sal*I.
D. MNK inserts cloned into pGEX-4T2 vector. Positive clones were picked and digested with *Eco*RI/*Sal*I.

3.1.2. GST-MNK expression clone

The verified pGex-4T2-MNK constructs (pGex-M1-1, pGex-M2-2, pGex-M3-2) were isolated from Top10 cells and transformed into BL21 CodonPlus (DE3) RIL cells for protein expression. The BL21 CodonPlus (DE3) RIL cells contain extra copies of genes encoding for arginine (*argU*), isoleucine (*ileY*) and leucine (*leuW*) tRNAs. In *E.coli* high level expression of heterologous proteins can lead to the depletion of certain rare tRNAs, which is abundant in other organism like mammals. Thus, the availability of these tRNAs in this *E.coli* strain can enable higher expression of recombinant proteins which is rich in arginine, isoleucine and leucine. The theoretical MNK domain has 274 amino acids (410-684) with 13 arginines, 21 isoleucines and 42 leucines. With a total of 27.7% of all amino acids being R, I or L for this protein, the BL21 CodonPlus (DE3) RIL *E.coli* strain is the best choice for MNK protein expression.

For each MNK construct, transformed BL21 clones were picked and grown in LB Ampicillin/Chloramphenicol medium overnight. 400 µl of the overnight culture was seeded in 4 ml culture medium and grown for 2 h at 37°C to an OD_{600} of about 0.5. The protein production is then

induced by adding a final concentration of 0.3 mM IPTG and cultured at 37°C overnight. The samples are then subjected to batch scale analysis.

The GST-MNK fusion can be expressed in the BL21 *E.coli* system (Figure 3.1.3). The expression of the GST-MNK2-2 (GM2-2) clone was highest at the given condition. Therefore, this clone was picked for further experiments.

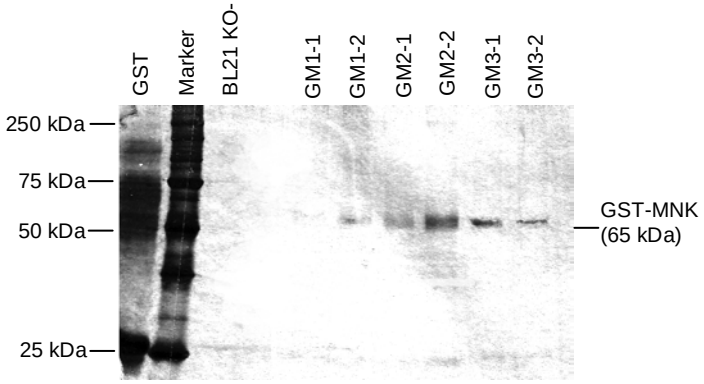

Figure 3.1.3: GST-MNK clone expression in different *E.coli* clones
SDS-PAGE analysis of different GST-MNK (GM) clones after batch scale purification.

3.1.3. GST-MNK expression condition

GM2-2 was seeded in LB selection medium, grown to an OD_{600} of 0.3-0.5 at 37°C, and separated in 4 ml fractions. These fractions are then cultured under different conditions: 0.1 mM, 0.3 mM, 1 mM IPTG; 12°C, 25°C, 37°C incubation temperature after IPTG induction and 1 h, 3 h, 5 h, 21 h incubation time. After these, different fractions are then collected via centrifugation at 4000 rpm for 10 min and used immediately or frozen at –20°C for later analysis. Also other medium compositions were tried, for example YT (16 g/l peptone, 10 g/l yeast extract, 5 g/l NaCl) and SOC (20 g/l peptone, 5 g/l yeast extract, 0.5 g/l NaCl, 4 g/l $MgCl_2$, 0.186 g/l KCl, 3.6 g/l glucose). But the effect on growth and expression level was not significant, so that LB was used as the standard medium.

The optimal OD_{600} value to induced protein expression was found to be between 0.3 and 0.5. With OD_{600} values higher than 1.0 the amount of expressed proteins is markedly reduced. One reason might be the lack of nutrients after extensive growth as well as the toxicity associated with overexpression of an exogenous protein. The concentration of IPTG used to induce protein expression can also vary between 0.3 mM and 1.0 mM without significant effect on protein yield.

The main factor influencing the expression was found to be the time and temperature of culturing after IPTG induction. The best expression is after 21 h at 12°C or 25°C (Figure 3.1.4). The highest yield under this condition was 120 µg crude GST-MNK in 1 ml cell suspension.

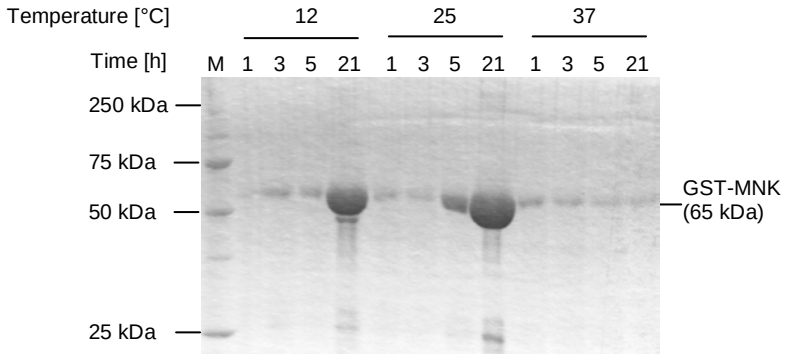

Figure 3.1.4: GST-MNK2-2 expression after IPTG induction for different incubation temperature and time

3.1.4. GST-MNK purification

While GST is a popular tag to produce fusion proteins, since it sometimes increases the yield of the target protein, GST needs to be removed for crystallization. Between the GST and MNK is a thrombin digestion site. Therefore, the GST-tag can be removed by thrombin digestion directly on the glutathione sepharose column or after the elution from the column.

Both approaches have advantages and disadvantages. The on-column approach is more convenient, because GST stays bound to the column after thrombin digestion and only free MNK is washed out after elution. The GST and MNK separation step can, therefore, be skipped. However, due to steric effects when GST-fusion proteins are still bound to the column, thrombin may have more difficulty to access the digestion site. The on-column thrombin digestion process may be less efficient as the off column approach. Therefore, both methods were tested to determine the best way to yield purified native MNK.

500 ml of GM2-2 was grown, collected and lysed. Each half of the lysate was subjected to a separate glutathione affinity column, incubated and washed well. One was eluted with 250 µl 10 mM GSH in Tris buffer (E1-E4), the other one was digested with 100 µl thrombin (10 U) overnight at room temperature and eluted with 250 µl PBS (T1-T3). Different fractions were collected and analyzed with SDS-PAGE (Figure 3.1.5).

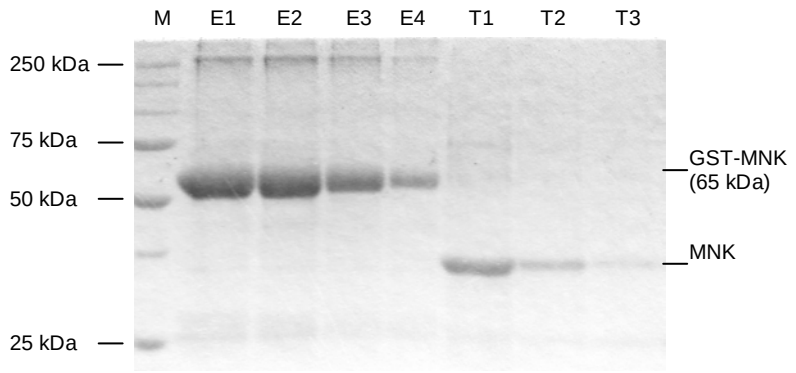

Figure 3.1.5: Glutathione affinity chromatography for purification of GST-MNK
E1-E4: 10 µl of 250µl elution sample of GST-MNK, T1-T3: 10 µl of 250µl thrombin digested sample on column

Relatively pure GST-MNK can be eluted from the column using this method (Figure 3.1.5, E1-E4). After on-column thrombin digestion MNK can be eluted down with PBS (T1-T3). As described before, this could mean that a major part of uncleaved GST-MNK is still bound to the column.

3.1.5. GST-MNK on-column thrombin digestion

The on-column digested fractions (T1-T3) were collected, concentrated and run on a Superdex™ 200 10/300 GL gel filtration column using PBS as gel filtration buffer (Figure 3.1.6). From the FPLC diagram one peak at Rv = 15.13 ml is visible (Figure 3.1.6A). Using a gel filtration protein standard this peak was calculated to be 56 kDa (Figure 3.1.6B). From the non-denaturing and non-reducing SDS-PAGE, MNK exists as monomer as well as dimer in solution (Figure 3.1.6C). These fractions (B3-B9) were tested for their enzyme activity and reveals specific kinase activity for ManNAc. The determined average specific activity is about 2.4 U/mg MNK protein. The protein yield after gel filtration using this method was 1.2 mg MNK per liter *E.coli* culture. The purity was good and fits for crystallization screening.

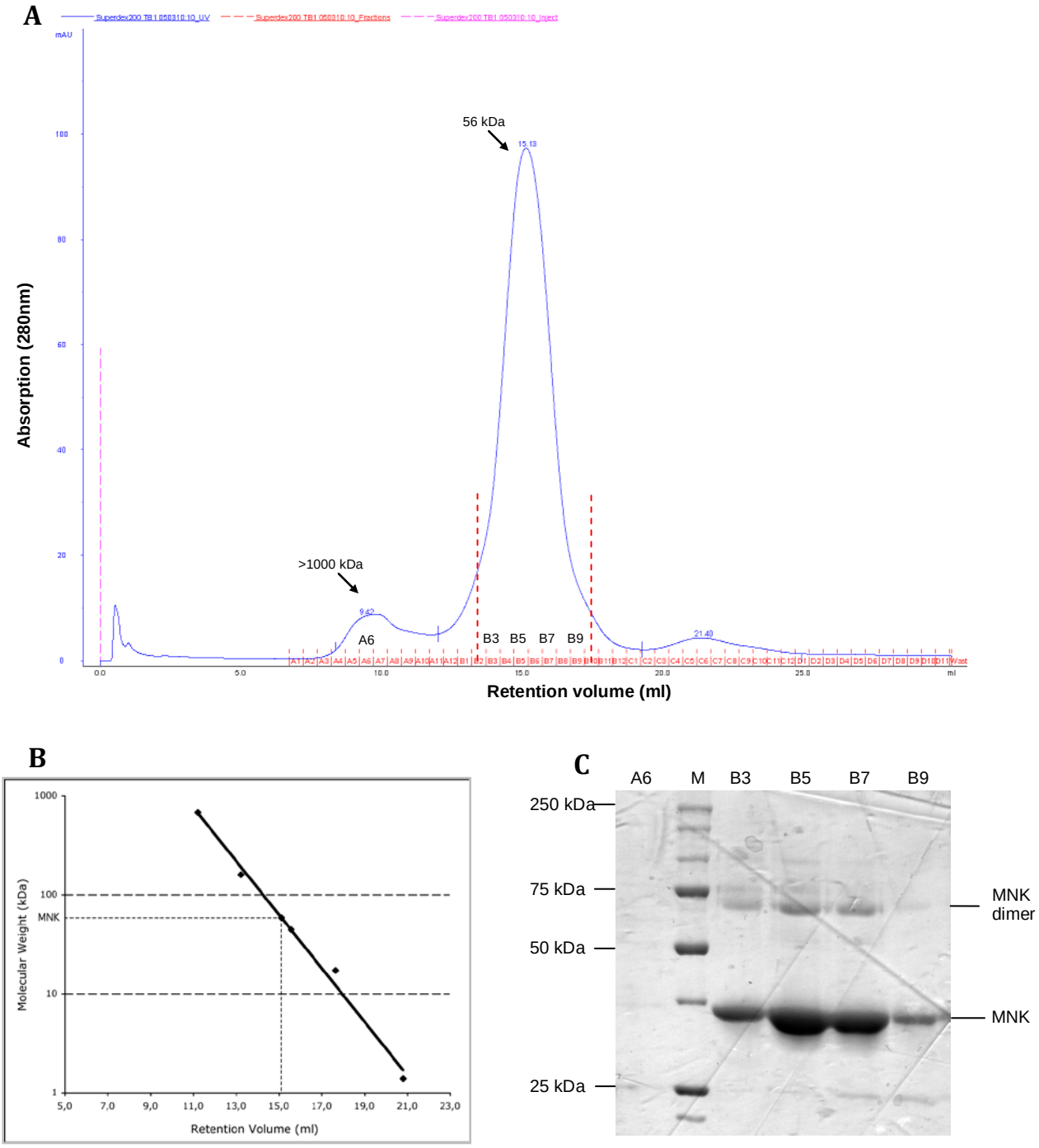

Figure 3.1.6: GST-MNK purification with on-column thrombin digestion
A. FPLC diagram of GST-MNK expression
B. FPLC protein standard (Biorad) on Superdex 200 10/30 column (thyroglobulin (670 kDa), γ-globulin (158 kDa), Ovalbumin (44 kDa), Myoglobin (17 kDa), Vitamin B12(1.35 kDa)). MNK eluted at 56 kDa.
C. Non-denaturing and non-reducing SDS-PAGE of different FPLC fractions (20 µl of 500µl), A6-B9: FPLC fractions

3.1.6. GST-MNK off-column thrombin digestion

The GST-MNK fractions (E1-E4) (Figure 3.1.5) were changed to PBS buffer and incubated with 100 µl Thrombin (10 U) overnight at RT. The whole sample was then subjected to Superdex™ 200 10/300 GL size exclusion chromatography. Fractions were collected and analyzed via non-denaturing and non-reducing SDS-PAGE and Western Blot with GST antibody (Figure 3.1.7).

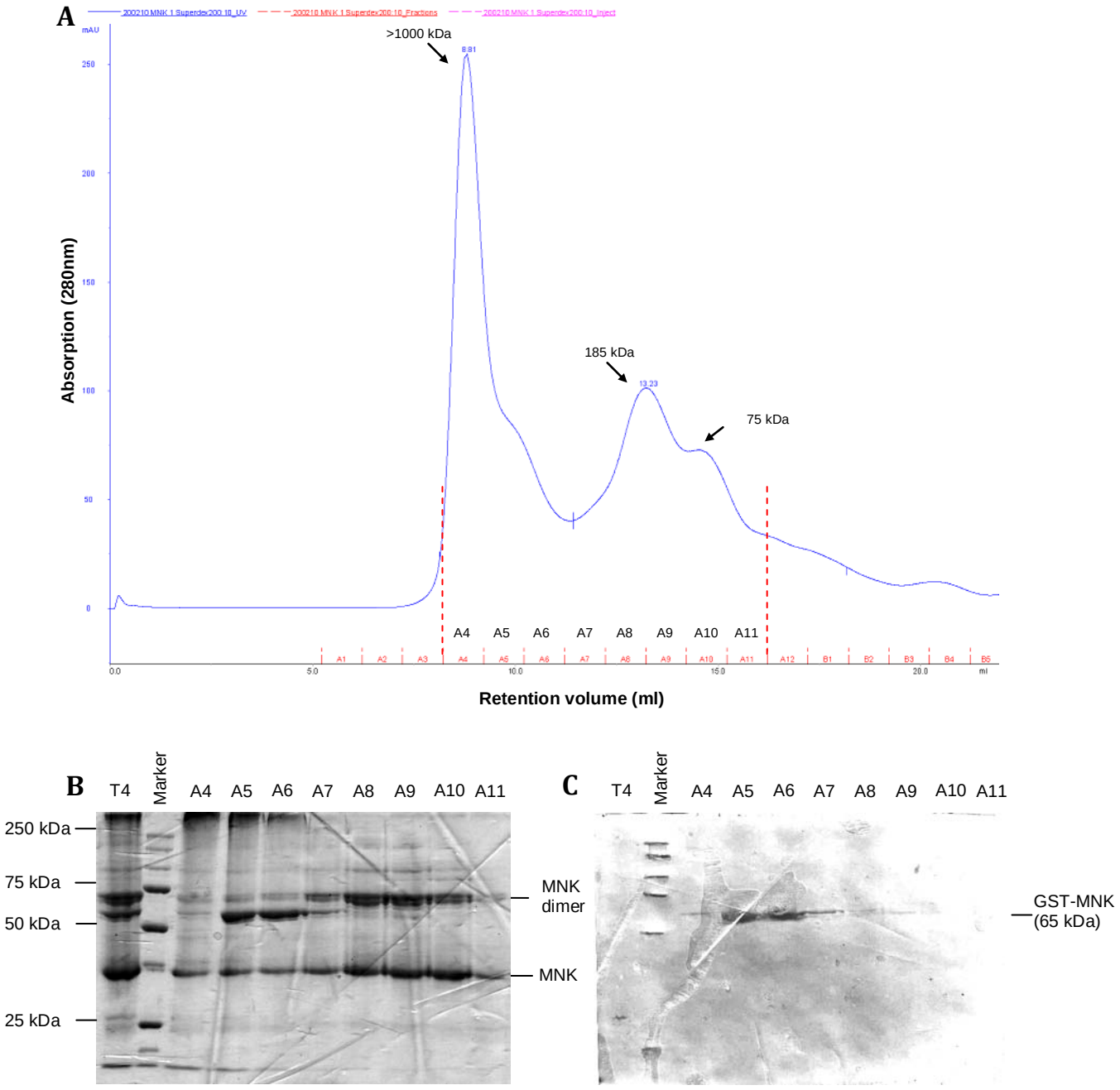

Figure 3.1.7: GST-MNK purification with off-column thrombin digestion
A. FPLC diagram of GST-MNK expression
B. Non-denaturing and non-reducing SDS-PAGE of different FPLC fractions (20 µl of 1 ml)
C. Western Blot of FPLC fractions with αGST antibody,
T4: Thrombin digested samples prior FPLC, A4-A11: FPLC fractions

From the FPLC the amount of undigested and aggregated MNK-GST was very high in the earlier fractions (Figure 3.1.7A, 3.1.7B, A4-A7). The Western Blot with anti-GST antibody detected the GST-MNK at 65 kDa in earlier fractions of the gel filtration (Figure 3.1.7C, A4-A7). In later fractions of the gel filtration (A8-A11) MNK exists predominantly as monomer and dimer. Under the non-denaturing and non-reducing SDS PAGE two dominant bands are visible. One is at 36 kDa as expected for a monomeric MNK, the other at 72 kDa common for dimeric MNK. Weaker bands represents most

likely GST (25 kDa), the hetero dimer of GST-MNK and MNK (100 kDa) and homo dimer of GST-MNK with itself (140 kDa) (Figure 3.1.7). Fractions (A8-A10) with reasonable purity of MNK could be collected but judging from the data, GST-MNK could also not be completely digested by thrombin under this condition. The protein yield was less than 1 mg MNK per liter *E.coli* culture.

Therefore, the on-column thrombin digestion of GST-MNK was favored. It was a simpler process, the purity was higher and the yield was slightly better than the off-column approach.

3.1.7. GST-MNK large scale expression

Under this optimized condition hMNK was then produced in large scale for crystallization purposes. GST-MNK *E.coli* cultures were grown to OD_{600}=0.5, induced with 0.3 mM IPTG to produce GST-MNK and collected 21 h after incubation at 25°C. For each liter cultures, the collected *E.coli* pellet is then resuspended in 10 ml lysis buffer and sonicated 3 times for 2 min. The cell lysis solution is then centrifuged for 60 min at 18000 rpm at 4°C to sediment cell debris and unbroken cells in the pellet. Subsequently, the supernatant is transferred on a glutathione affinity chromatography column to separate GST-fusion protein from the protein mixture. Using thrombin protease the GST-tag is then cleaved off on column or after elution over night. The eluate is then purified via gel filtration. As an option, thrombin could also be removed via a Benzamidine FF column before gel filtration.

3.1.8. GST-MNK crystallization screening

First crystallization attempts with purified GST free MNK samples were performed and MNK crystals could be collected via the sitting drop method at the crystallization condition of 5 mM ADP, 1% chymotrypsin (w/w), 15% PEG 3350, 0.2 M ammonium acetate, and 0.1 M sodium citrate pH 5.4 (Figure 3.1.8). These crystals produce low resolution structures of the apo-hMNK.

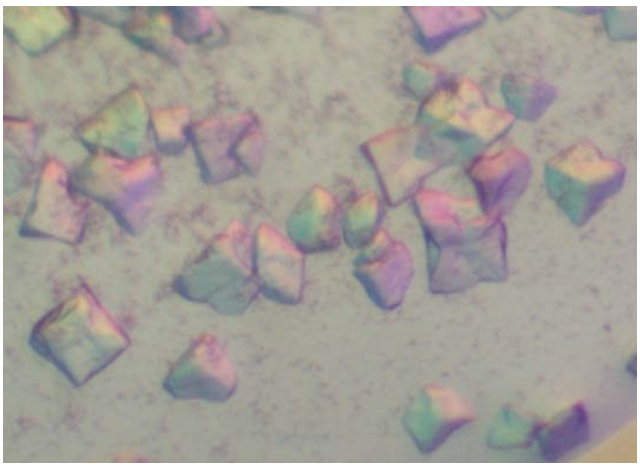

Figure 3.1.8: Presentation of apo-hMNK crystals
Ligand free hMNK crystals cultured with 5 mM ADP, 1% chymotrypsin (w/w), 15% PEG 3350, 0.2 M sodium citrate (pH 5.4)

3.1.9. His-MNK cloning, expression and purification

Since the yield of pure hMNK with the GST-tag is relatively low, another His-MNK construct was generated. MNK (aa 406-720) was cloned with two endonuclease sites *NdeI* and *XhoI* into a pET28a vector. Between the N-terminal 6xHis-tag a thrombin digestion site and a TEV-protease site were included (Figure 3.1.9). The total length of the His-MNK protein is 344 aa.

Figure 3.1.9: Schematic display of recombinant His-MNK fusion protein

PCR was performed using 100 ng of template DNA (pUMVC3-hGNE1) and 20 pmol of the described primer pair (Table 3.1.2, For HisMNK and Rev HisMNK). The PCR running conditions were 30 cycles of 30 s 94°C denaturation, 30 s 55°C annealing and 150 s 68°C elongation.

Table 3.1.2: MNK cloning primers for His-fusion construct

Primer name	Sequence (5' -> 3')	Tm [°C]
For His-MNK	GTACCATATGGAAAACCTGTATTTTCAGGGCACTCTAAGTGCCTTGGCCGTTG (53)	80,2
Rev His-MNK	GTACCTCGAGTTATTACCTGCGTGTTGTGTGTAGTCCAG (37)	69,5

A-*Nde*I site, A-*Xho*I, A-TEV sequence, A-GNE sequence, A-Stop codons (UAA)

MNK-PCR products were directly transferred into pET28a vector, amplified and sequenced. The verified plasmid was then transformed into BL21 RIL *E.coli* for protein expression. The cloning of the His-MNK construct was kindly carried out by Eva Tauberger at Prof. Dr. Wolfram Saenger's lab.

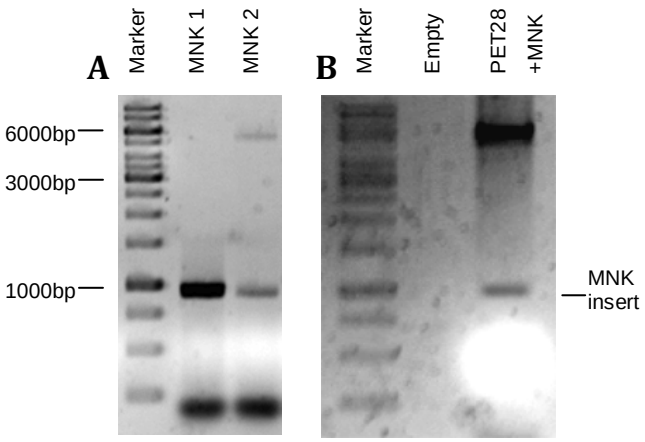

Figure 3.1.10: His-MNK DNA constructs
A. PCR product of MNK DNA, B. Positive pET28a-MNK plasmid verified by *Nde*I/*Xho*I double digestion

The PCR products are distinct DNA bands at the expected lengths around 1000 bp. No other unspecific bands were visible under this PCR condition (Figure 3.1.10A). Positive His-MNK plasmid constructs had the MNK insert in the pET28 vector and were confirmed by double digestion with *Nde*I/*Xho*I (Figure 3.1.10B). Sequencing results verified the construct to be correctly ligated, in the right orientation and without mutations.

3.1.10. His-MNK batch analysis

His-MNK BL21 clones, which are growing on Chloramphenicol and Kanamycin selective LB plates, were selected to optimize for expression in a batch scale. Similar to GST-MNK batch analysis, different *E.coli* samples were lysed and added on 40 µl Ni-NTA agarose (Qiagen). After incubating the samples for 1-12 h at 4°C, they are washed 3 times with Ni-NTA wash buffer and eluted with 30 µl Ni-NTA elution buffer. 20 µl of the elution supernatant are then analyzed on SDS-page. The optimal expression condition for His-MNK was found to be similar to the expression condition of GST-MNK.

3.1.11. His-MNK protein purification

For the expression and purification of His-MNK, the transformed bacteria culture was grown under LB Kanamycin and Chloramphenicol overnight. The overnight culture was seeded into fresh medium with a ratio of 1:100 and cultured to an OD_{600} of between 0.4-0.6. The protein production was induced with 1 mM IPTG and the culture was incubated at 25°C overnight at 225 rpm shaking frequency. The BL21 bacteria pellet was then collected, lysed and purified by Ni-NTA affinity chromatography and gel filtration according to the methods described.

For purification of up to 8 liters *E.coli* cultures the His-Trap FF 5 ml column was used instead of Ni-NTA affinity column and the HiLoad 26/60 Superdex 200 pg column for gel filtration instead of the Superdex 200 10/300 GL. These experiments were performed using the equipments in Prof. M. Wahl's lab (FU Berlin)

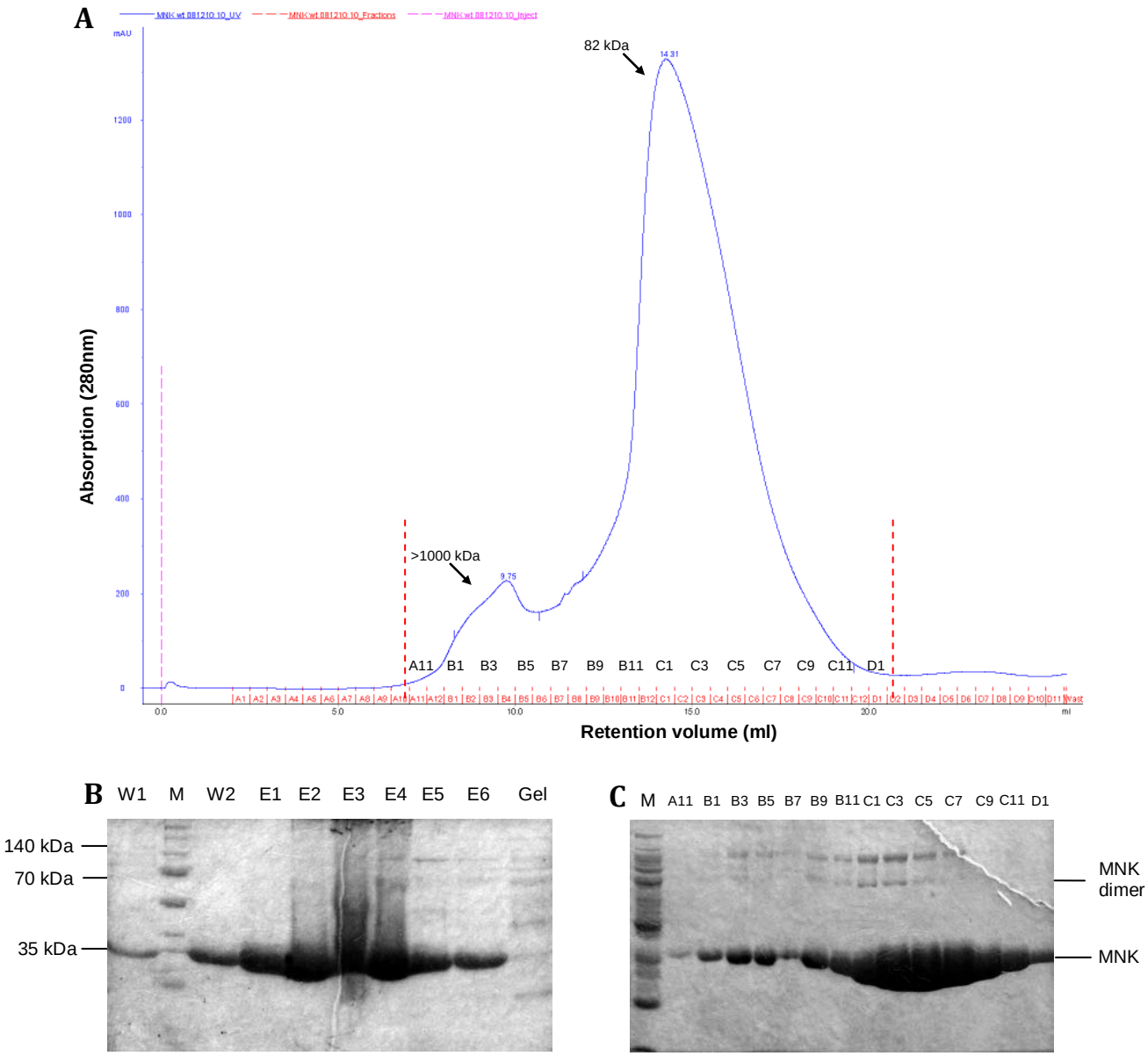

Figure 3.1.11: His-MNK purification
A. Chromatograph of His-MNK on Superdex 200 gel filtration
B. SDS-PAGE of His-MNK after Ni-NTA affinity chromatography
W1. W2: Washing fractions, E1-E6 (20 µl of 1 ml fractions)
C. Non-denaturing and non-reducing SDS-PAGE of His-MNK of Superdex 200 gel filtration fractions
A11-D1: FPLC fractions (10 µl of 500 µl fractions)

After Ni-NTA affinity chromatography a dominant single protein band at 35 kDa is observed on SDS-PAGE (Figure 3.1.11B), which corresponds to the MNK monomer. Running these concentrated fractions (E1-E6) using Superdex 200 gel filtration column yield a single protein peak at 14.31 ml retention volume (82 kDa), indicating that MNK in solution is a dimer. Some protein aggregation (>1000 kDa) could be observed in the first fractions (B1-B5). Compared to the total protein amount, however, this amount of aggregation is small (Figure 3.1.11A). The gel filtration peak contained purified MNK, in monomeric, dimeric and tetrameric forms, as can be observed in the non-denaturing and non-reducing SDS-PAGE (Figure 3.1.11C). With this method 20 to 30 mg of highly

purified His-MNK per liter *E.coli* culture could be produced. For crystallization experiments the His-tag was not cleaved off.

3.1.12. His-MNK characterization

The purified MNK was used for further characterization. The specific activity of MNK is 2.4 U/mg, which is comparable with the specific activity of the whole GNE [116]. This activity is stable in gel filtration buffer for several weeks at –20°C. At room temperature or 4°C this kinase quickly loses its activity just after a few days (Figure 3.1.12A).

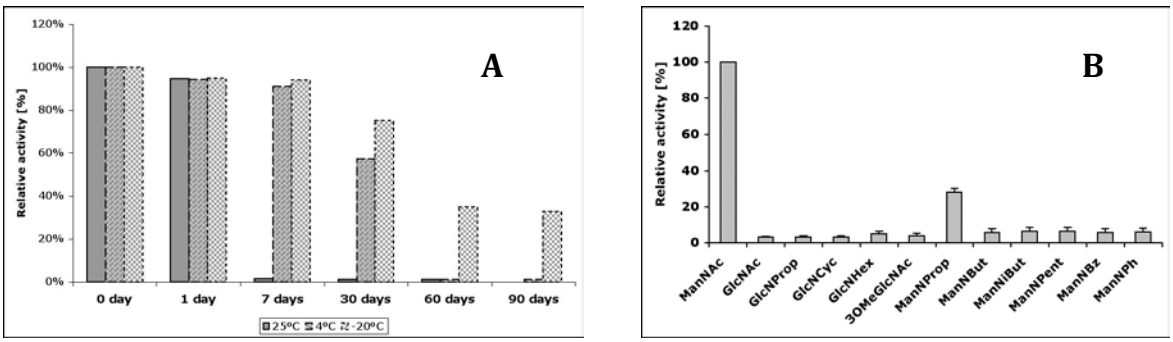

Figure 3.1.12: MNK stability and substrate specificity test
A. MNK stability dependency on time and temperature, enzyme activity test was carried out for MNK after the indicated time and temperature of storage
B. MNK substrate specificity, enzyme activity test was carried out for MNK using 10 mM of the indicated ManNAc analogs as substrate.

Through kinetic measurements the Km of MNK was determined to be 95 µM for ManNAc and 4.4 mM for ATP (Data not shown). This difference in substrate affinity would explain the difficulties faced in getting co-crystals of MNK with ATP or ATP analogs. Under physiological conditions ManNAc is in lower micromolar concentrations and ATP in millimolar range, which would explain this observation.

To verify MNK specificity, the kinase activity was tested with different HexNAc analogs as substitute for ManNAc (Figure 3.1.12B). The result confirmed that hMNK is specific for ManNAc, with almost no activity for other related structures. With ManNProp as substrate, MNK exerts a slight activity (25%). The related enzyme GlcNAc Kinase, which was purified as a control enzyme, on the other hand is less specific and can phosphorylate GlcNProp, GlcNCyc and GlcNHex, but not ManNAc, almost as good as GlcNAc (Data not shown). The specificity for ATP was also assessed by comparing the MNK activity with UTP, CTP and GTP. The relative MNK activity with UTP was 19%, with GTP 7% and with CTP 2% compared to ATP as a substrate, demonstrating that the specificity of hMNK for ATP is also very high.

3.1.13. MNK purification - conclusion

In this part of the work the hMNK was successfully cloned in a prokaryotic system using two different purification tags, GST and 6xHis. The expression conditions were assessed and optimized to yield the highest amount of pure hMNK in a most rapid way. With the use of the GST tag, pure hMNK could be obtained. After the removal of the GST tag via thrombin digestion about 1 mg/l hMNK could be obtained with the established methods. The protein quality was good enough to culture initial crystals. With the use of the 6xHis-tag, the purification process of this kinase could be greatly simplified. In a two-steps purification procedure high quantities (up to 30 mg/l) of highly pure hMNK could be generated. The hMNK was verified to be a dimer in solution with a monomeric weight of 35 kDa. The enzyme activity was verified to be in the same range of previously described whole GNE activity. The substrate specificity was intact and the enzyme was stable enough for further crystallization experiments.

3.2. ManNAc kinase crystal structure

MNK crystallization experiments were carried out together with Jacobo Martinez under the supervision of Dr. Sebastien Moniot of Prof. Dr. Wolfram Saenger's lab. Equipments and materials were kindly provided by Prof. Dr. Markus Wahl.

3.2.1. MNK crystallization

Using the described crystallization screening method, a reservoir containing 0.2 M calcium acetate, 0.1 M sodium cacodylate pH 6.5 and 40% PEG 300 yielded small crystals. Using hanging drop vapor diffusion at 18°C this condition could be reproduced and refined. Diamond shaped crystals, grew by mixing equal volumes (2 µl) of MNK and mother liquor containing 0.2 M calcium acetate, 0.1 M sodium cacodylate pH 6.5 and 38-46 % PEG 300. Crystals reached their maximal size within 5 days. Crystals were directly flash-frozen in liquid nitrogen prior to data collection. No further cryoprotectant was required for crystal freezing since the mother liquor contained high PEG 300 concentration.

No crystals could be obtained by co-crystallization of MNK with ManNAc and ADP, ATP, AMPPCP or AMPPNP. Neither the above described condition nor the screening for new conditions yielded crystals. Therefore, crystal complex of MNK and ManNAc were soaked with ADP or ATP to obtain the respective co-complex structures.

Under these conditions crystal of MNK/ManNAc, MNK/ManNAc/ADP and MNK/ManNAc-6-P/ADP could be obtained. The space group for the complexes MNK/ManNAc/ADP and MNK/ManNAc-6-P/ADP remained P41212 (primitive tetragonal) similar to MNK/ManNAc. The refinement of the latter complexes was performed as described in material and methods.

The data sets for MNK/ManNAc, MNK/ManNAc/ADP and MNK/ManNAc-6-P/ADP were completed at 1.65 Å, 1.80 Å, 2.40 Å resolutions respectively. Detailed statistics of the processed data for the 3 presented structures were summarized in Table 3.2.1. The atomic coordinates and structure factors have been deposited in the Protein Data Bank under accession 2yhw, 2yhy, 2yi1 respectively.

Table 3.2.1: Data collection and refinement statistics
Value in parentheses refer to the outermost resolution shell

	MNK/ManNAc	MNK/ManNAc/ADP	MNK/ManNAc6P/ADP
Data collection			
Beam line	BESSY MX 14.2	BESSY MX 14.2	BESSY MX 14.2
Space group	P 41 21 2	P 41 21 2	P 41 21 2
Unit Cell (Å)	a= b= 90.7; c= 100.8	a= b= 90.4; c= 101.2	a= b= 90.6; c= 101.4
	α= β= γ= 90°	α= β= γ= 90°	α= β= γ= 90°
Nominal resolution (Å)	45.3 – 1.64	50.0 – 1.82	41.40 - 2.15
Outermost resolution shell (Å)	1.73-1.64	1.92-1.82	2.16 – 2.27
Unique reflections	52083 (7584)	38183 (5567)	23574 (3484)
Completeness (%)	100 (100)	100 (100)	99.7 (100)
Redundancy	12.9 (12.9)	12.8 (12.9)	11.8 (3.9)
Rmerge	5.8 (72.5)	5.3 (69.4)	7.9 (64.7)
Rmrgd-F	5.9 (39.5)	6.0 (40.9)	9.3 (44.6)
Mean I/σ(I)	30.66 (4.37)	34.07 (4.40)	24.52 (4.0)
Refinement			
Rwork / Rfree (%)	14.8/17.0	15.2/18.2	17.2 / 20.0
r.m.s.d. Bond lengths (Å)	0.026	0.025	0.022
r.m.s.d. Bond angles (°)	2.068	2.097	1.788
Dihedral angles (°)	6.637	6.180	6.465
Mean B-factor (Å^2) Overall model	25.7	31.6	37.1
Mean B-factor (Å^2) Protein atoms	25.2	30.8	37.0
Sugar	12.5	16.2	18.7 (ManNAc) / 23.4 (ManNAc-6P)
ADP	-	58.0	66.3
PDB ID	2YHW	2YHY	2YI1

3.2.2. MNK sequence and structure homology

A primary sequence analysis identified GNE homolog proteins of pig, mouse, rat and chicken featuring 88%, 87%, 86%, 79% identity respectively, while the bacterial MNK proteins share around 30 % identity with the MNK domain from GNE and are listed as uncharacterized ROK (see below) family proteins, sugar kinases or transcriptional regulators (NagC and Mlc-like). Another structure similarity search using the DALI server conservation mapping in 3D [117] revealed a glucokinase (26 % amino acid sequence identity and 3.5 Å rms deviation of superimposed C α-atoms), a putative N-acetyl mannosamine kinase (26% and 2.3 Å), a fructokinase (22% and 2.3 Å), a NagC-like transcriptional regulator (22% and 2.5 Å) and a Mlc-like transcriptional regulator (22% and 3.1 Å) among the first 10 hits.

From these structural and sequential comparisons we can infer that human MNK belongs to the ROK family and more generally to the sugar-kinase/HSP70/actin superfamily that feature a common

ATPase domain characterized by five common structural motifs. Three of them, phosphate 1 (G416, T417), phosphate 2 (G543, T544) and adenosine are implied in ATP binding. The other two, connect 1 and connect 2 (helix α3 and helix α11 respectively), bridge from one domain to the other in opposite directions making close helix-helix contacts and defining the interdomain hinge region [118]. These characteristic sequence motifs conserved for this family can be found in the MNK as well (see information in parentheses).

As described in a previous publication by Tong et al in 2009, the MNK belongs to the ROK family [113], a functionally diverse enzyme family that was first described in 1994 by Titgemeyer et al. [119] encompassing transcriptional regulators, uncharacterized open reading frames and several sugar kinases. Comparing the primary structures of different ROK family members, Hanson et al proposed two consensus sequences as specific signature common to all family members [120]. Consensus motif 1 was a glycine rich 28 amino acids sequence with four glycines conserved among all the compared structures. The second motif was 14 amino acids long and contained 2 conserved cysteine residues and a histidine or another cysteine at the third position. In 2005, Schiefner et al. presented the structure of a ROK family member, the transcriptional regulator Mlc [121]. Using the novel structural information combined with a renewed sequence comparison of the ROK family members they merged the two consensus motifs to a single one, which contains a zinc (Zn^{2+}) binding motif. There are two variations of this motif: G<u>H</u>$X_{9\text{-}11}$CXCGX_2G(C/H)X<u>E</u> and G<u>H</u>$X_{11\text{-}17}$CX_2HX_2C<u>X</u><u>E</u> (the metal binding amino acids are printed in bold). MNK contains the first Zn^{2+} binding motif (G568-E588), and a Zn^{2+} is coordinated by three cysteines and one histidine (H569, C579, C581, C586). Interestingly, the underlined residues are conserved in many sugar kinases inside or outside of the ROK family. In the case of MNK, as was found out with the new MNK structures, these residues (H569 and E588) are also directly involved in ManNAc binding.

3.2.3. MNK overall structure of the monomer

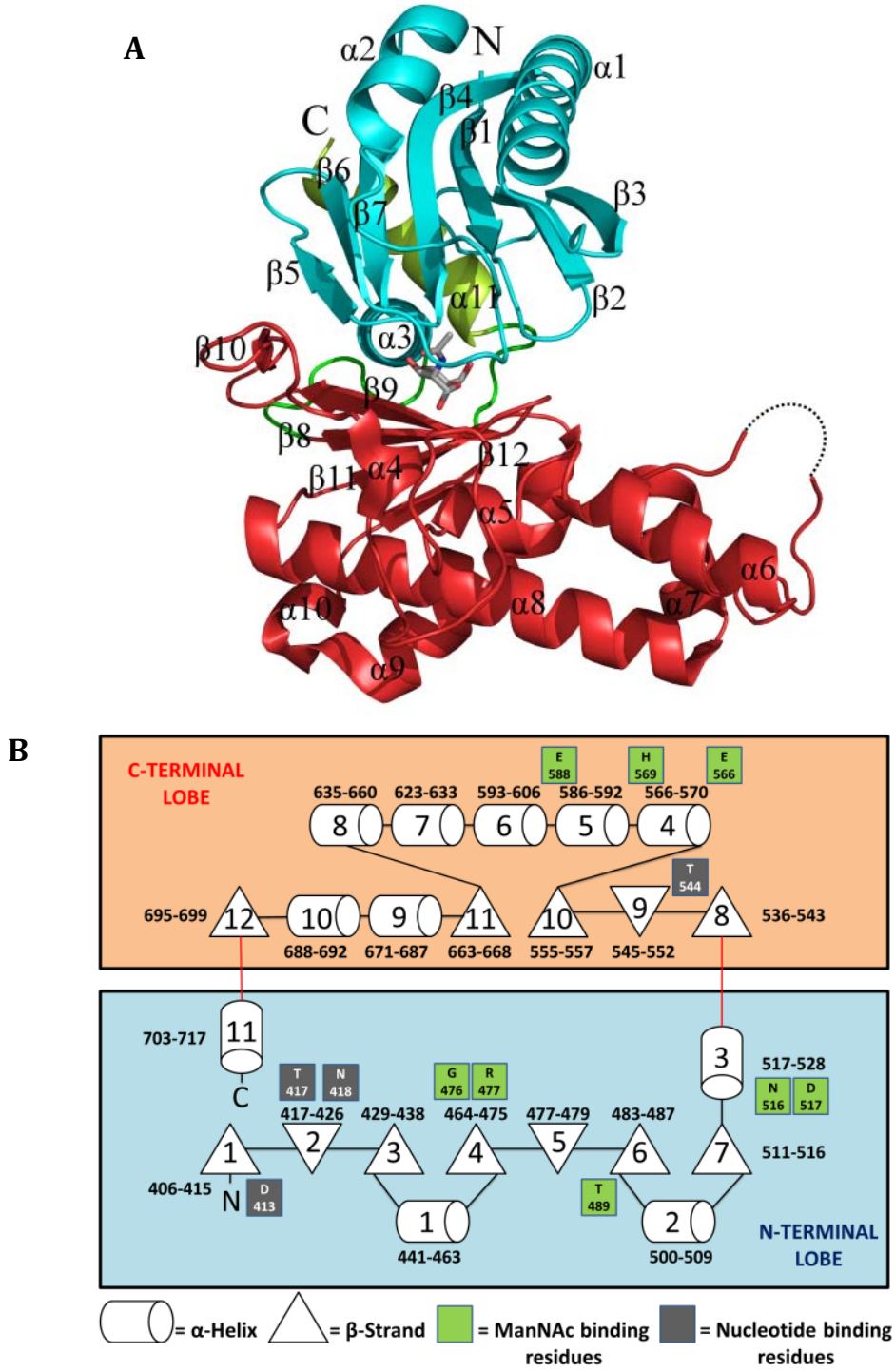

Figure 3.2.1: MNK topology and structure

A. Ribbon representation of MNK monomer in complex with ManNAc.

The N-terminal lobe is colored in blue, the C-terminal lobe in red. ManNAc is depicted as sticks in grey. The secondary structures are labeled as α (helices) or β (strands) followed by a number indicating their occurrence in the primary structure. The C-terminal α-helix (α11 in green) protrudes out of the C-terminal lobe into the N-terminal lobe. The dashed line in the loop connecting α6 with α7 indicates a flexible unmodeled region.

B. Schematic representation of the MNK topography.

The two lobes are boxed and colored according to (A) and connected by two red lines, indicating the hinge regions. The numbers close to each secondary structure indicate the first and last amino acid of the element. The residues forming the ManNAc and the ATP/ADP binding site are in green and grey rectangles respectively.

High quality electron density allowed the building of the structure model with reliability for the major part of the kinase domain of human GNE (amino acids 405-717) as well as for its native ligand, N-acetyl mannosamine. Only a loop region consisting of residues 601-625 has a poorly defined electron density. For residues 617-620, no electron density could be visible and therefore these residues are missing in the structure model.

As displayed in Figure 3.2.1, the secondary structure of the MNK is composed of two clearly differentiated domains: the N-terminal domain contains residues 406-528 and 703-717 (colored cyan and yellow respectively) and the C-terminal domain contains residues 543-699 (red). Both domains are connected by two flexible loops or hinges (colored green) allowing the MNK to change from an open conformation to a closed one upon substrate binding.

The N-terminal domain is composed of a central 5-stranded mixed β-sheet (β7, β4, β1, β2, β3), with β2 being antiparallel to the other strands, flanked by α1 and α2 on one side and by α11 and α3 (yellow) on the other side, protruding from the C-terminal domain. Two further β strands (β5 and β6) form a hairpin β-sheet in the loop connecting β4 with α2. The C-terminal domain is composed of a 4-stranded beta-sheet (β9, β8, β11, β12), with β9 being antiparallel to the other β-strands. The β-sheet is located on an α-helix cluster formed by (α4-α10). The presence of a well-coordinated zinc cation between α4 and α5 was confirmed by anomalous difference map (Figure 3.2.4). The two domains define a large cavity containing the active site, where ManNAc (gray) and ATP/ADP bind.

3.2.4. MNK multimeric state

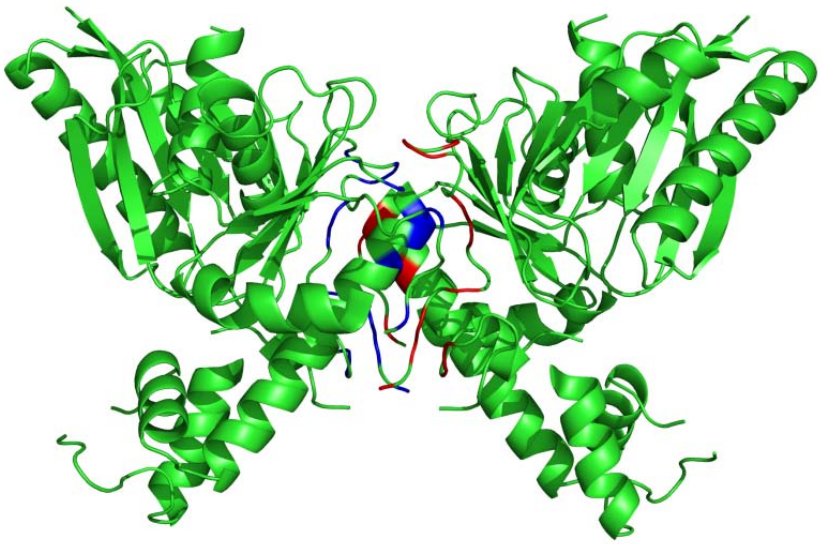

Figure 3.2.2: Representation of dimeric hMNK
The monomer-monomer interface residues have been colored in red and blue for each monomer respectively.

Table 3.2.2: Dimerization surface of MNK bound to ManNAc
Potential H Bond interaction between two homogenic structures

##	Structure 1	Structure 2	Dist. [Å]
1	ASN 661 [ND2]	HIS 558 [O]	3.77
2	HIS 658 [ND1]	HIS 569 [O]	2.86
3	ASN 655 [ND2]	VAL 571 [O]	2.88
4	LEU 574 [N]	VAL 572 [O]	3.22
5	GLN 686 [NE2]	SER 583 [OG]	3.04
6	GLN 686 [NE2]	HIS 584 [O]	3.68
7	VAL 571 [N]	ASN 655 [OD1]	2.63
8	ALA 565 [N]	HIS 658 [O]	3.18
9	GLU 566 [N]	HIS 658 [O]	2.82
10	ALA 565 [N]	THR 659 [O]	2.98
11	SER 560 [OG]	ASN 661 [OD1]	3.44
12	SER 561 [OG]	ASN 661 [OD1]	2.88
13	SER 560 [OG]	ASN 661 [O]	2.89
14	SER 560 [N]	ASN 661 [O]	2.89
15	SER 561 [OG]	SER 690 [O]	2.64
16	HIS 558 [O]	ASN 661 [ND2]	3.77
17	HIS 569 [O]	HIS 658 [ND1]	2.86
18	VAL 571 [O]	ASN 655 [ND2]	2.88
19	VAL 572 [O]	LEU 574 [N]	3.22
20	SER 583 [OG]	GLN 686 [NE2]	3.04
21	HIS 584 [O]	GLN 686 [NE2]	3.68
22	ASN 655 [OD1]	VAL 571 [N]	2.63
23	HIS 658 [O]	ALA 565 [N]	3.18
24	HIS 658 [O]	GLU 566 [N]	2.82
25	THR 659 [O]	ALA 565[N]	2.98
26	ASN 661 [OD1]	SER 561[OG]	2.88
27	ASN 661 [OD1]	SER 560[OG]	3.44
28	ASN 661 [O]	SER 560[N]	2.89
29	ASN 661 [O]	SER 560[OG]	2.89
30	SER 690 [O]	SER 561[OG]	2.64

Only one monomer is present in the asymmetric unit of the MNK-ManNAc crystals. However, an examination of the crystal structure using PISA [122] revealed that every monomer is sharing 13% of its solvent accessible surface with a symmetry related mate. The monomer-monomer interface area measures 1760 $Å^2$ per monomer (Figure 3.2.2). These findings correlate with biochemical results from analytical gel filtration and non-denaturing and non-reducing SDS-PAGE, which indicate a native molecular weight of MNK to be around 75 kDa compared to 35 kDa in denaturing SDS-PAGE.

Table 3.2.3: Dimerization surface of MNK without ManNAc
Potential H Bond interaction between two homogenic structures

##	Structure 1	Structure 2	Dist. [Å]
1	ASN 661 [ND2]	CYS 563 [SG]	3.20
2	HIS 658 [ND1]	HIS 569 [O]	2.61
3	ASN 655 [ND2]	VAL 571 [O]	2.87
4	LEU 574 [N]	VAL 572 [O]	3.54
5	VAL 571 [N]	ASN 655 [OD1]	2.86
6	GLU 566 [N]	HIS 658 [O]	2.77
7	ALA 565 [N]	THR 659 [O]	3.01
8	SER 560 [N]	ASN 661 [O]	2.68
9	SER 583 [OG]	GLN 686 [OE1]	2.97
10	CYS 563 [SG]	SER 690 [O]	3.01
11	HIS 558 [O]	ASN 661 [ND2]	3.55
12	HIS 569 [O]	HIS 658 [ND1]	2.54
13	VAL 571 [O]	ASN 655 [ND2]	3.12
14	VAL 572 [O]	LEU 574 [N]	3.41
15	ASN 655 [OD1]	VAL 571 [N]	2.93
16	HIS 658 [O]	GLU 566 [N]	2.70
17	THR 659 [O]	ALA 565 [N]	2.98
18	ASN 661 [O]	SER 560 [OG]	2.61
19	ASN 661 [O]	SER 560 [N]	2.99
20	ASN 661 [OD1]	SER 560 [OG]	3.80
21	GLN 686 [OE1]	SER 583 [OG]	2.75

All amino acids involved in dimerization belong to the C-terminal domain of the protein. A total of 30 hydrogen bonds stabilize this interaction (Table 3.2.2). The N-terminal domain is not implicated in dimerization and possesses therefore more freedom, which allows it to undergo the necessary conformational changes to bind ManNAc (Figure 3.2.3).

Comparison of the dimerization area between the MNK-ManNAc structure and the apo–MNK structure [113] shows an increment of the surface and the number of hydrogen bonds upon binding of the substrate. The apo-MNK structure has a monomer-monomer interface area of 1599 $Å^2$ with 21 hydrogen bonds stabilizing the dimer (Table 3.2.3) whereas for the MNK-ManNAc complex these values are increased to the already mentioned 1760 $Å^2$ (Figure 3.2.2) and 30 hydrogen bonds, respectively (Table 3.2.2).

3.2.5. MNK ManNAc binding site

One of the main goals of this work was to elucidate the active center of the MNK. This involves the elucidation of the ManNAc binding site, all amino acids involved and the conformation of ManNAc when bound to MNK. Co-crystallization of MNK with ManNAc yielded crystals diffracting at 1.65 Å.

After solving the structure, difference electron density maps clearly showed the position and conformation of ManNAc (Figure 3.2.3).

MNK binds the α-anomeric form of N-acetyl mannosamine in $^4C_1$ chair conformation. The average B factor for the sugar molecule has a value of 12.2 $Å^2$ which is even lower than the average B factor for the main chain of MNK (14.3 $Å^2$). This indicates that the sugar binding site is fully occupied and relatively rigid.

All the polar sugar atoms are hydrogen bounded by the surrounding residues of MNK. A total of eight amino acids and three water molecules are involved in the substrate binding network forming a total of 17 hydrogen bonds with the ligand. The N-terminal domain is the major contributor to this network with five amino acids (G476, R477, T489, N516 and D517). The other three residues belong to the C-terminal domain of MNK (E566, H569 and E 588).

The ManNAc binding network is displayed in figure 3.2.3 and all the interactions are summarized in table 3.2.4. The hairpin β-sheet formed by β5 and β6 orientates three of these residues: G476 and R477 are situated in the loop connecting β4 with the hairpin and T489 is in the loop region located at the end of β6 strand. The short connecting loop between β7 and helix α3 bears the other two N-domain residues involved in sugar binding, N516 and the presumed catalytic residue D517.

The active center residues of the C-terminal domain seem to be orientated by the Zn^{2+} binding motif. This is especially evident for H569, which directly coordinates both, the Zn^{2+} (ND1, 2.11 Å) and ManNAcO1 (over NE2, 2.74 Å). But also E566 and E588, which are close to two of the Zn^{2+} binding residues, H569 and C586 respectively. These findings underline the central role of the Zn^{2+} binding motif for MNK activity.

Table 3.2.4: Hydrogen bond contacts for ManNAc and MNK

Number	Sugar atom / H_2O	Protein atom / H_2O	Distance (A)
1	ManNAc [O1]	H569 [NE2]	2.7
2		E588 [OE1]	2.6
3	ManNAc [N2]	H_2O - 1	3.0
4	ManNAc [O3]	G476 [N]	2.9
5		R477 [NH2]	3.2
6		E566 [OE2]	2.6
7		N516 [ND2]	3.1
8	ManNAc [O4]	N516 [ND2]	3.2
9		H_2O - 3	2.8
10		D517 [OD2]	2.6
11	ManNAc [O6]	D517 [OD1]	2.6
12		H_2O - 2	2.7
13		H_2O - 1	2.9
14	ManNAc [O5]	H_2O - 1	3.2
15	ManNAc carbonyl	T489 [N]	2.9
16		R477 [NH2]	2.9
17	ManNAc [C7]	E476 [N]	3.2

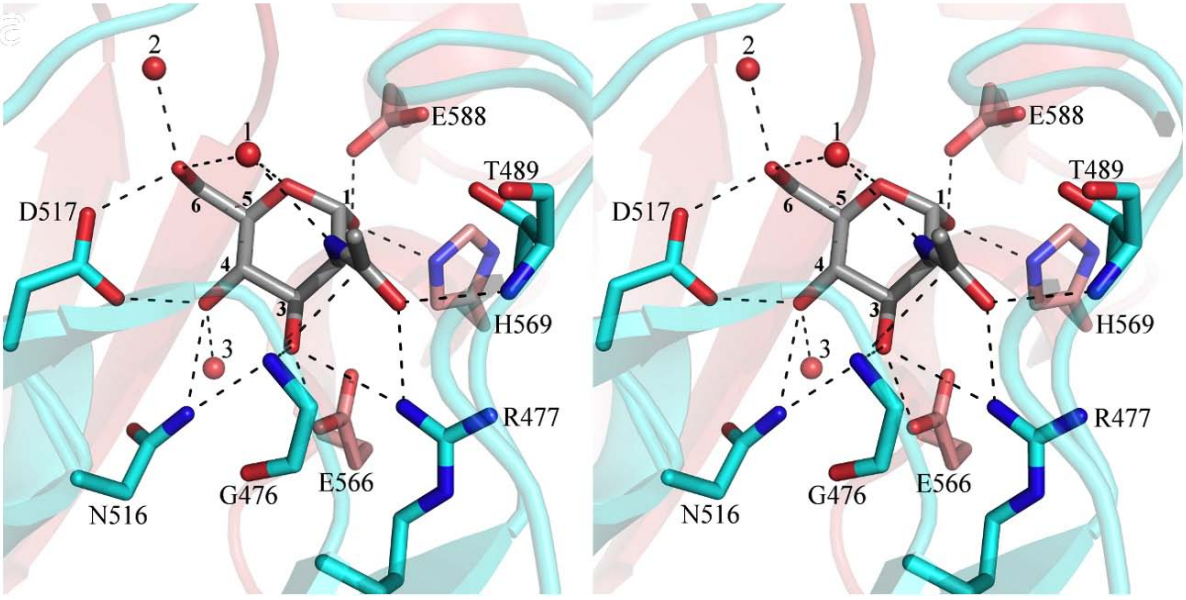

Figure 3.2.3: Stereo view of the ManNAc binding site.
The colors of the secondary structures are consistent with figure 3.2.1 indicating whether the residues arise from the N-terminal lobe (blue) or from the C-terminal one (red). The residues involved in ManNAc binding are represented as sticks, ManNAc atoms are numbered. Oxygen and nitrogen atoms are displayed in red and blue, respectively. The 3 water molecules are shown as red spheres and numbered. Broken lines show the extensive hydrogen bond network between hMNK and ManNAc.

3.2.6. MNK domain movements upon substrate binding

A comparison of the apo-MNK structure [113] with the MNK-ManNAc structure using DYNDOM [123] showed a clear conformational change. Upon substrate binding the N-terminal domain rotates 12° against the C-terminal domain (Figure 3.2.4). This closure allows MNK to embrace and tightly

coordinate the ManNAc molecule (Figure 3.2.3). Both domains behave as rigid bodies, and the flexibility is conferred by the two hinge regions (amino acids 529-535 and 700-702) (Figure 3.2.1).

Interestingly, the DYNDOM software suggests residues N516 and D517, which belong to helix α3, to form a third hinge. Both residues are directly implied in sugar binding (Figure 3.2.3). The orientation change of the side chains induced by ligand binding might be the driving force for domain movement. Notably, no significant conformational changes take place upon ADP/ATP binding.

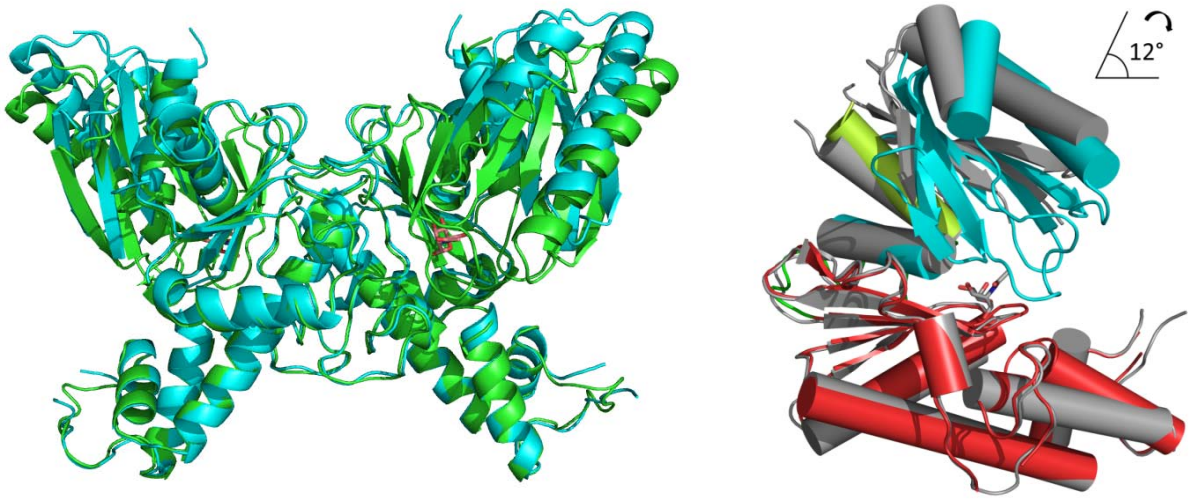

Figure 3.2.4: Superimposed structures of the MNK
A. MNK changes its structure from an open ligand free conformation (blue) to a closed ligand bound conformation (green) B. The helices have been displayed as cylinders for clarity. Upon ManNAc binding, the N-lobe (blue and gray for MNK/ManNAc and apo-MNK respectively) pivots 12° towards the C-lobe (red and gray) over the hinge region (green loops). Based on these representations we can clearly differentiate an open ligand-free conformation (gray) from a close ligand-bound conformation (blue and red).

3.2.7. MNK nucleotide binding site

Since attempts to co-crystallize hMNK with ManNAc and ADP, ATP, or AMPPCP were unsuccessful, crystals of the binary complex hMNK/ManNAc were soaked either with ATP or ADP. The structure of the ternary complex between MNK, ManNAc and ADP could be determined at 1.82 Å resolution (Figure 3.2.5). The electron density difference maps clearly showed the presence and position of the α- and β-phosphate groups of ADP as well as of the Mg^{2+} necessary for catalysis. The ribose moiety was partially defined but no electron density was found for the adenine moiety which is probably due to weak coordination that is also indicated by the dissociation constant of 4.4 mM for ATP. All the interactions of ADP with MNK are summarized in table 3.2.5.

Table 3.2.5: Hydrogen bond contacts for ADP/ATP and MNK

Number	ADP atom / H_2O	Protein atom / H_2O	Distance (A)
1	β-phosphate O1	T417 N	3.0
2		N418 N	3.0
3	β-phosphate O2	T544 OG1	2.4
4		T544 N	2.8
5		H_2O 429	2.8
6	β-phosphate O3	H_2O 449	3.1
7		H_2O 452	3.0
8		Mg	2.3
9	α-phosphate O1	R420 NH2	2.9
10		N418 ND2	2.8
11		H_2O 452	3.1
12	α-phosphate O2	H_2O 452	2.2
13		H_2O 268	2.9
14	Ribose hydroxyl O2	H_2O 453	2.6
15	H_2O 453	A624 N	2.5
16		G593 O	3.1

The β-phosphate of ADP is stabilized by a total of eight interactions (Figure 3.2.5). On one side, the β-phosphate interacts with the backbone NH of T417, N418, and T544, as well as with T544-OG1. On the other side, the β-phosphate is stabilized by hydrogen bonds to 3 water molecules that are further hydrogen bonded to ManNAc-O6H and the NH group of G545 (water molecule #1 in figure 3.2.5), D413-OD1 and D517-OD1 (#2) and to R420-NH2 (#3).

Mg^{2+} is octahedrally coordinated with the β-phosphate-O3 atom and D413-OD2 in the axial positions while four water molecules occupy the equatorial sites. The side-chain of D413 does not directly bind one of the oxygens of the β-phosphate but is necessary for Mg^{2+} coordination and consequently crucial for ATP binding.

The α-phosphate of ADP is mainly coordinated by the side-chains of R420-NH1 and N418-ND2 and further stabilized by 2 water-mediated hydrogen bonds (#3, #4).

All the amino acids involved in pyrophosphate coordination are located within strand β2 of the N-terminal lobe (T417, N418, R420) and in the loop connecting β8 and β9 of the C-terminal lobe (T544).

In the hMNK/ManNAc/ADP complex, the O3'H group of ADP is only stabilized by a hydrogen bond to Q597-Oε1 that is mediated by water #5 (Figure 3.2.5). In the ternary complex hMNK/ManNAc-6P/ADP, however, O3'H of ADP engages in two direct hydrogen bonds with T417-OG1 and T544-OG1, and O2'H is stabilized by a water-mediated hydrogen bond to the side chain of Q597 (Figure 3.2.6).

In the hMNK/ManNAc/ADP complex, the adenine group is located in a hydrophobic pocket where it

is stacked between the side-chains of L625 and V670 (Figure 3.2.5). The conformation of both the 8 ribose and the adenine moieties observed here is consistent with the one observed for ADP in the previously published crystal structure of fructokinase YdhR from *Bacillus subtilis* (19). The conformation of adenine is different in the complex with ManNAc-6P, its plane being rotated by ~100°, and it stacks on top of L625 and V670. In both complexes, the adenine base is poorly defined in electron density maps, which indicates flexibility that is also reflected by the relatively low binding affinity of hMNK for ATP (*Km* of 4.4 mM). However, one cannot exclude that spatial rearrangements by hMNK to properly accommodate the nucleotide and especially the adenine base could occur in solution.

Prolonged soaking of hMNK/ManNAc crystals with ATP afforded the structure of the ternary complex hMNK/ManNAc-6P/ADP at 2.10 Å resolution (Figure 3.2.6). In this case also, no electron density could be found for the adenine moiety of ADP, however, additional electron density extending from the ManNAc-O6 atom was attributed to the partial presence of the phosphorylated product of the reaction, ManNAc-6P (0.4 occupancy) in coexistence with the substrate ManNAc (0.6). This indicates that the kinase reaction has taken place in the crystal and that the γ-phosphate of ATP has been transferred to ManNAc. In essence, we have determined the crystal structures of the reaction educt hMNK/ManNAc and of the product hMNK/ManNAc-6P/ADP.

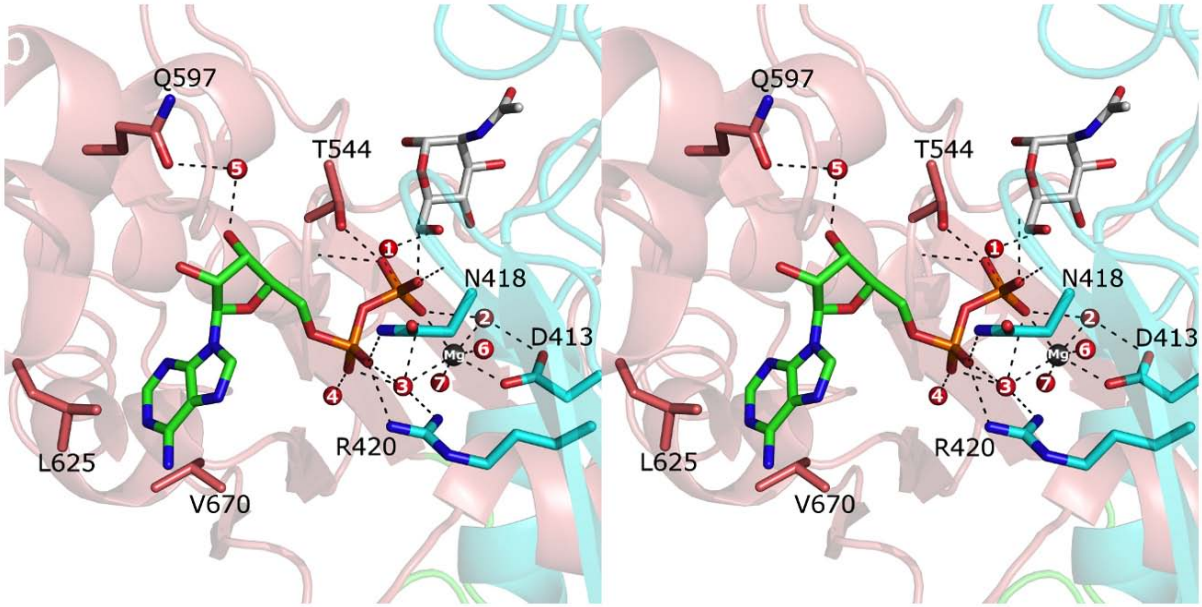

Figure 3.2.5: Stereo view of the ADP binding site.
Oxygen and nitrogen atoms are displayed in red and blue, respectively. The seven water molecules involved in ADP binding are displayed as red spheres and numbered in white. (1 corresponds to 179 in the PDB file 2YHY, 2 to 192, 3 to 195, 4 to 112, 5 to 196, 6 to 193 and 7 to 194). Broken lines show hydrogen bonds. ADP is shown in green (adenine moiety and ribose) and orange (phosphates). Mg^{2+} (gray sphere) is octahedrally coordinated, axially between D413 and the β-phosphate O3 and equatorially by four water molecules (2, 3, 6, 7). The ManNAc molecule is also shown (C atoms white, in the back of the picture), hydrogen bonded with O6H to water molecule 1. This gives a first impression of the distance separating the β-phosphate and the sugar phosphorylation site, hydroxyl O6H.

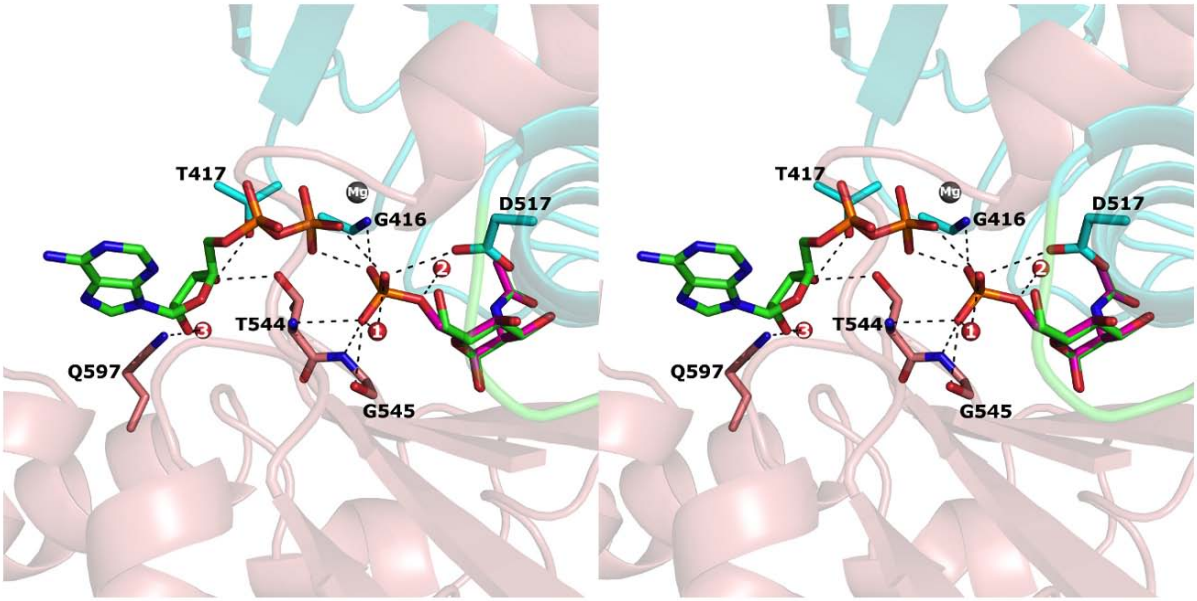

Figure 3.2.6: Stereo view of the ManNAc-6P phosphate coordination.
Oxygen and nitrogen atoms are displayed in red and blue, respectively. Short distances between phosphate oxygens (2.7Å) are represented by dashed lines and indicate protonation of one of these oxygens. Water molecules involved are displayed as red spheres and numbered in white. (1 corresponds to 68 and 2 corresponds to 87- PDB 2YI1). Broken lines show the hydrogen bond network surrounding the phosphate (orange) at the O-6 position. The ManNAc-6P molecule (0.4 occupancy) is displayed with pink backbone whereas the unphosphorylated ManNAc molecule (0.6 occupancy) is shown in green.

In the ternary complex MNK/ManNAc-6P/ADP the ribose engages in only one single water (H_2O453) mediated hydrogen bond between ribose O2'H and G593O and A624N. The adenine moiety was modeled in a hydrophobic pocket and is stacked between V670 and L625, again similar as in the above mentioned structure of fructokinase YdhR in complex with ADP.

3.2.8. MNK zinc binding site

Using anomalous difference maps we could confirm the presence of a Zn^{2+} located between α4 and α5 and tetrahedrically coordinated by three cysteines (C579, C581 and C586) and one histidine (H569) arising from the loop between these two α-helices (Figure 3.2.7). The Zn^{2+}-S distances are 2.35 Å for C579, 2.33 Å for C581 and 2.26 Å for C586. The Zn^{2+}-ND distance measures 2.11 Å for H569. The four residues implied in the Zn^{2+} binding form part of the specific ROK-family motif signature. The Zn^{2+} binding site is in close proximity to the ManNAc binding site. Indeed, the NE2 of H569 is in hydrogen bond distance (2.74 Å) with the C1 hydroxyl group of ManNAc. Zn^{2+} is properly orientating the H569 side chain for sugar binding. The observed B factor for Zn^{2+} correlates with the B factor of the atoms in the surrounding space indicating full occupancy, although no zinc has been added during purification. This indicates the endogenous strong binding of Zn^{2+} and underlines its central role for MNK activity.

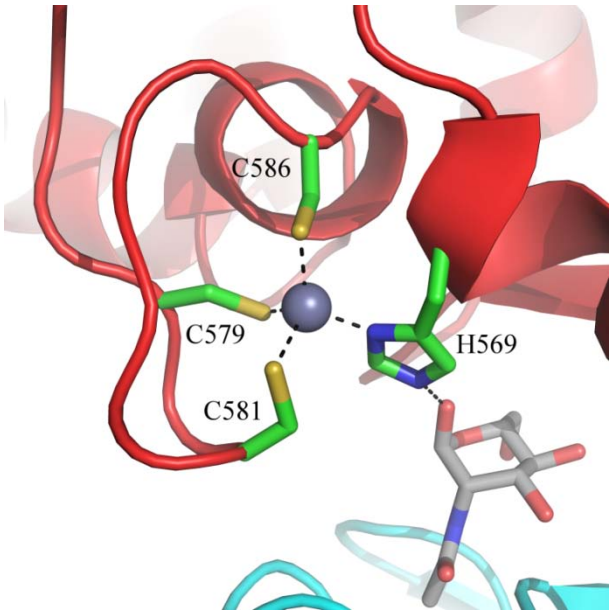

Figure 3.2.7: Zinc binding site.
The zinc atom (gray sphere) is tetrahedrichally coordinated by 3 cysteine residues (sulfur atoms in yellow) and a single histidine (nitrogen in blue). Zinc coordinates H569 in the right orientation for ManNAc binding.

3.2.9. MNK crystal structure - conclusion

High resolution crystal structures of the hMNK could be successfully obtained in this part of the work. The apo structure of the protein as previously described by Tong et al could be reproduced and verified [113]. As previously deducted from sequence and structure homology analysis the hMNK belongs to the ROK family, which are mostly prokaryotic proteins that possess sugar kinase activity and a transcriptional repressor function. With the novel crystal structures of the MNK/ManNAc, MNK/ManNAc/ADP and MNK/ManNAc-6-P/ADP we succeeded in characterizing the first human ROK in complex with its natural ligands (ManNAc and ADP). From these results, a detailed description of the active center was possible. ManNAc's binding conformation as well as its interaction with the network of amino acids in the binding pocket could be clarified. Also the nucleotide (ADP) binding pocket could be described and the reaction mechanism of ManNAc to ManNAc-6-P could be understood. The role of the two ions in the protein (Mg^{2+} and Zn^{2+}) could be better understood. Mg^{2+} is involved in the coordination and stabilization of ATP while Zn^{2+} is involved in the binding of ManNAc. Lacking those ions would significantly impair the activity of MNK. The MNK is a dimer in the crystal structure which correlates biochemical data for this enzyme in solution. The MNK undergoes a conformational change from an open conformation to a close conformation upon ManNAc binding enabling the reaction with ATP. D517 is found to be the essential amino acid for the transfer of the γ-phosphate form ATP to the 6-O of ManNAc. Through site directed mutational studies this finding will be verified in follow up experiments.

3.3. ManNAc kinase mutations

3.3.1. Hereditary inclusion body myopathy mutations of MNK

HIBM is a neuromuscular disease caused by mutations in both domains of the GNE. Two main hypotheses exist to why GNE mutations would cause HIBM. One relates the pathology of this disease to the decreased enzyme activity of the GNE which leads to hyposialylation and malfunction of important glycoproteins. The other believes that changes in the structure of the GNE, which often lead to decreased enzyme activity, may in fact disturb binding of other interaction partners which are essential in the proper development and function of muscle cells.

Even though solving this dilemma is out of the scope for this thesis, one purpose of this work was to use the novel insights about the MNK structure in combination with biochemical data to gain novel insights about the different MNK mutants, and further understand the molecular basis of HIBM pathogenicity.

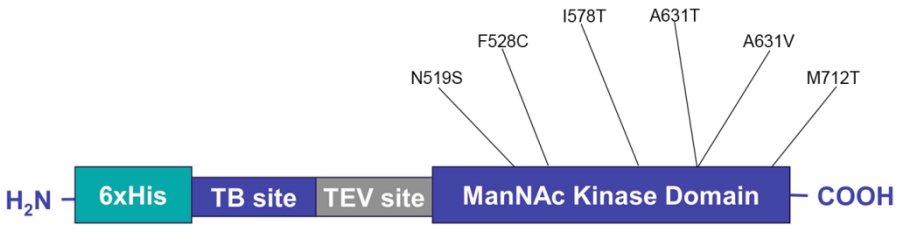

Figure 3.3.1: Schematic presentation of His-MNK HIBM mutant proteins

For this reason, the MNK domain of relevant HIBM GNE mutants, were cloned into the pET28a expression system using PCR with the given primers for His-MNK with *NdeI* and *XhoI* as endonuclease sites. These constructs contain a thrombin site (TB) and a Tobacco Etch Virus (TEV) protease site between the His-tag and the protein. The length of these constructs is 344 aa.

PCR was performed using 100 ng of template DNA (pFastBac-hGNE1 HIBM mutants for N519S, F528C, I587T, A631T, A631V and pBluescript-hGNE M712T mutant, which were kindly provided by Prof. Hinderlich) and the same primers for His-MNK. These PCR products were then subsequently cloned into pCR blunt vector. The amplified plasmids were then double digested with *Nde*I and *Xho*I endonuclease- The digested MNK fragments were then inserted into the pET28a vector. Positive clones were sequenced and verified to have the desired mutation at the given location. Positive and verified constructs were transformed into BL21 RIL *E.coli* cells for protein expression. Clones were cultured and purified according to the methods described for His-MNK. Purified proteins were then subjected to MNK enzyme activity assay, CD analysis, and crystallization attempts.

3.3.2. D517A and D517N mutations

Based on the insights from the determined active center of MNK, D517 was suggested to be the major catalytic residue of the kinase, since it engages in a direct hydrogen contract to ManNAc-6-O (Figure 3.3.2). To verify the fact that D517 is essential for MNK activity, two MNK mutants were prepared (D517A and D517N) and analyzed together with the HIBM mutants. Mutants were created according to the protocol of the "Quikchange™ Site-Directed-Mutagenesis Kit" with the primers given in the material and methods and pET28a-MNK construct as template. After the correct MNK mutation was verified by sequencing, the constructs were transformed into BL21 RIL *E.coli* cells. His-MNK mutants were expressed using the established method.

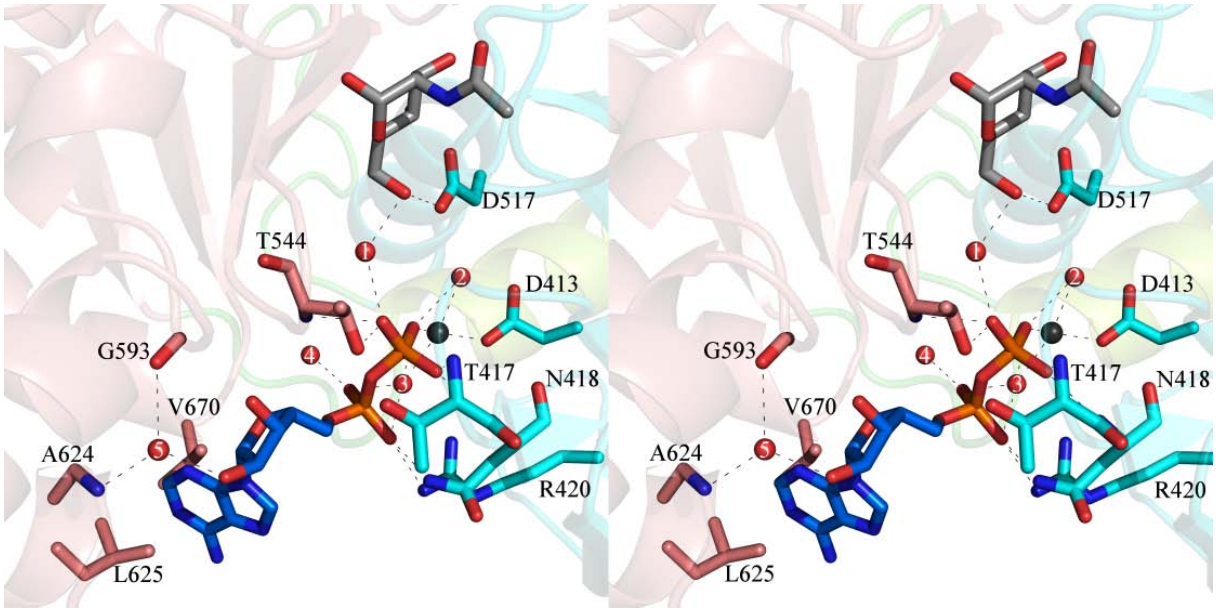

Figure 3.3.2: Stereo view of the ADP binding site.
The residue D517 is also depicted between the ManNAc and ATP binding pocket. Even though it is not directly involved in ADP binding, it is believed to be the key residue in the enzyme catalytic process.

3.3.3. MNK mutants purification

MNK N519S purification

One liter of E.coli culture containing MNK N519S mutant plasmids were collected and purified according to the described methods. The elutions from the Ni-NTA affinity column contain a high amount of purified MNK at 35 kDa on SDS-PAGE (Figure 3.3.3A, E1-E5), which were subjected to FPLC. From the gel filtration chromatograph a dominant protein peak at 55 kDa is visible, which indicates a mixture of monomer and dimer of this protein in solution (Figure 3.3.3B). After gel filtration protein aggregations (>140 kDa) and protein degradation (<35 kDa) could be still be observed in all the fractions (Figure 3.3.3C). However, the concentration of N519S MNK (35 kDa) is highest in the fractions A7-A11. For further analysis, therefore, the fractions A8-A10 were used.

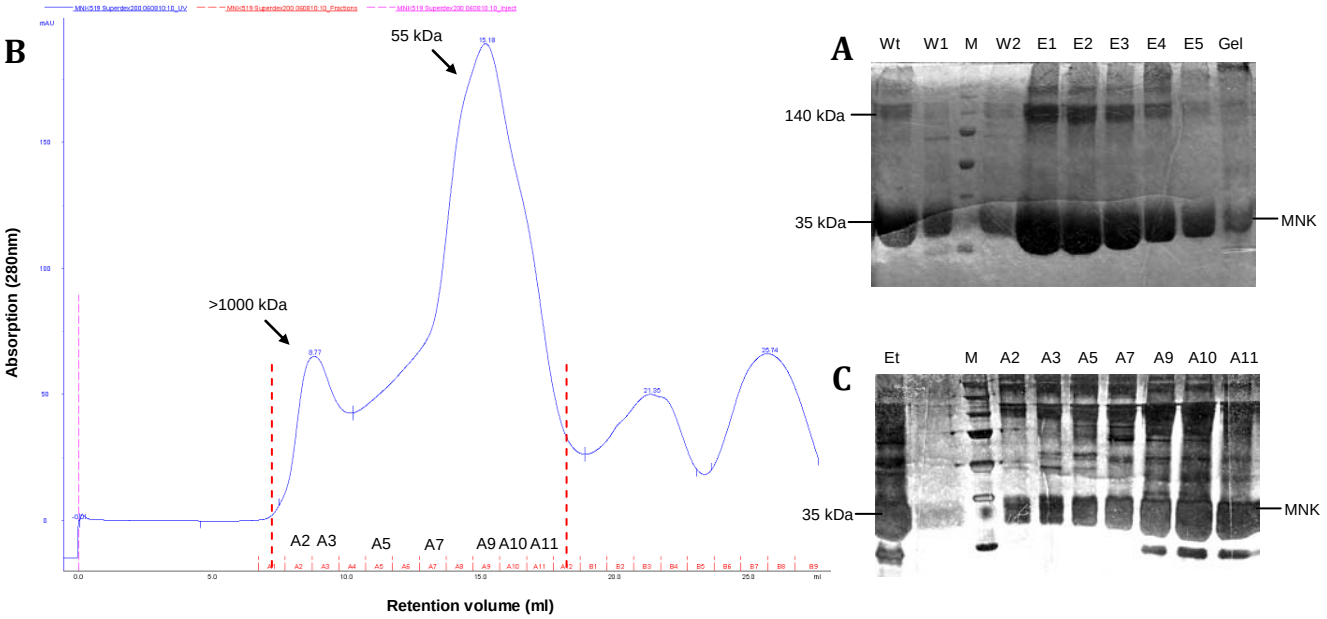

Figure 3.3.3: His-MNK N519S mutant purification

A. SDS-PAGE of His-MNK N519S after Ni-NTA affinity chromatography (20 µl of 500 µl fractions) Wt: wild-type MNK, W1/W2: Wash 1 & 2, E1-E5: Elutions, Gel: Ni-NTA gel after elution

B. Chromatograph of His-MNK N519S on Superdex 200 gel filtration

C. SDS-PAGE of His-MNK N519S Superdex 200 gel filtration fractions, (20 µl of 1 ml fractions), Et: Total elution prior gel filtration, A2-A11 FPLC fractions

MNK F528C purification

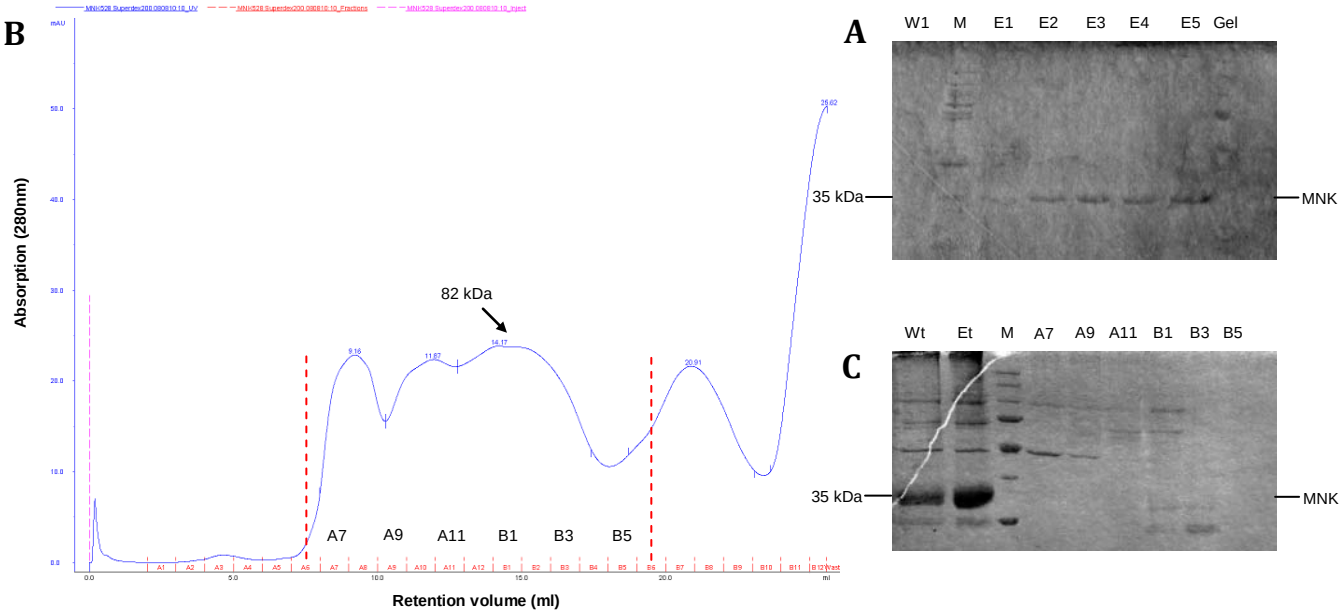

Figure 3.3.4: His-MNK F528C mutant purification

A. SDS-PAGE of His-MNK F528C after Ni-NTA affinity chromatography (20 µl of 1 ml fractions) W1: Wash, E1-E5: Elutions, Gel: Ni-NTA gel after elution

B. Chromatograph of His-MNK F528C on Superdex 200 gel filtration

C. SDS-PAGE of His-MNK F528C Superdex 200 gel filtration fractions (20 µl of 1 ml fractions)
Wt: Wild-type MNK, Et: Total elution prior gel filtration, A7-B5: FPLC fractions

F528C mutant is successfully expressed and purified by Ni-NTA chromatography. From the SDS-PAGE one could see that a single 35 kDa MNK band could be obtained (Figure 3.3.4A). The protein concentration was low so that for gel filtration all fractions E1-E5 were used. No dominant peak was visible in the gel filtration chromatogram (Figure 3.3.4B). The SDS-PAGE after the gel filtration shows a very low yield of purified proteins (Figure 3.3.4C). Therefore, for further activity assays the fractions prior to gel filtration (Et) was used.

MNK I587T purification

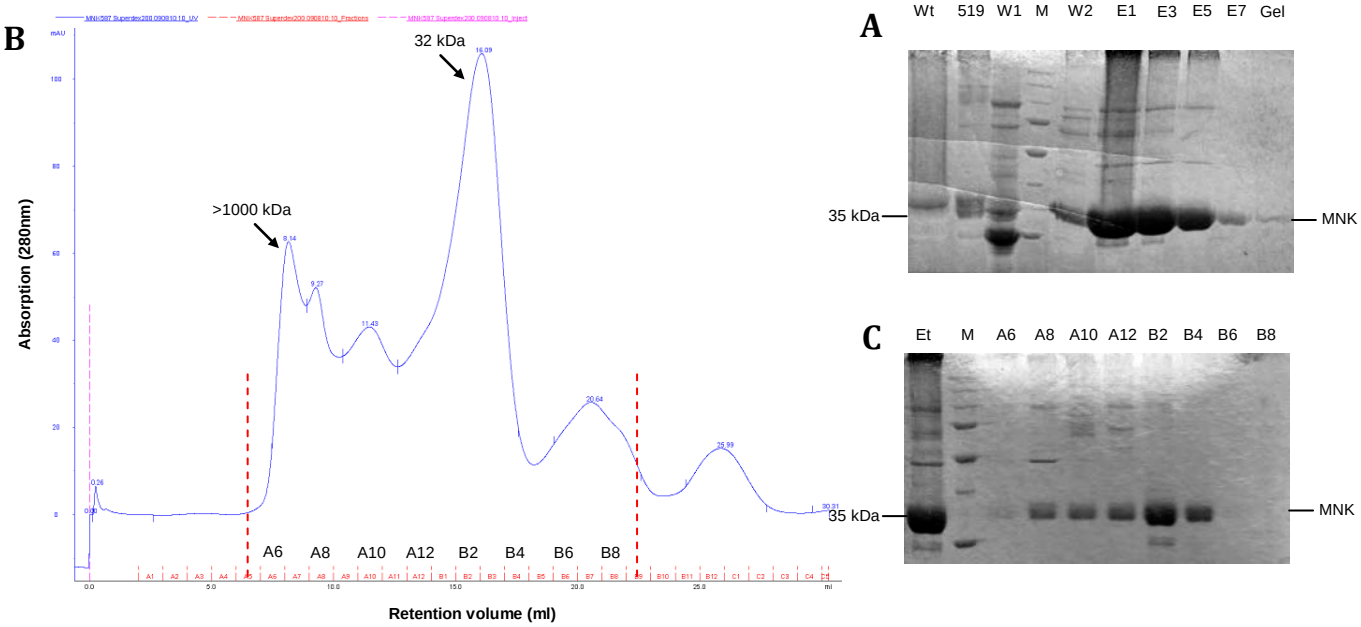

Figure 3.3.5: His-MNK I587T mutant purification
A. SDS-PAGE of His-MNK I587T after Ni-NTA affinity chromatography (20 µl of 1 ml fractions)
Wt: Wild-type MNK, 519: MNK N519S, W1/W2: Wash 1 & 2, E1-E7: Elutions, Gel: Ni-NTA gel after elution
B. Chromatograph of His-MNK I587T on Superdex 200 gel filtration
C. SDS-PAGE of His-MNK I587T Superdex 200 gel filtration fractions (20 µl of 1 ml fractions)
Et: Total elution prior gel filtration, A6-B8: FPLC fractions

The protein yield for I587T His-MNK was good. On SDS-PAGE this mutant after Ni-NTA elution is visible as a single band at 35 kDa (Figure 3.3.5A). In analytical gel filtration experiments the dominant peak of I587T is at Rv = 16.09 ml (32 kDa), which indicates a major monomeric state of this mutant in solution (Figure 3.3.5B). Fractions B2-B4 were also the purest fractions on SDS-PAGE and were selected for further experiments (Figure 3.3.5C).

MNK A631T purification

The protein yield of A631T MNK was high, which can be seen in the dominant protein band at 35 kDa in fractions E1-E5 (Figure 3.3.6A). The gel filtration of these fractions is associated with high degree of aggregation (Rv = 8.98 ml) and moderate yield of active MNK at Rv = 14.79 ml (72 kDa) (Figure 3.3.6B). For further analysis fractions A10-B1 were used (Figure 3.3.6C).

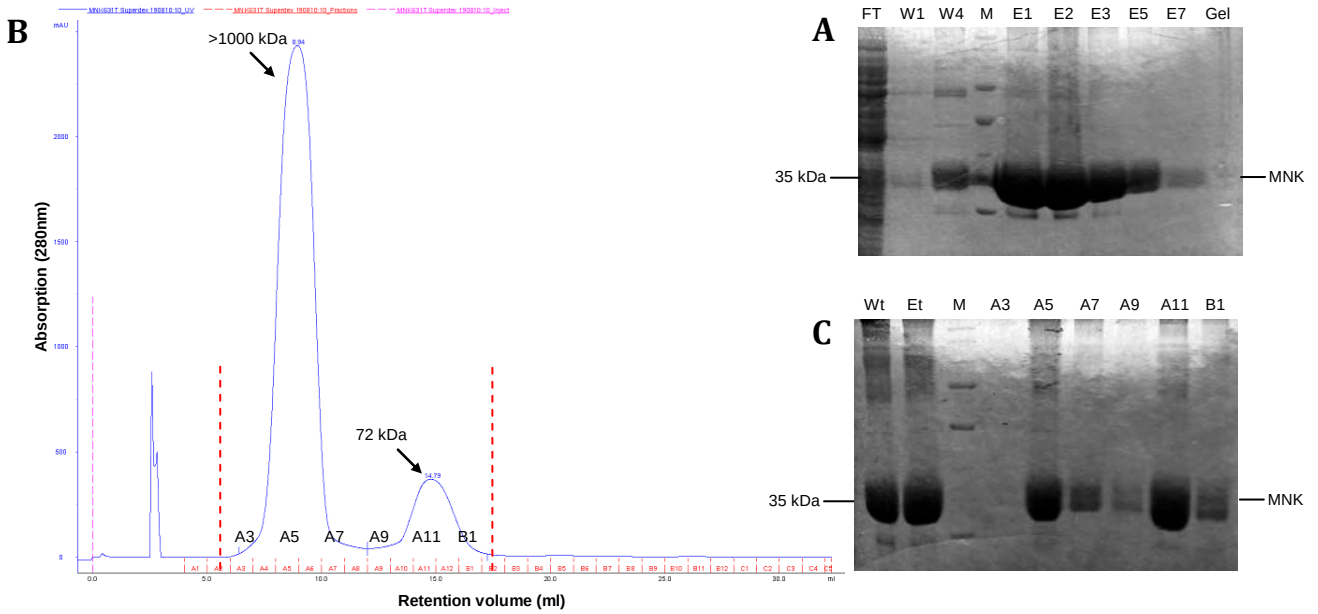

Figure 3.3.6: His-MNK A631T mutant purification
A. SDS-PAGE of His-MNK A631T after Ni-NTA affinity chromatography (20 µl of 1 ml fractions)
FT: Flow through, W1/W4: Wash 1 & 4, E1-E7: Elutions, Gel: Ni-NTA gel after elution
B. Chromatograph of His-MNK A631T on Superdex 200 gel filtration
C. SDS-PAGE of His-MNK A631T Superdex 200 gel filtration fractions (20 µl of 1 ml fractions)
Wt: Wild-type MNK, Et: Total elution prior gel filtration, A3-B1: FPLC fractions

MNK A631V purification

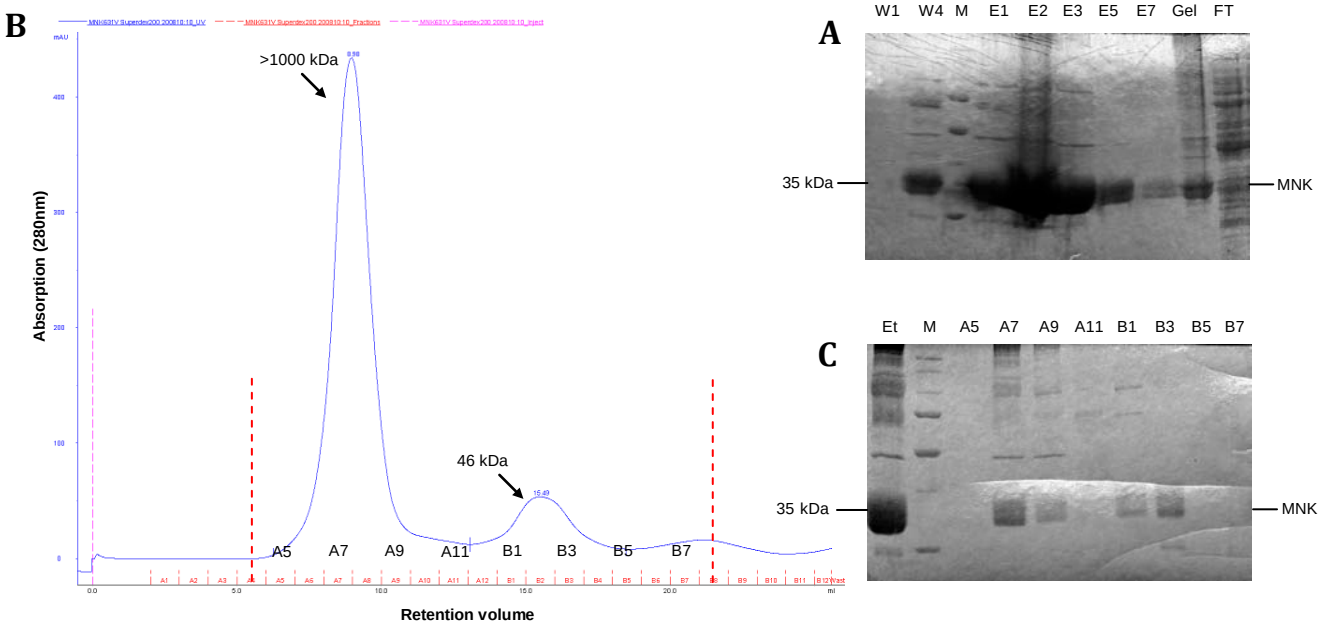

Figure 3.3.7: His-MNK A631V mutant purification
A. SDS-PAGE of His-MNK A631V after Ni-NTA affinity chromatography (20 µl of 1 ml fractions)
FT: Flow through, W1/W4: Wash 1 & 4, E1-E7: Elutions, Gel: Ni-NTA gel after elution
B. Chromatograph of His-MNK A631V on Superdex 200 gel filtration
C. SDS-PAGE of His-MNK A631V Superdex 200 gel filtration fractions (20 µl of 1 ml fractions)
Et: Total elution prior gel filtration, A5-B7: FPLC fractions

Compared to the A631T mutant, for the A631V MNK mutant purified protein yield was equally high (Figure 3.3.7A, E1-E5). On the gel filtration, protein aggregations are dominant. The MNK fraction is found at Rv = 15.49 ml (46 kDa), which makes it difficult to define the oligomeric state of this mutant in solution (Figure 3.3.7B). For further experiments the gel filtration fractions B1-B3 were selected. SDS-PAGE confirms that there is pure MNK in these fractions (Figure 3.3.7C).

MNK M712T purification

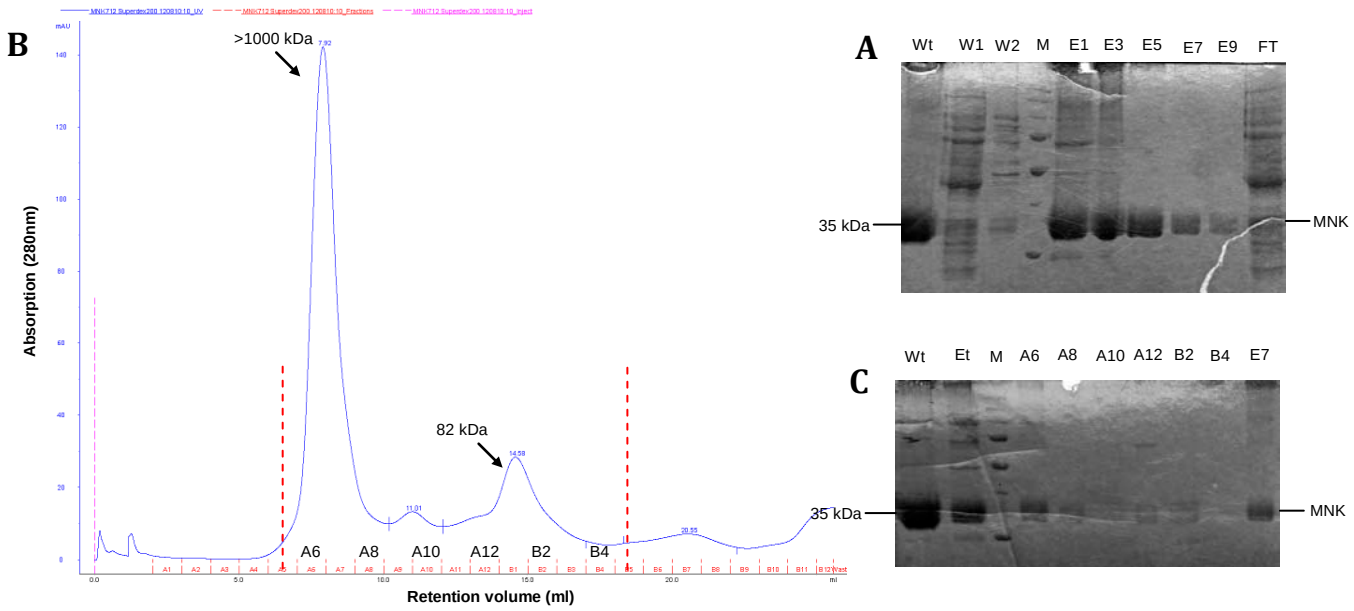

Figure 3.3.8: His-MNK M712T mutant purification
A. SDS-PAGE of His-MNK M712T after Ni-NTA affinity chromatography (20 µl of 1 ml fractions)
FT: Flow through, Wt: Wild-type MNK, W1/W2: Wash 1 & 2, E1-E9: Elutions, Gel: Ni-NTA gel after elution
B. Chromatograph of His-MNK M712T on Superdex 200 gel filtration
C. SDS-PAGE of His-MNK M712T Superdex 200 gel filtration fractions (20 µl of 1 ml fractions)
Wt: Wild-type MNK, Et: Total elution prior gel filtration, A6-B4: FPLC fractions, E7: M712T elution

A good amount of M712T MNK mutant could be eluted from the Ni-NTA column. It was verified on SDS PAGE with a clear band at 35 kDa in fractions E1-E9 (Figure 3.3.8A). The soluble protein fraction is visible at Rv = 14.58 ml (82 kDa) in the gel filtration chromatogram, which represents a dimeric state of this protein in solution (Figure 3.3.8B). Aggregations of M712T MNK protein are also very dominant. After confirming with SDS-PAGE, the fractions A12-B2 were collected for further experiments (Figure 3.3.8C).

MNK D517A purification

The purified protein yield of the D517A mutant was equally high as the wild type MNK. Very strong protein bands (E1-E5) are visible in the SDS-PAGE after Ni-NTA affinity chromatography (Figure 3.3.9A). The gel filtration shows a clear single band at 49 kDa without any aggregation formation (Figure 3.3.9B). In the fractions B9-C11 most of the purified proteins are collected (Figure 3.3.9C)

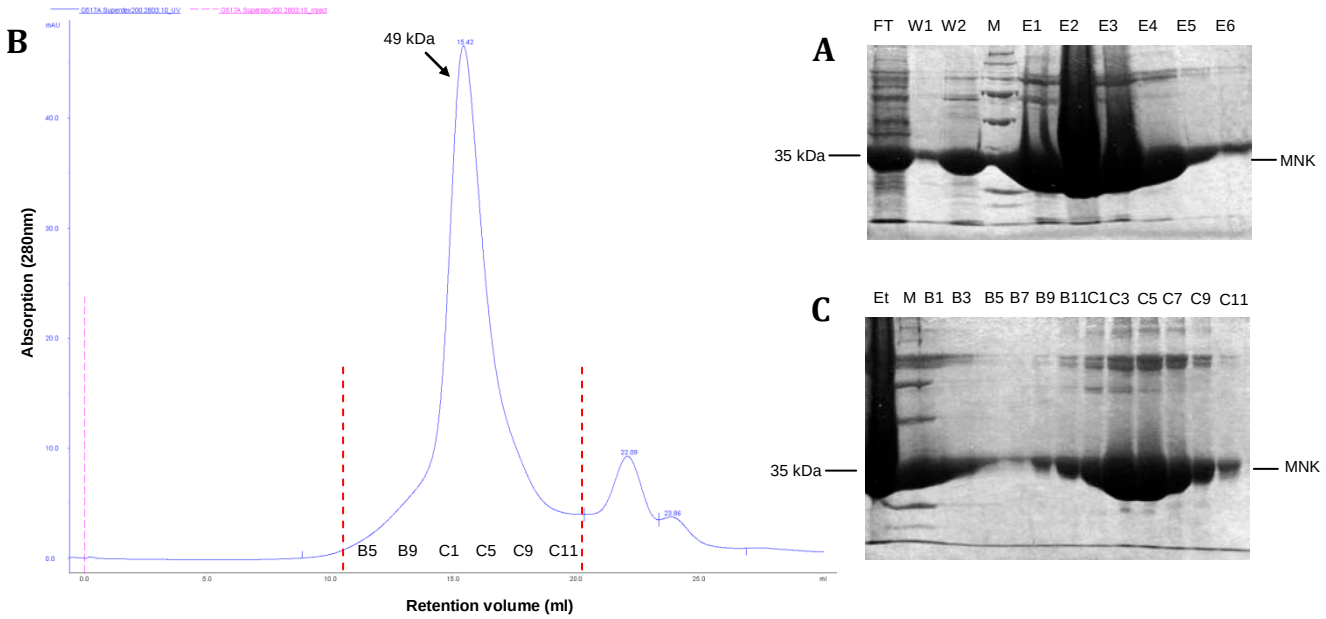

Figure 3.3.9: His-MNK D517A mutant purification
A. SDS-PAGE of His-MNK D517A after Ni-NTA affinity chromatography (20 µl of 1 ml fractions)
FT: Flow through, Wt: Wild-type MNK, W1/W2: Wash 1 & 2, E1-E6: Elutions
B. Chromatograph of His-MNK D517A on Superdex 200 gel filtration
C. SDS-PAGE of His-MNK D517A Superdex 200 gel filtration fractions (20 µl of 500 µl fractions)
Et: Total elution prior gel filtration, B1-C11: FPLC fractions

MNK D517N purification

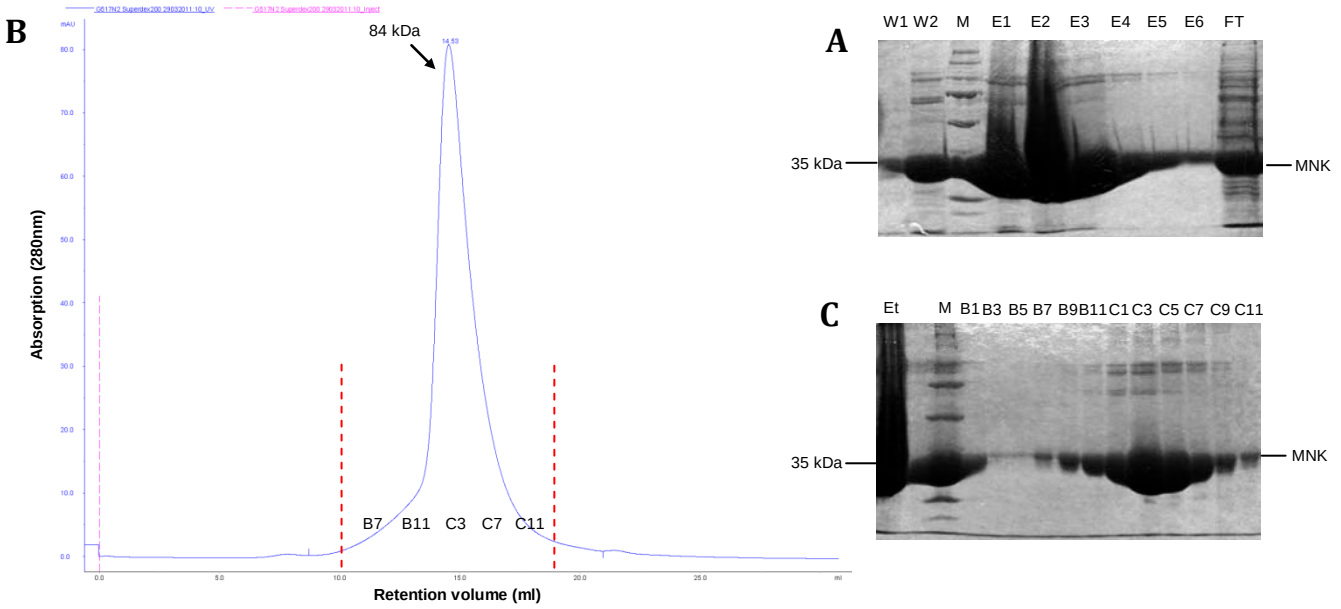

Figure 3.3.10: His-MNK D517N mutant purification
A. SDS-PAGE of His-MNK D517N after Ni-NTA affinity chromatography (20 µl of 1 ml fractions)
FT: Flow through, W1/W2: Wash 1 & 2, E1-E6: Elutions
B. Chromatograph of His-MNK D517N on Superdex 200 gel filtration
C. SDS-PAGE of His-MNK D517N Superdex 200 gel filtration fractions (20 µl of 500 µl fractions)
Wt: Wild-type MNK, Et: Total elution prior gel filtration, B1-C11: FPLC fractions

The yield of D517N MNK mutant in the Ni-NTA eluate is high (Figure 3.3.10A). These protein fractions (E1-E6) on gel filtration showed a clean single peak at 84 kDa, indicating a dimeric state of this protein in solution (Figure 3.3.10B). The FPLC fractions were analyzed with SDS-PAGE and demonstrated that fractions B7-C11 contained the highest concentration of MNK (Figure 3.3.10C)

3.3.4. MNK mutants characterization

The most important characteristics of the MNK mutants are summarized in table 3.3.1. After gel filtration the concentration of selected purified MNK protein fractions were measured. Protein yield was normalized at one liter *E.coli* culture. The specific activity was measured for each mutant and compared with the activity of the wild-type MNK set at 100%. Substrate specificity was assessed by comparing the activity of the mutants with different substrates (GlcNAc, ManNAc, ManNProp). A low specificity means that the kinase reaction took place equally well for all three indicated substrates. The oligomerization state in solution was determined from analytical gel filtration results. The stability of the proteins is an empiric measure of activity reduction after storage and repeated use.

Table 3.3.1: Characterization of MNK mutants
MNK mutants: name of the different MNK mutants, purified MNK yield: amount of pure hMNK after purification procedure for 1 l E.coli culture. Relative specificity: MNK enzyme activity for different mutants compared to wild-type. Substrate specificity: estimate of substrate specificity by comparing MNK activity for GlcNAc, ManNAc, ManNProp as substrate. Oligomerization: oligomerization state of MNK in solution. Stability: empiric value based on changes in MNK activity after storage at -20°C.

MNK mutants	Purified MNK yield [mg/l culture]	Relative specific activity [%]	Substrate specificity	Oligomerization	Stability
MNK	26.0	100	high	dimer	very good
N519S	11.5	25	low	monomer/dimer	good
F528C	3.7	78	low	monomer/dimer	good
I587T	10.9	24	low	monomer	very good
A631T	11.2	4	high	dimer	good
A631V	6.6	26	high	monomer/dimer	good
M712T	8.5	40	high	dimer	very good
D517A	25.5	0	n.A	monomer/dimer	n.A
D517N	25.7	0	n.A	dimer	n.A

For each mutant CD spectra were taken as described in the material & methods using the instruments in Prof. Koksch's lab. These results depict changes in the secondary structure of different mutants compared to the wild-type MNK.

Table 3.3.2: CD measurement results of MNK mutants
Secondary content of MNK mutants based on CD spectra results analyzed by CDNN with 31 base spectra

Samples	α-helix [%]	β-sheet [%]	β-turn [%]	Random coil [%]	Tm [°C]
MNK	20	24	18	38	44.6
N519S	15	27	18	40	49.9
F528C	10	31	18	41	n.A
I587T	11	30	18	41	n.A
A631T	10	31	17	42	n.A
A631V	12	29	17	42	n.A
M712T	11	30	17	42	n.A
D517A	16	26	18	40	45.3
D517N	23	22	18	37	50.5

MNK N519S

This mutation at the position 519 of the MNK changes an arginine to the shorter polar serine amino acid. This single point mutation resulted in major changes in the protein character. The soluble protein yield is less than 50% of the wild-type MNK and minor aggregations can be found. The specific activity for ManNAc is lost and the enzyme activity is reduced to 25% (Table 3.3.1). From the CD measurement results N519S has a slight increase in β-sheet and random coil content. These changes resemble the ones of D517A the most, which is closest in the primary sequence (Table 3.3.2). In the crystal structure N519 is located on α3 and hydrogen bounded to D515 over the side chain (ND2 to OD1) (Figure 3.3.11). This interaction orientates N516 and D517, two of the sugar binding residues. In the variant N519S no hydrogen bound with D515 is possible, which consequently diminish the binding affinity of the sugar, which would explain the observation of decreased activity and low specificity.

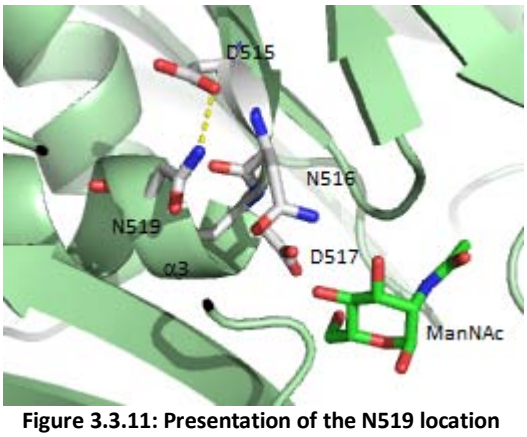

Figure 3.3.11: Presentation of the N519 location

MNK F528C

The protein yield of this mutant, which changes a bulky non-polar phenylalanine to a cysteine at position 528, is lowest compared to other mutants. From FPLC gel filtration experiments this mutant may exist as a mixture of dimer and monomer in solution (Figure 3.3.4B). Its enzyme activity is 78% compared to wild-type and, as for N519S, its specificity for ManNAc was low (Table 3.3.1). From the

CD results, a significant change in the secondary structures could be observed. The α-helix content is decreased, parallel to an increase in β-sheet and random coil (Table 3.3.2). From the crystal structure, F528 is located at the very C-terminus of α3 in a hydrophobic interface with α11. The mutation of a bulky hydrophobic residue like phenylalanine to a small polar one can disrupt this interaction and affect the orientation of the sugar binding residues at the end of α3 (Figure 3.3.12).

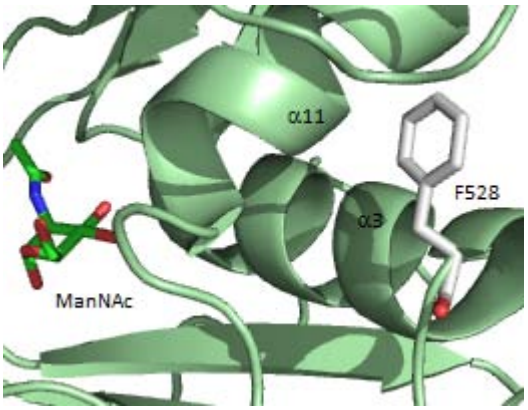

Figure 3.3.12: Presentation of the F528 location

MNK I587T

The mutation from a hydrophobic isoleucine to a polar threonine resulted in a big decrease in activity and destabilization of the enzyme. The enzyme activity of this mutant is 24% of the wild-type, also with low specificity for ManNAc (Table 3.3.1) and a lot of aggregations were formed during gel filtration. MNK I587T also appears to be predominantly a monomer in solution (Figure 3.3.5B). CD measurements showed similar structural changes compared to the F528C mutant. Based on the crystal structure, I587 is found buried and solvent inaccessible in the α5. Its location between C586, which is involved in zinc binding, and E588, which is involved in sugar binding, suggests that a mutation to a polar residue like threonine may disturb both, zinc and sugar binding (Figure 3.3.13). Since zinc is a very important stabilizing element of this enzyme, the impairment of I587T to bind zinc may disturb the propensity of this mutant to form dimers.

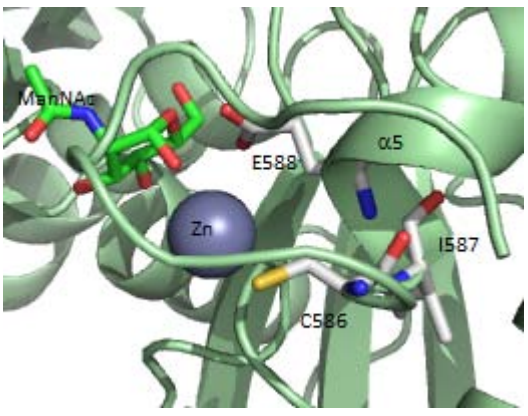

Figure 3.3.13: Presentation of the I587 location

MNK A631T and A631V

A631T and A631V, despite being a mutation at the same site, have very different character, relating to purification and activity. The soluble protein yield of A631T is relatively high (11.2 mg/l) but the enzyme activity is almost non-existent (4%). A631V, on the other hand, has a very low protein yield (6.6 mg/l) but the activity is significantly higher (26%) than that of A631T (Table 3.3.1). Both mutants produced very intensive protein bands at 35 kDa on SDS-PAGE after Ni-NTA chromatography (Figure 3.3.6/7A) but form a lot of aggregations during gel filtration (Figure 3.3.6/7B). The soluble A631T is found in fractions around 72 kDa, while A631V comes down a little bit later at 46 kDa, which may indicate a mixture of monomeric and dimeric proteins in solution. Changes in secondary structures are similar for both mutants as observed by CD measurements. The concentration of random coil is highest for all mutants (42%), together with M712T. For A631T the percentage of β-sheet (31%) is slightly higher than that of A631V (29%) (Table 3.3.2). From crystallographic data, A631 is located at the C-terminal end of α7 (Figure 3.3.14). It is far away from the sugar binding site and a mutation of this residue is likely to impair rather the ATP binding, which fits with the low activity observed for the two mutants and the conservation of the specificity for ManNAc. The change from a small non-polar alanine to a non-polar valine or a polar threonine may have different structural effects which may account for the differences in their character.

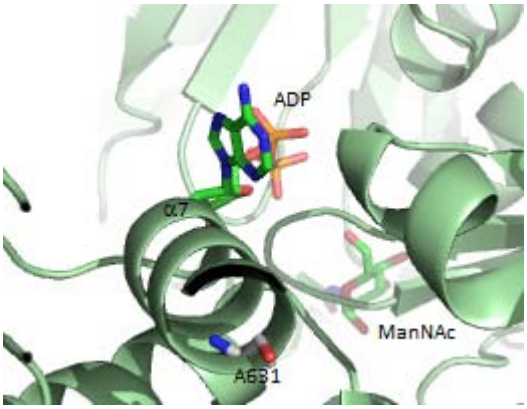

Figure 3.3.14: Presentation of the A631 location

MNK M712T

The change from the hydrophobic methionine to a polar threonine at position 712 is the most common mutation in HIBM. As can be observed by gel filtration results aggregations of this mutant are also dominant (Figure 3.3.8B) causing the protein yield to be moderate (8.5 mg/l) (Table 3.3.1). The activity of the dimeric protein is 40% of wild-type MNK and the specificity is intact. As other HIBM mutants, CD results demonstrated an increased in random coil (42%) and β-sheet (30%) and decrease in α-helix structures (11%) for the M712T mutant (Table 3.3.2). From crystallographic data, one can see that M712 is located on the α11 and stabilizes β4 and β7 by hydrophobic interactions.

β4 and β7 bear four of the sugar binding residues in a loop at its C-terminus. Threonine is shorter than methionine and unable to make these interactions, which might explain the impact of this mutation.

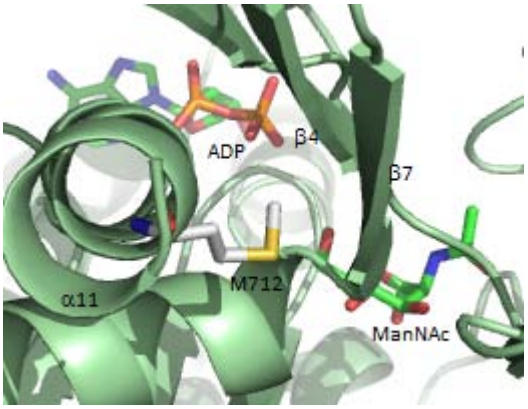

Figure 3.3.15: Presentation of the M712 location

MNK D517A and D517N mutants

CD517 mutants compared to HIBM mutants have a very high protein yield (Table 3.3.1) and very low aggregation formation during purification procedure (Figure 3.3.9/3.3.10A). The CD spectra also showed very similar curves compared to wild-type MNK unlike other HIBM mutants. No major differences were found for the variant D517N, whereas D517A showed a small increase of the random coil content (40%) with respect to the wild type (38%) (Table 3.3.2). The enzymatic activity for both D517 mutants was zero, which was predicted by crystallographic data (Figure 3.3.16).

Since D517 is involved in ManNAc coordination, it was important to find out how these mutations affect ManNAc binding. Therefore, isothermal titration calorimetry (ITC) experiments were carried out together with Jacobo Martinez. The dissociation constants (K_D) for wild type wt-MNK/ManNAc were determined to be 2.5 µM and for D517N/ManNAc to be 259 µM. D517N shows 100-fold lower affinity compared to wt-MNK, but this binding affinity would still be sufficient for enzyme activity. All other mutants (HIBM mutants) tested in this study showed a weaker binding affinity for ManNAc, and no K_D could be obtained for them with ITC, but yet partial enzyme activity could be observed (Table 3.3.1). These biochemical results confirm that D517 is an essential amino acid for MNK enzyme activity, which had been predicted by crystallographic analysis before.

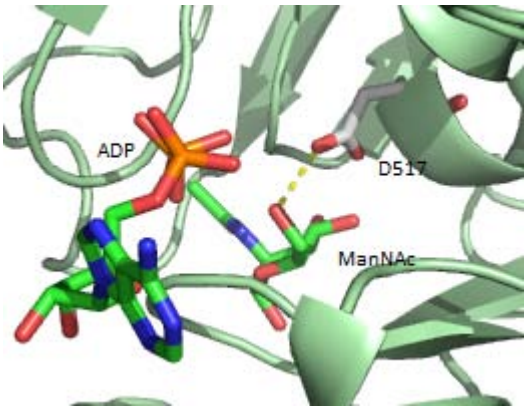

Figure 3.3.16: Presentation of the D517 location

3.3.5. MNK mutants - conclusion

All in all, significant changes could be observed for different HIBM mutations. The yield of these mutants after gel filtration in general is lower than this of wild type MNK, due to stronger aggregation formation. In general, the activities of all MNK HIBM mutants were also reduced (Table 3.3.1). CD measurements indicated that the secondary structures HIBM mutants have been changed. The content of α-helices is reduced, accompanied by a slight increase in β-sheets and random coils (Table 3.3.2). The specificity of the different mutants was also significantly changed. For mutants N519S, I528C, I587T there were no significant differences in activity when exchanging ManNAc for GlcNAc or ManNProp. Other mutants (A631T, A631V, M712T) are highly specific for ManNAc. Most of the HIBM mutants remain predominantly dimeric in solution. N519S, F528C, 631V appears to also have monomeric structure in solution. Only I587T seems to be predominantly monomeric.

A universal feature of the HIBM mutants was the higher propensity to form aggregations. If the samples are not held on ice permanently white precipitations gradually forms. This effect is worsened when protein concentrations were high. For the crystallization of the wild-type MNK at least 10 mg/ml protein concentration was needed. Therefore, this character of these mutants poses a limitation on further crystallization attempts.

Given the highly compact overall MNK fold, however, it is understandable that many single point mutations are prone to disrupt the MNK architecture. An extensive structural mapping of these disease-associated mutations has been performed previously [113, 124]. Therefore, this work focused only on six HIBM point mutations biochemically characterized. Structural mapping were performed with the newly gained structural information about the ManNAc and nucleotide binding sites. With these insights a better understanding could be gained about the different loci of mutations and their effects on activity and specificity.

From the crystal structures, the position D517 was predicted to be the key catalytic residue of this kinase, since it appears to stabilize the O6 of ManNAc for the phosphate transfer. After expressing and analyzing two D517 mutants (D517A and D517N), it could be confirmed that even though binding of ManNAc was still intact for the D517N mutant, the activity was completely lost. Except the lack of activity, purification profile and CD measurement results are similar to wild-type MNK (Table 3.3.1/2).

3.4. MNK inhibition study

A goal of this work was to find an inhibitor for sialic acid expression on cell surface. In previous attempts, predominantly the 2-epimerase domain of the GNE was the target for inhibition search. Substrate and transition state analogs of the 2-epimerase domain were usually big hydrophilic molecules which cannot penetrate well the plasma membrane and be effective in cells. In order to avoid these complications, this study aimed to design smaller more membrane permeable structures as an inhibitor of the MNK. Parallel to the X-ray structures, lead inhibitor modeling and chemical synthesis, *in vitro* as well as cellular assays are needed to verify their effects.

Consequently, in this part of the work biochemical and cellular assays were established to access the activity of MNK in relation to cell surface sialic acid expression. Potential structures like GlcNProp and 3-O-MeGlcNAc, which were published to be inhibitors in cell-free systems [98, 99], were re-evaluated. Other cellular assays were used to determine the biological effects of these inhibitors.

Since the GNE as a whole enzyme is very instable and hard to work with, the MNK kinase activity assays would be a convenient and reliable substitute to test for the kinase activity of the GNE. New potential inhibitors can be directly tested on these established biochemical and cellular systems.

3.4.1. Inhibition of MNK with different GlcNAc analogs in vitro

GlcNAc and ManNAc analogs, which were kindly provided by Prof. Reutter, have usually a single modification at the C2 position as substitution for the N-acetyl group (Figure 3.4.1).

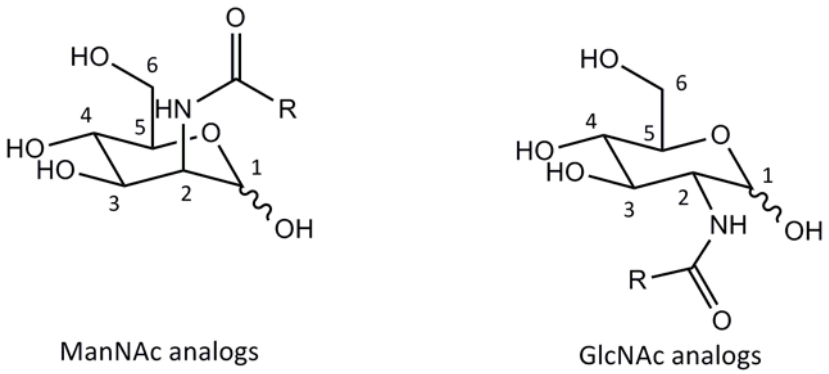

Figure 3.4.1: Schematic presentation of ManNAc and GlcNAc analogs
GlcNAc (R=methyl), GlcNProp (R=ethyl), GlcNCyc (R=cyclopropyl), GlcNHex (R=pentyl), 3OMeGlcNAc (3-O-methyl-N-acetyl-glucosamine), ManNProp (R=ethyl), ManNBut (R=propyl), ManNiBut (R=isopropyl), ManNPent (R=butyl), ManNBz (R=benzyl), ManNPh (R=phenyl)

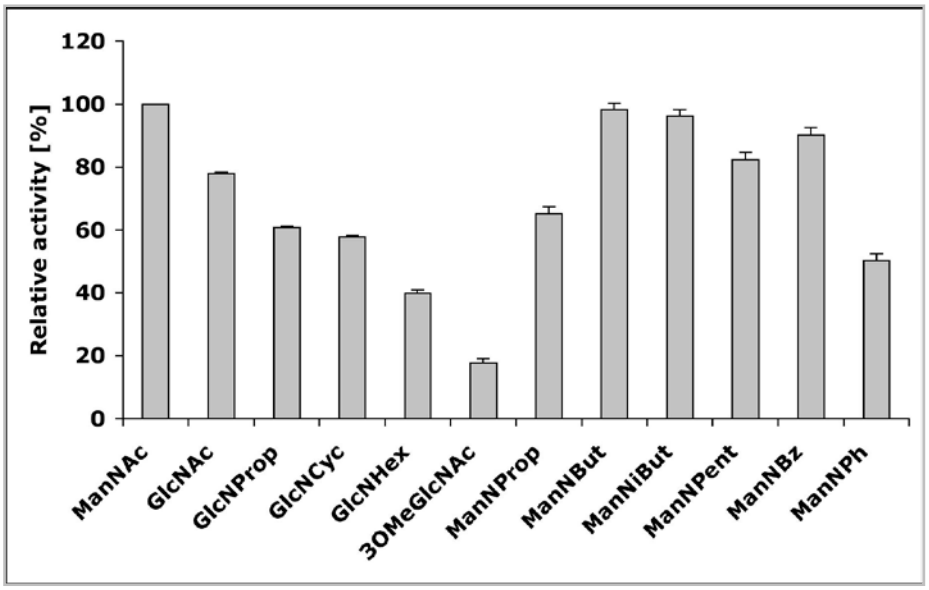

Figure 3.4.2: ManNAc kinase activity with GlcNAc and ManNAc analogs as inhibitors
2.5 µg MNK, 200 µM ManNAc, 10 mM HexNAc analogs were added together with other reagents as described in methods for MNK activity assay. The inhibitory effects of those substances are expressed as reduced kinase activity compared to ManNAc treated samples. Absorption of the substrates at 340 mM has been deducted. Results depicted are mean values of 3 independent measurements.

GlcNAc and other GlcNAc analogs at high concentration (10 mM) can reduce the activity of MNK (Figure 3.4.2). The strongest inhibitory effect was observed for 3-O-MeGlcNAc, with up to 80% inhibition. ManNAc analogs exert less inhibitory effects on the MNK with the exception of ManNProp, which is also a substrate, and ManNPh. All in all, at concentrations of 10 mM these substrates cannot be classified as specific inhibitors and are only valid as a model structure for further compounds.

In a previous publication by Grünholz et al. [98] GlcNProp was claimed to be a good inhibitor of sialic acid de novo synthesis. More likely, they concluded, it is the phosphorylated form of this sugar which is responsible for this effect. In cell lysates GlcNProp would be phosphorylated to GlcNProp-6-phosphate via the rather unspecific GlcNAc kinase and may in this way inhibit the MNK. In protein assays with pure MNK this effect cannot be observed. The proposal that metabolites of the substrate could be better sialic acid synthesis inhibitors in cells, was the premise for further cellular experiments on GlcNAc analogs: GlcNProp, GlcNCyc and GlcNHex.

3.4.2. Inhibition of cell proliferation with GlcNAc analogs

In order to do a series of experiment on cells, first the toxicity of these substrates on certain cellular systems has to be assessed. For further analysis a certain number of cells are needed for subsequent assays, so the parameters of cell growth with these exogenic reagents were established in the beginning. Therefore, proliferation assays were performed for GlcNProp, GlcNCyc and GlcNHex on

various cell lines. Included were different human tumor cell lines, sarcomas as well as carcinomas. Adhesive and suspension cells were equally studied. As controls, a non-tumor cell line Hekl, primary fibroblast provided by Dr. M. Kontou, and a non-human cell line “A-Zellen”, murin adenocarcinoma kindly provided by Dr. A. Klein, were included.

Different concentrations of substrates (2 mM, 5 mM, 10 mM) were applied for different time frames (1 d, 3 d, 5 d) on different initial cell concentrations (20000 cells/ml, 40000 cells/ml, 80000 cells/ml) to establish the growth pattern. For the purpose of comparability, data for 5 mM of different substrates incubated for 3 days with the initial cell concentration of 40000 cells/ml are presented in table 3.4.1.

Table 3.4.1: Cell proliferation of different cell lines treating with 5 mM of GlcNAc analogs for 3 days
GlcNAc analogs were diluted in PBS. Relative proliferation rates are presented in % compared to PBS as control (100%). Results are mean values of 3 independent measurements.

Cell lines	GlcNAc	GlcNProp	GlcNCyc	GlcHex
Mela-2	94	65	77	51
Saos-7	93	104	93	93
LN 405	92	95	92	92
Mcf-7	91	67	93	91
Bon-1	85	98	76	85
Panc-1	99	84	94	97
Raji	94	36	73	71
HL60	95	53	74	73
Jurkat	95	30	89	89
U266	106	52	70	74
A-Zellen	99	75	76	47
Hekl	98	100	96	98

In general GlcNProp is the most potent anti-proliferative substrate compared to GlcNCyc and GlcNHex (Table 3.4.1). From the results one could see that quickly growing and aggressive cell lines are inhibited by these substances the most. On primary fibroblast, Hekl, those analogs have almost no effect. Based on these results, 4 tumor cell lines (Panc-1, Mela-2, HL60, Raji) were selected for further studies. Two cell lines (Panc-1 and Mela-2) are adhesive cells. The other two (HL60 and Raji) are suspension cell lines. The susceptibility on proliferation inhibition of these cell lines ranges from low (>80% Panc-1), middle (40-80% Mela-2, HL60) to high (>40% Raji) (Table 3.4.1). They also have different growth rates and cell surface sialic acid expression (Figure 3.4.3).

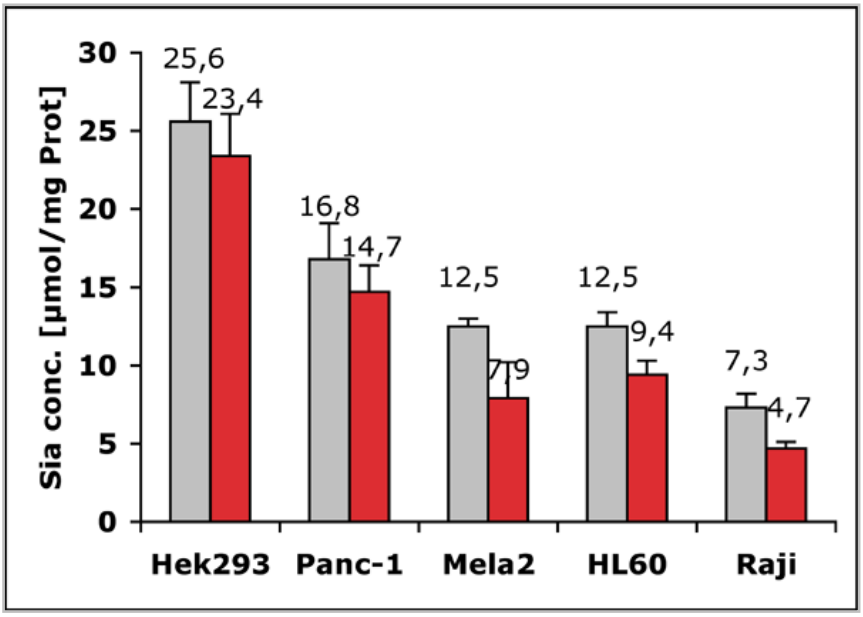

Figure 3.4.3: Sialic acid expression in different cell lines
Cells were cultured under standard conditions as described and measured for sialic acid expression using the periodate-resorcinol method. Total sialic acid expression ( ) and bound sialic acid expression ( ) were measured according to Jourdian et al [107]. Sialic acid concentrations for each cell line were normalized with protein concentration.

3.4.3. Inhibition of sialic acid expression in cells

In the following experiments the growth rate of these cells are more precisely determined using cell counting assays. A closer look was also taken at the effects of GlcNAc analogs on cell morphology. The total cellular amount of sialic acid, the amount of bound sialic acids as well as cell surface sialic acid expression were determined in order to assess the effect on sialic acid expression of these substances in cell. The results will be presented for each of the four cell lines.

Panc-1: Human Pancreas Carcinoma

Panc-1 is an adhesive cell line from human pancreas carcinoma. Under normal conditions the shape of the cells are round. The growth rate of this cell line is slow with doubling time of about 52 h. Panc-1 cells are used as an *in vitro* model of non-endocrine pancreatic cancer for tumorigenicity studies. The cells possess the type B phenotype for glucose-6-phosphate dehydrogenase (G6PD) and overexpress heregulin/human epidermal growth-factor receptor 2 (HER2/neu) oncogene (which is present in 60-70% of human pancreatic carcinomas), but are estrogen receptor (ER) negative. Cells are also negative for MUC4 (sialomucin complex SMC, an intramembrane ligand for ErbB2) and positive for Smad4 (a TGF-β signaling cascade protein inactivated in human gastrointestinal cancers).

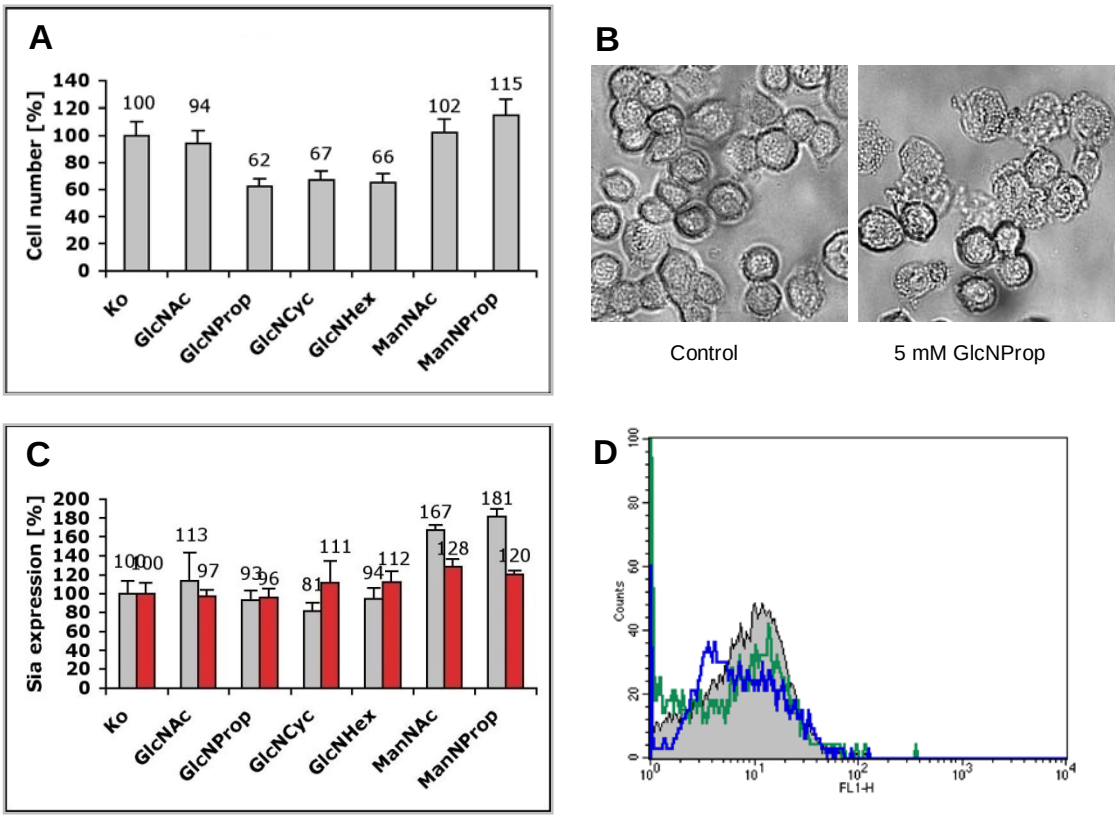

Figure 3.4.4: Effect of GlcNAc analogs on Panc-1
A. Effect of GlcNAc on Panc-1 growth. Cells were cultured under standard condition with addition of 5 mM analog in the medium. After 3 days the cell count of living cells were determined and compared with control.
B. Morphology of Panc-1 cells treated with 5 mM GlcNProp for 3 days.
C. Total sialic acid expression (▭) vs. bound sialic acid expression (▭) of Panc-1 cells after treatment with 5 mM of the indicated GlcNAc analogs for 3 days.
D. LFA-FITC stained FACS analysis of Panc-1 cells treated with PBS (grey), 5 mM GlcNAc (green) and 5 mM GlcNProp (blue) for 3 days.

This cell line experienced changes in morphology for some cells and effect on growth rate after treatment with GlcNAc analogs (Figure 3.4.4A). The growth rate of this cell line is 2/3 of the control when cultured with GlcNAc analogs. This effect is rather unspecific for all GlcNAc analogs. Some groups of cells as shown are destroyed with broken cell membranes and a flattened cell shape (Figure 3.4.4B). Signs of apoptosis, which was tested by microscopic and Anexin IV FACS analysis could not be observed (Data not shown). The effect of the substances on sialic acid expression is insignificant. There were no changes in the expression of total or bound sialic acid (Figure 3.4.4C) nor cell surface expression of sialic acid (Figure 3.4.4D). Noteworthy was the significant increase in total sialic acid expression after culturing the cell on enriched ManNAc and ManNProp medium. A significant increase of total sialic acid expression could also be observed for ManNAc (167%) and ManNProp (181%) (Figure 3.4.4C). These data indicate that excess ManNAc and also ManNProp can be transformed into an excess sialic acid expression in this cell line.

Mela-2: Human Melanoma

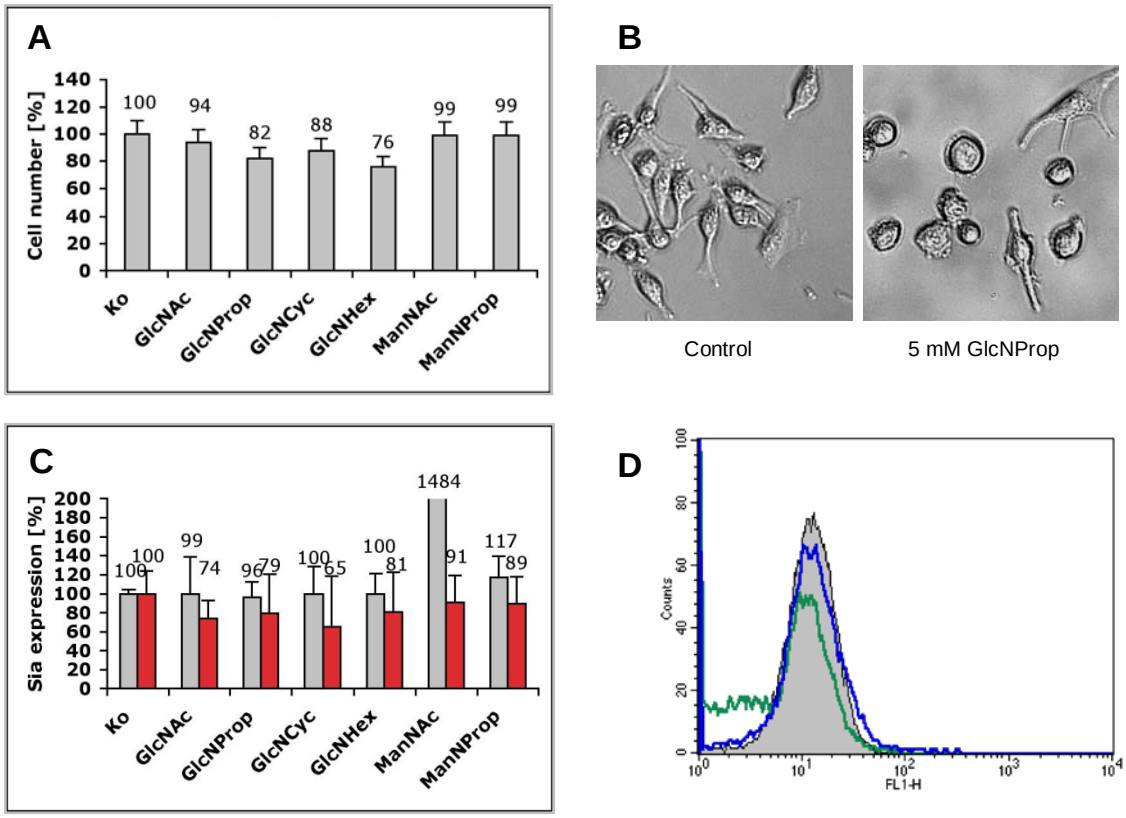

Figure 3.4.5: Effect of GlcNAc analogs on Mela-2
A. Effect of GlcNAc on Mela-2 growth. Cells were cultured under standard condition with addition of 5 mM analog in the medium. After 3 days the cell count of living cells were determined and compared with control.
B. Morphology of Mela-2 cells treated with 5 mM GlcNProp for 3 days.
C. Total sialic acid expression ( ) vs. bound sialic acid expression ( ) of Mela-2 cells after treatment with 5 mM of the indicated GlcNAc analogs for 3 days.
D. LFA-FITC stained FACS analysis of Mela-2 cells treated with PBS (grey), 5 mM GlcNAc (green) and 5 mM GlcNProp (blue) for 3 days.

Mela-2 is a human melanoma cell line, which originates from a malignant, metastatic melanoma [125]. It is a malignant, adhesive, relatively quick growing (doubling time = 48 h) tumor cell line from human metastatic melanoma. The cell shape in culture is more lengthily and stretched. Under the influence of GlcNAc analogs the growth rate is slightly inhibited (about 80% growth rate) (Figure 3.4.5A). There is an increased number of round not strongly adhesive cell groups (Figure 3.4.5B), but in general the morphology of the cells was intact, with no signs of membrane leakage or apoptosis. There is a slight decrease in the bound sialic acid concentration of treated samples (Figure 3.4.5C), which may correlate with the weaker adhesive potential. FACS analysis of cell surface sialylation reveals, however, no significant changes between treated and untreated cell samples (Figure 3.4.5D). An interesting observation is the insignificant increase in total sialic acid level after treatment with ManNProp (117%) compared to ManNAc (1484%) (Figure 3.4.5C). Unlike Panc-1, ManNProp appears not to be readily accepted and transformed into the respective sialic acid residues in this cell line.

HL60: Human leukemia cell line

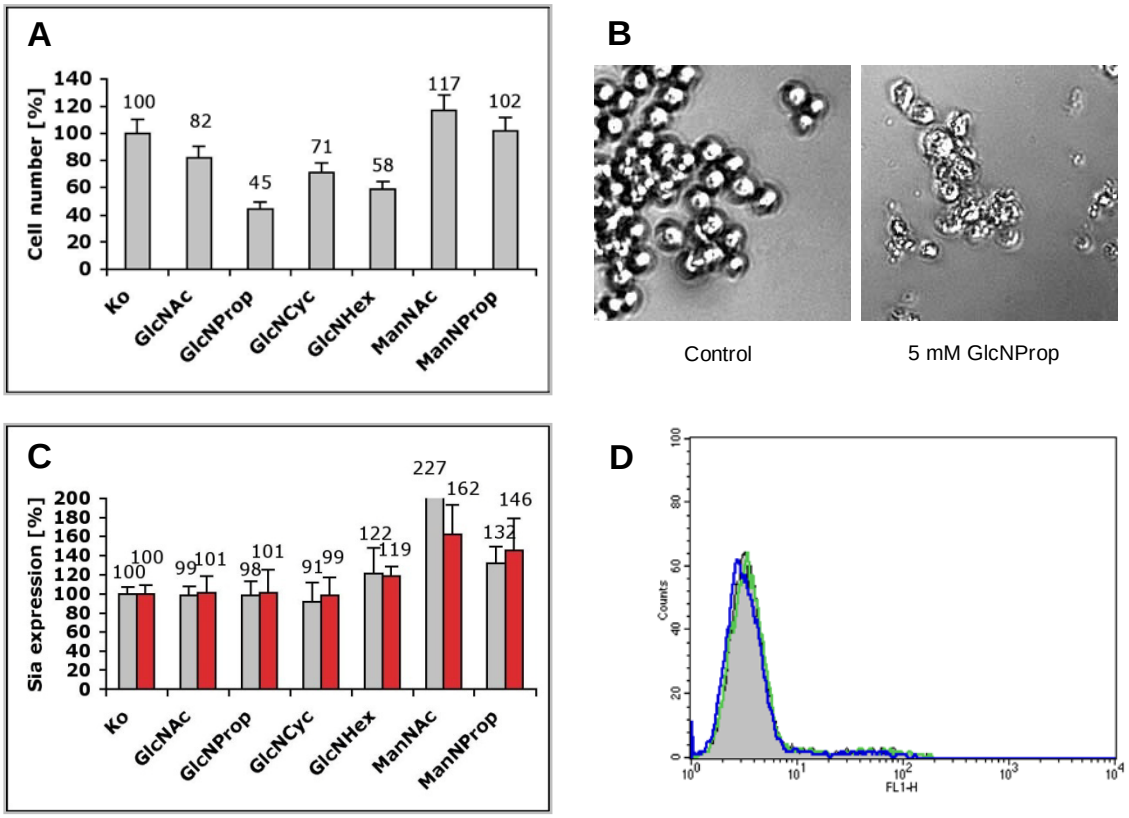

Figure 3.4.6: Effect of GlcNAc analogs on HL60
A. Effect of GlcNAc on HL60 growth. Cells were cultured under standard condition with addition of 5 mM analogs in the medium. After 3 days the cell count of living cells were determined and compared with control.
B. Morphology of HL60 cells treated with 5 mM GlcNProp for 3 days.
C. Total sialic acid expression ( ) vs. bound sialic acid expression ( ) of HL60 cells after treatment with 5 mM of the indicated GlcNAc analogs for 3 days.
D. LFA-FITC stained FACS analysis of HL60 cells treated with PBS (grey), 5 mM GlcNAc (green) and 5 mM GlcNProp (blue)

HL60 is a human acute myeloid leukemia cell line. They grow well as suspension cells rather separately from each other. The shape is round and the growth rate is high (doubling time = 36 h). This cell line can be induced to conduct differentiation studies. They exhibit phagocytic activities and respond to DMSO, phorbol ester (e.g. TPA) and other chemotactic reagents. They were very susceptible to exogenous reagents like GlcNProp with growth inhibition up to 50% (Figure 3.4.6A). Many cells are deformed and grouped together (Figure 3.4.6B). The effect of GlcNAc analogs on sialic acid expression was almost non-existent. Resorcinol periodate assay as well as LFA FACS analysis revealed no significant changes in total or cell surface sialylation (Figure 3.4.6C/D).

Raji: Burkitt's lymphoma cell line

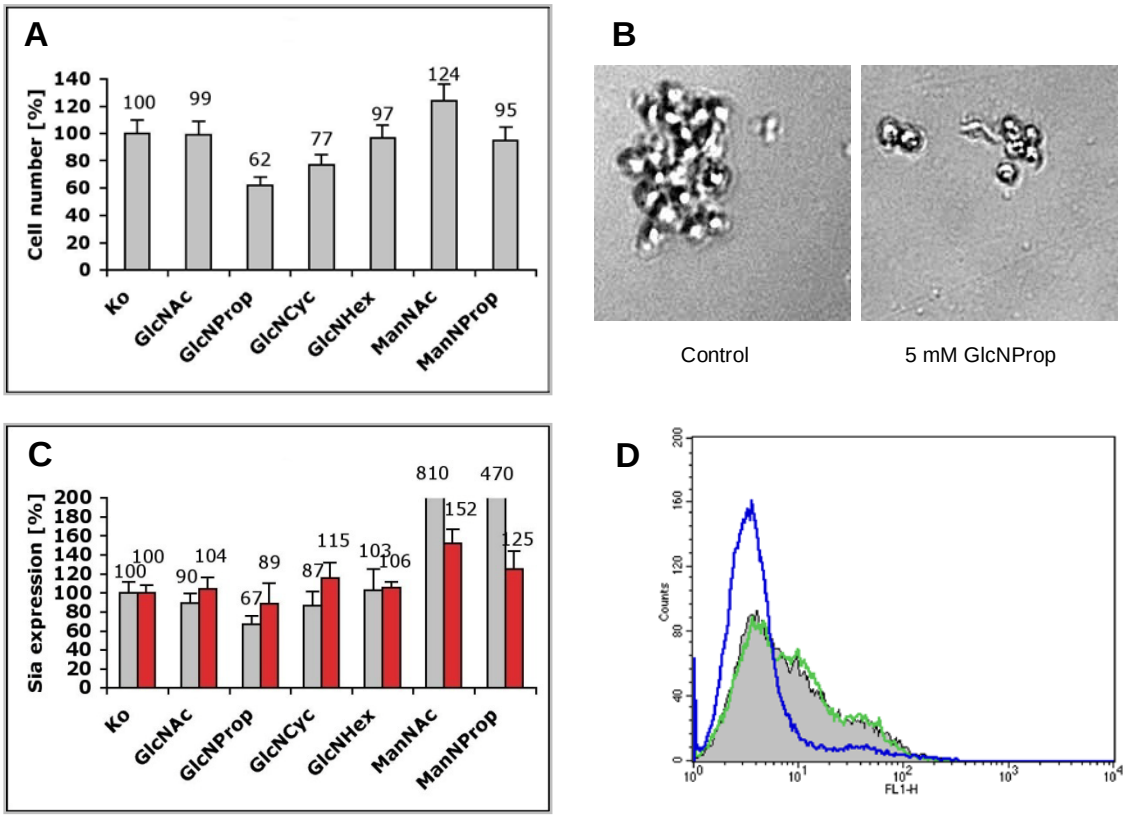

Figure 3.4.7: Effect of GlcNAc analogs on Raji
A. Effect of GlcNAc on Raji growth. Cells were cultured under standard condition with addition of 5 mM analogs in the medium. After 3 days the cell count of living cells were determined and compared with control.
B. Morphology of Raji cells treated with 5 mM GlcNProp for 3 days.
C. Total sialic acid expression ( ) vs. bound sialic acid expression ( ) of Raji cells after treatment with 5 mM of the indicated GlcNAc analogs for 3 days.
D. LFA-FITC stained FACS analysis of Raji cells treated with PBS (grey), 5 mM GlcNAc (green) and 5 mM GlcNProp (blue)

Raji is a human Negroid Burkitt's lymphoma cell line. They grow as suspension lymphoblast-like, round cells, single or in clumps. The growth rate is very high (doubling time = 24 h). They possess numerous receptors for certain complement components such as Fc receptors for immunoglobulin G and is therefore widely used for immunological studies. In this study Raji's growth rate is specifically impaired by GlcNProp. With GlcNCyc and GlcNHex this effect is rather low (Figure 3.4.7A). They tend to be less grouped and more disperse throughout the suspension culture. Their shape is also a little bit smaller than the normal cells after treatment with GlcNAc analogs (Figure 3.4.7B). With GlcNProp the total sialic expression of this cell line is significantly reduced (Figure 3.4.7C), followed by a slight decrease in conjugated sialic acid. The decreased of cell surface sialylation could also be observed by LFA-FITC FACS analysis (Figure 3.4.7D). For this cell line the effect of GlcNProp on sialic biosynthesis could be observed at rather high concentrations (5mM).

From the results with tumor cells, one could see that GlcNAc analogs have different effects on different cell lines. They inhibit the proliferation rate of cells without obvious effect on apoptosis. Morphological changes are visible but can usually only be observed by a small group of cells with the given concentration and testing conditions. For Raji cells the inhibitory effect of GlcNProp on total sialic acid and cell surface sialic acid could be assessed. A biological implication of this inhibition is a matter of future research.

3.4.4. Inhibition of GABA uptake in Hek-GAT1 cell line

For another cell system the effect of sialic acid inhibition could be studied on a defined biological effect. The Hek-GAT1 cell line was created by Jing Hu in this lab. She verified that lack of cell surface sialylation would lead to decreased GABA uptake activity of GAT-1, a major GABA uptake transporter in presynaptic membranes [40]. In previous work, sialidases were used to remove the outer layer of sialic acid with the result that GABA uptake activity was reduced. A CHO cell line with a defective GNE mutant transfected with GAT-1 could also not take up GABA to the normal extend. In order to test for the effect of GlcNAc analogs on GABA uptake activity Hek-GAT1 cell line was treated with the indicated substrate at two different concentrations (5 mM and 10 mM) for 3 days and sialic acid quantization assays as well as GABA uptake activity test were performed.

There is an anti-proliferative effect of these substances on cell growth (Figure 3.4.8B). The morphology of the cells indicated no serious modifications or excessive membrane leakage (Figure 3.4.8A). At 10 mM concentrations of GlcNProp a significant reduction of total sialic acid (48%) (Figure 3.4.8C) as well as GAT-1 conjugated sialic acid (60%) (Figure 3.4.8D) could be detected. To a lesser extend this effect could also be observed with GlcNCyc and GlcNHex. This effect is dose dependent and is not significant at 5 mM. 10 mM GlcNProp reduces GABA uptake activity of this transfected cell line (75%), affecting a distinct biological function, which has been associated with sialic acid expression [40]. It is therefore possible to conclude that high dose of GlcNProp has the potential to inhibit sialic acid expression in this cell lines. Combined with *in vitro* MNK inhibition results (Figure 3.4.2), this inhibition is most likely linked to the inhibition of the MNK domain of the GNE.

These results support the fact that inhibiting the MNK domain of the GNE could limit the expression of sialic acid on the cell surface. With the defined effect on GABA uptake, it also indicates that MNK inhibitors can be used to research distinct biological effects of sialic acids.

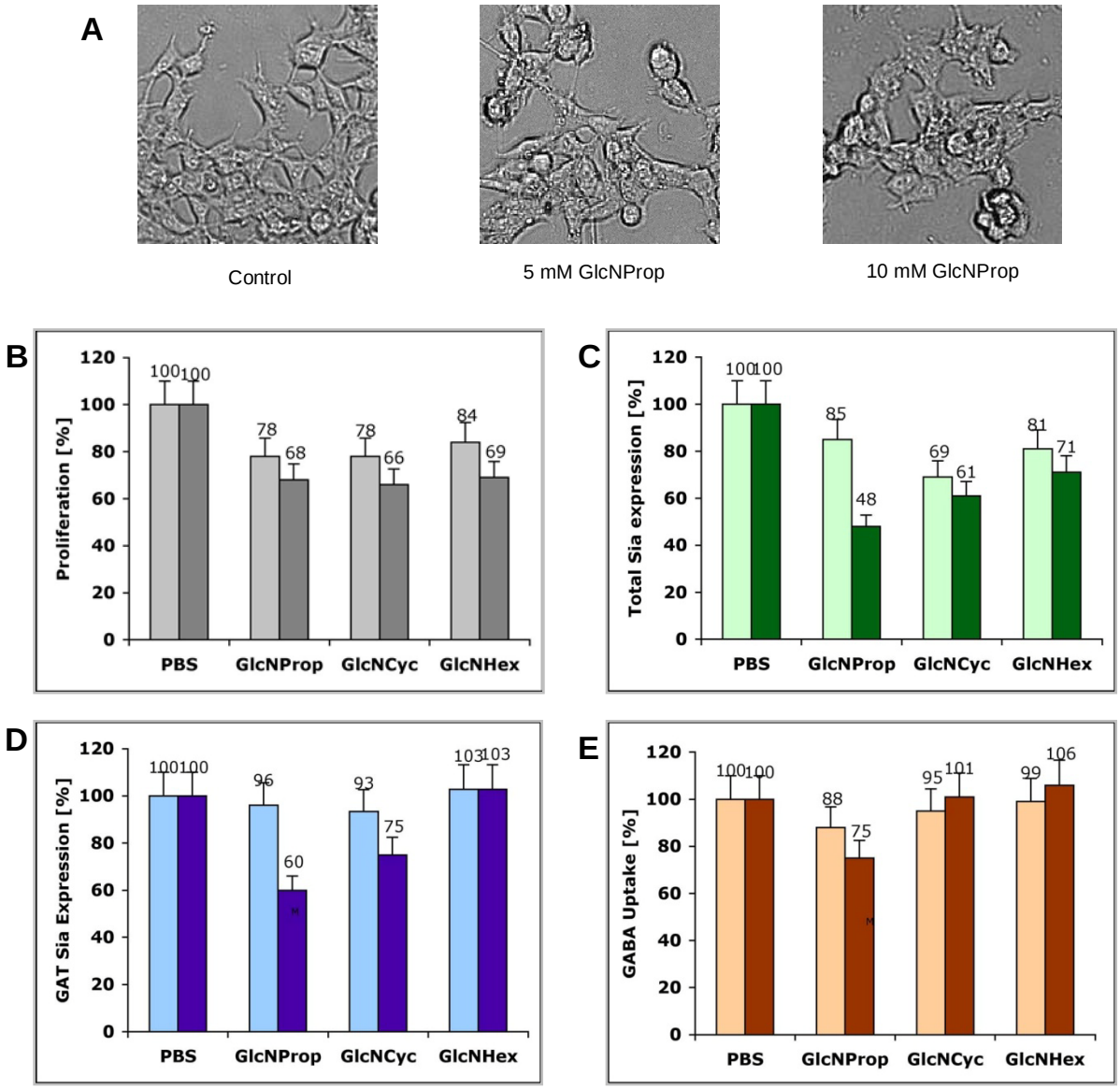

Figure 3.4.8: Effect of GlcNAc analogs on GAT-1 transfected Hek293 cell line
Cells were treated with 5 mM or 10 mM GlcNAc respectively and incubated for 3 days. After this cells were collected and following assays performed. Experiments were performed together with Dr. Jing Hu.
A. Morphology of Hek-GAT.
B. Proliferation of Hek-GAT with AlamarBlue assay 5 mM ( ) / 10 mM ( ).
C. Total sialic acid expression of Hek-GAT with Periodate-Resorcinol assay 5 mM ( ) / 10 mM ( ).
D. Quantitative estimate of sialic acid expression on GAT-glycans based on intensity of MAA lectin and anti-GAT-GFP blot of anti-GAT-GFP immunoprecipitation 5 mM ( ) / 10 mM ( ).
E. GABA uptake activity of Hek-GAT 5 mM ( ) / 10 mM ( ).

In conclusion, the given inhibitors only work at very high concentrations for a limited number of cell lines. At these concentrations, unspecific side effects on proliferation and morphology of cells could be observed making the effect on sialic acid expression less specific. On the basis of these assays, however, new and more potent inhibitors can be tested and verified.

3.4.5. Novel MNK inhibitor from crystal structure

From the X-ray structure, one could observe that the active center is tightly coordinated (Figure 3.4.9). Only in the C2, C4 and C6 position there is a small room for modifications. The C2 modifications have been used extensively in glycan engineering processes, where the modified ManNAc derivates is transformed into the corresponding NANA derivates in vivo [126]. The C-6 modification does not fit with the concept of glycan engineering, since it would interfere with the phosphorylation process. A modification at the C6 for our purpose, however, is very interesting since it would generate a potential competitive inhibitor for MNK.

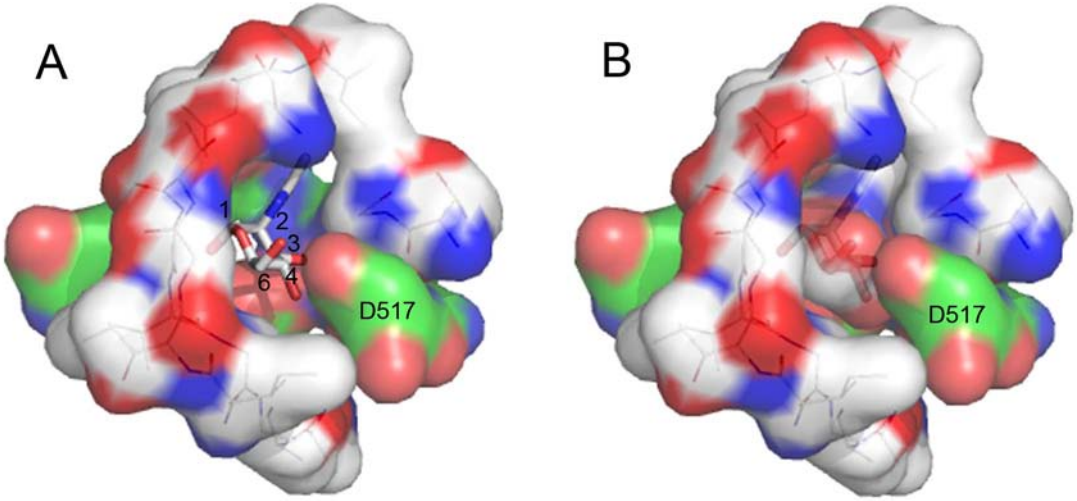

Figure 3.4.9: Surface expression of ManNAc in MNK active center
A. ManNAc is represented as sticks. Amino acid residues around the ligand are shown as lines and surfaces. ManNAc C-atoms are numbered. C-Atoms are white, N-Atoms blue, and O-Atoms red. Residues involved in ManNAc binding are colored in green. Residues not directly involved in ManNAc binding are colored in white.
B. Surface representation of ManNAc, demonstrating a tight coordination of the active center.

6-O-Ac-ManNAc, which was kindly provided by Dr. R. Zimmer, was tested for its inhibition activity for MNK. With an Ki = 1.4 mM, this substrate was found to be the best *in vitro* inhibiting substrate so far for the MNK compared to GlcNProp (Ki > 5 mM) and 3-O-Me-GlcNAc (Ki =2.2 mM) (Figure 3.4.10). The inhibition mode was confirmed to be competitive.

Unfortunately, this inhibitor would be deacetylated in cells by unspecific esterases. Therefore, the effect of this inhibitor cannot be tested in cellular assays. The syntheses of novel inhibitors, which can be used in cells, are ongoing.

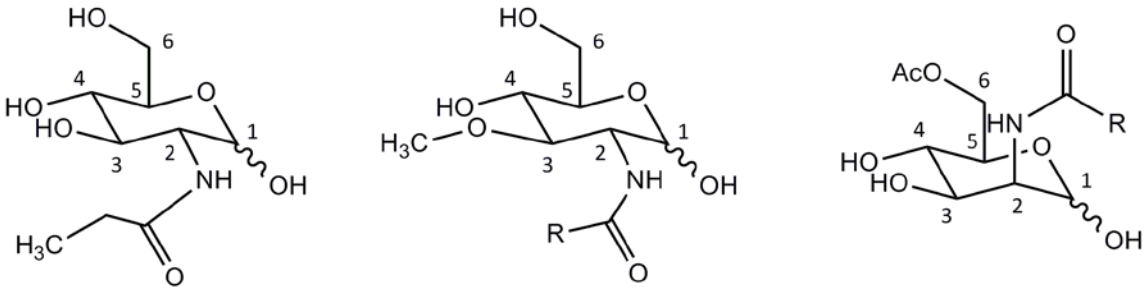

Figure 3.4.10: Presentation of inhibitors of hMNK
Ki are mean values of 4 independent measurements.

3.4.6. MNK inhibitor - conclusion

In this part of the work, cellular assays for various cell lines was established to test for the effect of MNK inhibitor on sialic acid expression. With these assays various tumor cell lines were tested. Intensive study was performed on Panc-1, Mela-2, HL60 and Raji. GlcNProp, GlcNCyc and GlcNHex were found to have little effect on inhibiting sialic acid expression in general. Although different cell lines react differently on the given substrates, the proliferation rate is in general reduced and the cell morphology was altered.

The inhibitory effects of these substrates on MNK were observed at very high concentrations *in vitro* (5 mM and 10 mM). In Raji cells sialic acid expression was reduced after GlcNProp treatment. At very high concentration (10 mM), GlcNProp could also inhibit sialic acid expression in Hek293 cells. These results using the periodate resorcinol assay could be verified with MAA lectin binding assays for GFP-GAT1. The GABA uptake activity of GAT was decreased due to the treatment with GlcNProp. In previous studies a decreased sialic acid expression on GAT1 was associated with reduced GABA-uptake activity in the given cell line [40]. Whether these effects are a direct result of MNK inhibition or due to unspecific influences of other enzymes or sialylation processes could not be verified. By discovering a more potent MNK inhibitor we hope to be able to more clearly access the specific effect of MNK inhibition on sialic acid expression.

With the analysis of the X-ray structure and the active center of the MNK, a novel inhibitor could be created. With the 6-O-Ac-ManNAc we currently have the best *in vitro* inhibitor for MNK so far. The inhibitory effect of 6-O-Ac-ManNAc demonstrates that more potent novel MNK inhibitors can be generated with the help of the MNK crystal structure. By substituting the acetyl residue on the 6-O with other residues, the unspecific esterase reactions in the cell could be avoided, opening ways to test these potential substances on established cellular assays.

4. Discussion

In this thesis, the human N-acetylmannosamine kinase (hMNK), which is part of the bifunctional UDP-GlcNAc-2-epimerase/ManNAc-kinase (GNE), could be crystallized. With the knowledge of the crystal structures, the enzyme mechanism could be revealed and new insights about mutant characteristics and potential inhibitors could be obtained. Inhibition of the hMNK is linked to sialic acid biosynthesis and would be of great biological significance.

4.1. MNK purification and characterization

For the different biochemical experiments required as well as structural studies through X-ray crystallography, soluble and active proteins in high quantity is an inevitable foundation. From rat liver Hinderlich et al succeed in isolating GNE from rat liver [63]. Blume et al successfully expressed recombinant His-GNE in mg amount in Sf9 cells [100]. The MNK domain of rat GNE could be recombinantly purified by Darius Ghaderi, but attempts to determine the crystal structure of these proteins were not successful [127].

MNK purification

In a series of experiments, the cloning, expression and purification of the MNK domain of the human GNE has been achieved in the *E.coli* system. Initial expression attempts were conducted in the pGex-4T vector system, which produces N-terminal GST-MNK fusion proteins. Previous experiences indicated higher expression and solubility of the target protein using this approach. In order to increase the chance of crystallization success, constructs with different lengths were generated. Various clones were optimized for protein expression and purified GST-MNK could be obtained after a single glutathione affinity chromatography step. Because the bulky GST-tag may alter the structure of MNK and influence the crystal structure, attempts were made to remove this tag via thrombin digestion prior to gel filtration. Using this approach 1 mg protein per liter *E.coli* culture of soluble and active MNK could be obtained. The 355 aa construct of hMNK formed protein crystals, which was very encouraging. However, due to the big protein lost by thrombin digestion, it was necessary to adapt another protein purification procedure.

With the use of the 6xHis-tag, the yield of purified hMNK could be improved to more than 26 mg per liter *E.coli* culture, making it very convenient for crystallization attempts. Compared to the whole His-GNE expressed in *E.coli* the protein yield of His-MNK with this system is much higher [128].

MNK characterization

The 6xHis-tag is constructed in the N-terminus of the MNK domain, in a linker region between the 2-epimerase and the kinase domain of the GNE. Kinase activity assays demonstrated that the MNK activity for ManNAc was not affected. The specific MNK activity was found to be 2.4 U/mg, which is in the same range as the kinase activity of the whole His-GNE [116].

The molar mass of the monomer is 35 kDa under denaturing conditions as shown by SDS PAGE, which was expected for a 335 aa protein. Non-denaturing and non-reducing PAGE as well as gel filtration analysis confirmed the dimeric nature of this enzyme in solution, as previously shown by biophysical methods on the GNE [75, 113].

Kinetic assays determined the substrate affinity of MNK for ManNAc to be similar to the whole GNE (Km = 95 µM (MNK), Km = 121 µM (GNE)). Although there are differences in the binding affinities for ATP, they are also in the same millimolar range (Km = 4.4 mM (MNK), Km = 1.67 mM (GNE)) [129]. The small difference may indicate structural changes in the binding environment of ATP in the MNK domain compared to the whole structure with the UPD-GlcNAc-2-epimerase domain. Because the GNE is a bifunctional enzyme where a product acts as an educt for the next reaction, it is possible to postulate that the active centers of these two domains are closely connected. Removing one domain of the GNE does not change the active site for ManNAc but could destabilize the binding pocket for ATP and consequently reduced its affinity for ATP. This structural determination may contribute to the understanding of this enzyme, since until now no crystal structure for the whole GNE exists.

Another noticeable difference between the whole GNE and MNK is their protein yield when expressed in the prokaryotic system. While purified His-GNE yields 0.3-0.5 mg/l [128], expressing His-MNK in the same system produces up to 26 mg/l. Due to the difference of protein expression in prokaryotic and eukaryotic systems, overexpression of a eukaryotic protein often result in formation of insoluble inclusion bodies. In prokaryotes the proper folding apparatus for a eukaryotic protein is missing as well as the post-transcriptional modification apparatus, which is often essential for enzymatic activity and stability. In the case of His-GNE, for example, expression in insect cells using a baculovirus system could significantly increase yield and activity [128]. For His-MNK, maybe due to the relatively small nature of this protein, expression and folding is facilitated. In addition, the MNK belongs to the ROK (Repressor ORF Kinase family), a kinase family mostly found in prokaryotes, making it possibly more suitable to a prokaryotic protein expression system.

Lastly, a significant difference of MNK and GNE is their propensity to form crystals. Using His-GNE, crystallization could not be achieved. One reason is the instability of the enzyme in solution. GNE loses 2-epimerase activity after 48 h at 4°C. The main reason, however, is the dynamic change in

conformation between tetramer and dimer of GNE in solution, preventing it from crystal formation. The MNK, on the other hand, is stable and active for weeks in solution. Its main dimeric state in solution may facilitate the formation of homogeneous crystals under the given conditions.

4.2. MNK crystal structure

The apo-structure of the hMNK we obtained has been published by Tong et al [113]. In addition to that, we succeeded in characterizing novel structure complexes of MNK/ManNAc (1.65 Å), MNK/ManNAc/ADP (1.80 Å) and MNK/ManNAc-6-P/ADP (2.40 Å).

In this work, the first human member of the ROK family in complex with its ligands and co-factors was structurally characterized. One of the structural signatures common to all ROK family members is the presence of a Zn^{2+}, which has been confirmed for MNK by anomalous difference electron density measurements. Our structural data demonstrated that the Zn^{2+} binding motif is in close proximity of the substrate binding site. As a matter of fact, the key amino acid H569 coordinates both Zn^{2+} and ManNAc (C1 hydroxyl group). Without this Zn^{2+} coordination the hMNK may not be active, which underlines the structural key role of the metal for enzyme activity.

The MNK is found also in the crystal structure as a dimeric protein. The previous apo-MNK structure featured a crystallographic hexamer, which was discussed to be biologically relevant [113]. This hexamer is formed by interaction between the N-terminal domains of symmetry related mates. With our new data, it is assumed that this interaction is a crystallographic artifact rather than a naturally occurring multimer, since this would reduce the flexibility of the N-terminal domain which changes conformation upon substrate binding.

The basic structure consists of two rigid lobes with a flexible hinge region where the active site is located. Upon ManNAc binding, MNK undergoes a conformational change, from an open substrate-free conformation to a closed sugar-bound one. This phenomenon has been observed for other sugar kinases like human N-acetylglucosamine kinase [130] or hexokinase from Sulfolobus tokodaii [131]. Interestingly, this is not the case for the closely related YdhR, a bacterial fructokinase also belonging to the ROK family [132]. Upon sugar binding no major structural change for YdhR is induced.

MNK active center

Given the high resolution structure of MNK in complex with its natural substrate, ManNAc, the active site of the enzyme and the binding conformation of the ligands (ManNAc and ATP) were identified and structurally characterized.

The high affinity (Km = 95 µM) and specificity of MNK for ManNAc correlate with the structural findings. The N- and C-terminal domains of MNK form a V-shaped structure. The active site cavity

formed at the inner lower side of the V coordinates ManNAc with a network of 17 hydrogen bonds, and the 8 residues involved in these interactions sterically determine the specificity of MNK. In contrast, the affinity of MNK for ADP is relatively low (Km = 4.4 mM). While ManNAc is closely engulfed in the binding pocket, ADP binding is not well coordinated; the adenine moiety is for example not even in hydrogen bonding contact with MNK.

These data can be compared with the STD NMR data collected for ligands interaction with the whole GNE [101]. With the STD NMR measurements it was postulated that modifications at positions C1, C3 and C4 would result in a loss of binding affinity toward the MNK, whereas the C2 and C6 modifications can be well tolerated. With the crystal structure data of the MNK active site, these results can be confirmed and better understanding could be gained. The hydroxyl group at C6 is coordinated by N517, as described before. At this position there is a hole for the access of ATP allowing modifications at this site, which would correlate with the STD NMR results. Also at position C2, even though the amino and the carbonyl group of the acetate are well coordinated, there is a hydrophobic hole behind these residues allowing an extension and modification of the methyl group. ManNAc derivates with C2 modifications, like ManNProp, have been used for glycan engineering purposes and can be transformed to the respective NANA derivates, 5-N-propionylneuramic acid [126]. On the other hand, the inversion of ManNAc to GlcNAc, as was suggested to be possible by STD NMR measurements, was found with crystallographic data to be intolerable. Even though there is room for this inversion in the active center, which would explain the similar affinity for MNK, the coordination in this conformation is not stabilized. The induced conformational changes necessary for enzyme activity are not possible rendering the enzyme inactive for GlcNAc. At position C1, the hydroxyl group is H-bonded to E588 favoring the α-anomere of ManNAc. At C3 and C4 of ManNAc the hydroxyl groups are tightly coordinated by G476 and E566 as well as N516 and D517 respectively, allowing no drastic modifications in these polar pockets. In addition, at C3 no room for further extension is available, while at C4 a small non-polar pocket can be found. This little pocket could explain why, a novel 4-N_3-ManNAc structure worked as substrate for sialic acid glycan engineering (Hinderlich et al. personal communication).

As for the binding of ATP, its affinity for MNK is 40 times weaker than that of ManNAc. The lack of close coordination for example of adenine could explain this phenomenon. The specificity for ATP, however, stays almost intact, rendering enzyme activities with other co-factors like UTP, CTP, and GTP insignificant.

In STD NMR measurements with the whole GNE a very close proximity to the protein surface was found for the hydrogen at C1 of adenine (100%). In the crystal structure of the MNK, one cannot

observe this coordination. The ATP affinity for the whole GNE is also two times higher than that for MNK. One explanation for these observations is the involvement of the 2-epimerase domain in the stabilization of ATP binding. Most likely, the active center of the 2-epimerase is very close to the active center of the kinase, resulting in cross interactions between the two domains. This question would be answered when the crystal structure of the whole GNE could be obtained.

As shown previously, in the nucleotide binding site of the MNK, Mg^{2+} interacts directly with the β-phosphate of ATP. Usually, kinases need Mg^{2+} for ATP binding. In the case of MNK weak kinase activity could be detected for the enzyme without Mg^{2+} [101]. Therefore, Mg^{2+} is not essential for MNK activity but would strongly enhance the reactions. The coordination of Mg^{2+} to ATP stabilizes the interaction with this enzyme. As Lowe and Potter [133] and Pollard-Knight et al [134] suggest, Mg^{2+} appears to play a role in coordinating the negative charge of the β- and γ-phosphate, facilitating the nucleophilic attack of the C6 hydroxyl group of ManNAc on the γ-phosphate of ATP.

MNK catalytic mechanism

Taken these data together, the following mode of action for the MNK domain of the GNE could be suggested. After the binding of ManNAc, MNK undergoes a conformational change. The active center is tightly coordinated and offers the binding energy to stabilize the novel conformation. In this closed conformation, ATP is now recruited to the binding pocket. Even though the affinity for ATP is low, excess cellular concentration of ATP still allows a quick reaction of the γ-phosphate with the hydroxyl group of C6. The nucleophilic attack of the hydroxyl group is facilitated by the coordination of the hydrogen atom with the carboxyl group of D517. Without this coordination the MNK is inactive even in the presence of excess ManNAc, as demonstrated by site directed mutagenic studies. On the other side, in the ATP binding pocket the coordination of the oxygen of the β- and γ-phosphate with Mg^{2+} renders the phosphate groups more positive. Thus, allowing the transfer reaction to take place. The affinity for ManNAc-6-phosphate is lower than for ManNAc, due to the lack of hydrogen interaction with D517. The energy needed to stabilize the close conformation is lost. MNK returns to its relaxed open conformation after releasing the product of the reaction, ManNAc-6-phosphate and ADP.

MNK and DNA binding

Sequential and structural homology studies classify MNK as member of the ROK family and more generally as member of the sugar-kinase/HSP70/actin superfamily [113]. The ROK family encompasses transcriptional regulators, sugar kinases and uncharacterized open reading frames. A common feature of ROK proteins as transcriptional repressors of sugar catabolic operons, is their ability to bind DNA [119] . A multiple alignment of many ROK family protein sequences showed that

all ROK-transcriptional regulators possess an N-terminal extension of approximately 80 aa with a helix-turn-helix motif responsible for DNA binding in contrast to the ROK-kinases, which lack such an extension. In the MNK domain this 80 aa long structure motif cannot be found. Sequence alignment of the whole human GNE with the known ROK HTH primary motif sequences [119] also reveals no defined locus for this motif in the epimerase domain. Therefore, from the given data we cannot deduct a binding of the GNE to DNA. However, besides its role as the key enzyme for sialic acid biosynthesis, the GNE was found to regulate ST3Gal5 and ST8Sia1 mRNA level and protein expression [91]. It is located in the nucleus [135]. And the fact, that it is structurally closely related to bacterial transcription factors, strongly indicates its interaction with DNA. Furthermore, without the crystal structure of the epimerase domain we cannot exclude the fact, that the secondary HTH structure motif or other DNA binding motifs, which could not be found in the MNK crystal structure, may still be located within the 2-epimerase domain of this bifunctional enzyme.

The hMNK, as part of the GNE, is a eukaryotic protein. Due to the differences of eukaryotic and prokaryotic gene transcription, further studies are needed to fully understand the role of the GNE in DNA binding and regulation. The crystal structure of the whole GNE or the 2-epimerase domain would offer a clearer understanding about the role the GNE and DNA binding.

4.3. MNK HIBM mutants characterization

To further understand the underlying reason of this myopathy, experiments were conducted to elucidate the characteristic changes in the structures of MNK HIBM mutants. For this purpose, different MNK HIBM mutants were expressed, purified and characterized. The hypoactivity of the MNK mutants were confirmed *in vitro*. These results correlate with previous *in vitro* measurements for HIBM mutant of the whole GNE [87, 90, 116].

The specificity of the mutants was measured. For mutants N519S, I528C, I587T specificities were low, while he specificity of A631T, A631V, M712T mutants are virtually intact. It should be noted that there is no close correlation between enzyme activity and specificity. I528C has very high relative activity (78%) while specificity is very low. On the other hand, the activity of A631T is relatively low (4%) but its specificity for ManNAc is completely intact. With the resolved active center of the MNK, the reasons for that observation became evident. Mutations like N519S, I528C, and I587T are close to the binding site of ManNAc. Therefore, changes at these positions result in activity decrease as well as specificity loss. Other mutations like A631T, A631V, and M712T are found predominantly on the surface of the enzyme. They may disturb ATP binding or block conformational changes after substrate binding and prevent therefore enzyme activity but does not affect the specificity of the ligand binding pocket itself.

The expression level and consequently protein yield for different mutations are dramatically altered, suggesting that this single mutation do create significant changes in structure and protein folding that are less accepted by the prokaryotic expression system. Reduced expression level is a result of reduced proper folding and stability or the protein itself is toxic at high concentration. Although the expression level in prokaryotic system cannot be directly transferred to eukaryotic systems, deductions can be made on the expression level of these mutants in mammalian cells. Unpublished data from GNE HIBM mutant expression in insect cell system depicts the same characteristic of MNK HIBM mutants. Their expression level compared to wild-type is usually decreased (S. Hinderlich personal communication). In mammalian cells a reduced expression of GNE can very likely affect the function of healthy cells. Together with the decreased activity of the enzyme, these changes may determine the onset of the disease at different times.

From the CD spectra analysis, changes in the secondary structure of the mutants are observed. These changes appear to be similar for all HIBM mutations. An increase in the β-sheet and the random coil percentage as well as a decrease in α-helices is characteristic. The discrepancy reflected in the CD results correlates with the amount of aggregation of the mutants. Most of the aggregations can be found for A631T, A631V and M712T. The secondary structure content of these mutants is 10-12% α-helices, 29-31% β-sheet and 42% random coil compared to 20%, 24% and 38% for wild-type MNK respectively. These strong discrepancies in the CD results cannot be observed in the D517N mutant and are rather mild in D517A and N519S (15-16%, 26-27%, 40%), which has very low aggregation formation and are not associated with HIBM. Besides that, attempts to prepare protein samples for crystallization failed due to stronger aggregation formation at higher concentrations for all HIBM mutants.

Hypothesis about HIBM pathogenesis

A common feature of HIBM is rimmed vacuoles with inclusion bodies. One possible explanation for this phenomenon is that GNE HIBM mutants self-aggregate, which is reflected in the results presented here. The proteolytic machinery of the body can keep up with clearing misfolded proteins. But for reason still not clearly understood, also in other diseases like Alzheimer or BSE, at a non-defined threshold a cascade for disease progression will be triggered. This may explain the unpredictable onset of this disease in the afflicted HIBM population.

Upon ManNAc binding, MNK changes its conformation from an open to a closed conformation. So that aggregation might be avoided by supplying the cells with a sufficient dose of ManNAc. In experiment with mice/rats by Galeano et al (2007) [136] disease symptoms can be relieved by additional ManNAc supplement in food, which they credited to the effect of increased sialylation.

Reduction of GNE aggregation, beside higher GNE activity, may offer an alternative explanation for these results.

Many hypotheses on the onset of HIBM in GNE mutants exist, but yet no clear answer is found. That's why, I looked forward to solving the X-ray structure for some of the mutants, in order to gain insights into the conformational changes HIBM mutants have in common. Unfortunately, due to difficulties with protein aggregations until now it is not possible to create crystals for these proteins. However, optimized protein expression systems for different MNK HIBM mutants have been established, different characters of the mutants could be assessed and analyzed, and a novel hypothesis for the molecular causes of this disease, in that HIBM is caused by self-aggregation of GNE mutant proteins, was formulated. To further verify these initial findings the composition of HIBM inclusion bodies needs to be verified. Cellular assays with MNK mutants would also be helpful to further research about the changes in a biological system.

4.4. MNK and sialic acid biosynthesis inhibitor

As previously described, sialic acid plays a diverse and important role in the interaction of cells. Tools to study the biological effects of sialic acid modifications like sialidase treatment, hyposialylated cell strains, inhibition of selective sialic acid transferases or glycoengineering of the N-acyl side chain are widely used. However, a potent inhibitor for the key enzyme of sialic acid biosynthesis, GNE, is still missing. There is a high value associated with the ability to inhibit sialic acid expression on the cell surface. Not only would it be a key for further studies on the biology of sialic acid, but also an alternative approach in the search for cancer treatment remedies, since sialic acid overexpression is very common in tumor cells.

As demonstrated in previous studies by Keppler et al., a reduction of the GNE/MNK activity could diminish the concentration of sialic acid expression on the cell surface [69]. The reduction of GNE activity, 2-epimerase as well as ManNAc kinase activity, in many HIMB mutated cell lines also lead to decreased sialylation of the cell surface [87]. Therefore, the GNE is a promising target for sialic acid inhibition. Many inhibitors of the 2-epimerase domain have been tested as a way to inhibit sialic acid expression on the cell surface. Unfortunately, due to the bulky nature of UDP-GlcNAc analogs and transition state analogs these substances are blocked by the plasma membrane. The MNK domain has been neglected since. But with ManNAc analogs, which are less bulky as UDP-GlcNAc analogs, it is very possible to design an inhibitor that is membrane permeable.

MNK inhibition with GlcNAc analogs

In previous studies GlcNAc analogs were found to inhibit ManNAc kinase activity in liver homogenate [98, 99]. Grünholz et al (1982) could show that sialic acid biosynthesis is markedly inhibited by

GlcNProp and GlcNProp-6-phosphate. Zeitler et al (1990) did the same experiments for 3-O-Me-GlcNAc and found that it was a non-competitive inhibitor for MNK. In my studies, these substrates were used for inhibition experiments on purified MNK and cells.

At millimolar concentrations (10 mM) GlcNAc analogs were able to inhibit the activity of MNK to lower than 20% *in vitro* (3-O-Me-GlcNAc). Their Ki were calculated to be in low millimolar range. Their weak competitive inhibitory effects on the MNK can be explained by the selective ManNAc active site.

For further cellular experiments GlcNProp, GlcNCyc and GlcNPent were used. Due to the low physiological concentrations of MNK and ManNAc, we hoped to see partial inhibition of sialic expression with millimolar concentrations of the given substrates. As GlcNProp is transformed to GlcNProp-6-phosphate by the unspecific GlcNAc kinase in cells, an inhibitory effect of metabolites of the given substrate was also anticipated. The intention was to determine the link between MNK inhibition and sialic acid expression on the cell surface, establishing cellular assays for new lead structures.

In this work, for two cell lines, Raji (Burkitt's lymphoma) and Hek 293 (human embryonic kidney), the connection between MNK inhibition and sialic acid expression could be established. With the treatment of 5 mM GlcNProp over the course of 3 days total sialic acid expression in Raji decreased to 67%. Glycoconjugates bound sialic acid content decreased to 89% compared to the control group. This decrease in the sialic acid content could be verified for cell surface sialic acid expression using LFA-FITC FACS. Raji has the lowest sialic acid expression of the cell lines tested and may have a very sensitive de novo sialic acid expression system. Therefore, GlcNProp may have the highest impact this cell system.

Further tests on a stably transfected Hek-GAT1 cell line confirmed this effect on sialic acid inhibition has a defined biological implications. In previous studies it has been established that sialic acid expression on GAT1, a major GABA reuptake transporter in the synapse, is essential for GABA reuptake activity. GABA uptake was diminished by removing sialic acid on the cell surface of normal transfected Hek cell lines with sialidase. This activity was also decreased when GAT1 was transfected on CHO cell lines with deficiencies in the GNE [40]. In this work, upon treating Hek-GAT1 cell lines with 5 mM or 10 mM GlcNProp, total sialic acid expression was decreased to 85% and 48% respectively and in correlation to that GABA uptake activity was decreased to 88% and 75%. These results indicate a connection between MNK inhibition, sialic acid expression and changes in biological functions.

For the other cell lines tested no significant reduction of sialic acid expression could be observed in a similar setting. The total level of sialic acid on Panc-1, human pancreas carcinoma, Mela-2, human melanoma, and HL60, human acute myeloid leukemia were changed insignificantly.

Due to the high concentrations of the given inhibitors, a clear conclusion about their efficacy to inhibit the MNK in cells cannot be made. Part of the cell population experienced abnormal morphology changes. Overall, cell proliferation assay as well as cell counting experiments revealed a slower growth rate in all cell lines with these substrates. Even though, no apoptosis could be observed. These observations are most likely the result of unspecific side effects of the given substrates at millimolar concentrations.

GlcNAcs are the two first building blocks of N-glycan chains, which are directly connected to asparagine residues on proteins. GlcNAc derivates may be substituted for GlcNAc, modifying the structure of this sugar chain. This would contribute to the change in glycosylation of cells and ultimately cell surface sialylation. As GlcNAc analogs they are also likely to influence the biosynthesis pathway of GlcNAc. Particularly, the interaction with O-GlcNAc transferase (OGT) or β-N-acetylglucosaminidase (O-GlcNAcase) is very likely. The disturbance of O-GlcNAc formation has impact on the dynamic crosstalk with phosphorylation [137], leading to cellular disturbances in cellular homeostasis and an increased stress response, which would explain the observed changes in proliferation and morphology.

In summary, with this series of experiments cellular assays to test the effect of MNK inhibitors have been established. The first indication that MNK inhibition can affect cell surface sialylation could be shown.

Novel sialic acid biosynthesis inhibitor

Based on the novel crystal structures and the information about the active center, it was possible to model novel lead structures as inhibitors of the MNK. Computer modeling data suggest that a modification of ManNAc at position C6 with a relatively small polar group would yield a potential MNK inhibitor. In a first approach to verify this idea, 6-O-Ac-ManNAc was synthesized and tested for its inhibitory capacity on MNK compared with other previously tested inhibitors of MNK. With a Ki = 1.4 mM, 6-O-Ac-ManNAc was verified to be the best MNK inhibitor ever discovered so far. Further inhibitors with different and stable modifications are being synthesized to be also tested in cells.

4.5. Future outlook

In this work the crystal structure of the MNK domain of the GNE with its ligands was successfully solved. The access to this structural information offers explanations about the activity of the MNK, as well as mutational influences and inhibitor design. But the results also created a lot of new questions. As a part of a bifunctional enzyme it would be relevant to further elucidate the interplay between the kinase domain and the 2-epimerase domain. Are the two active centers closely located or is there a tunneling of ManNAc as product of the 2-epimerase? Is the missing HTH loop, common in DNA binding of ROKs, present in the 2-epimerase domain? How is the character of the active center of the 2-epimerase?

The difficulties for the crystallization of GNE lie not in the expression but in the dynamic equilibrium of different oligomeric states, namely dimer and tetramer, of the GNE in solution. A solution to overcome this problem is to use stabilizing agents, e.g. inhibitors, selective antibodies, or protein crosslinks to get stable crystals. Different attempts like construct length variations, limited proteolysis, co-crystallization with antibodies or mutational modifications could be tried to access the crystal structure of the whole GNE, the key enzyme for sialic acid biosynthesis.

With the detailed description of the MNK active site, it is now possible to use computer modeling to design novel inhibitors for the MNK. With the established *in vitro* and cellular systems these inhibitors can be verified. Crystal structures of the MNK with newly determined inhibitors could also be conveniently generated, since the expression and crystallization conditions of the MNK are well-optimized.

The cloning, expression and purification conditions for HIBM MNK mutants are determined. It will take some effort to overcome the aggregation difficulties associated with high protein concentrations. Different buffer conditions need to be tried. The optimal concentration of detergents and reducing reagents can help stabilize the mutants in solution. By having access to the crystal structure of a HIBM MNK mutant, structural changes in the MNK could be understood.

To test the hypothesis that GNE aggregations is the source of inclusion bodies accumulation in HIBM muscle tissues. Fibroblast cell lines could be transfected with HIBM GNE variants to access this effect in cell culture. Isolation of inclusion bodies in these cells and analyzing it composition would offer important insights into the pathomechanism of HIBM.

5. Supplemental data

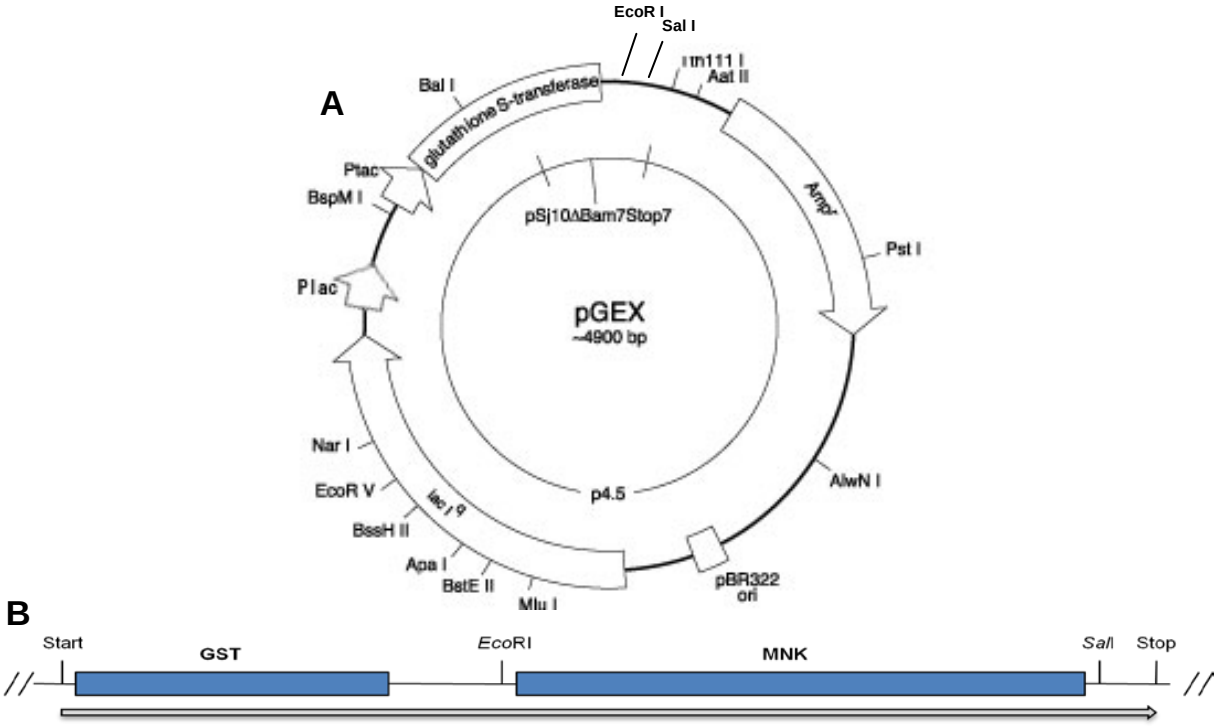

Figure 5.1: GST-MNK plasmid design
A. pGex-4T vector map, B. DNA construct of GST-MNK: arrow represents open reading frame and translational orientation

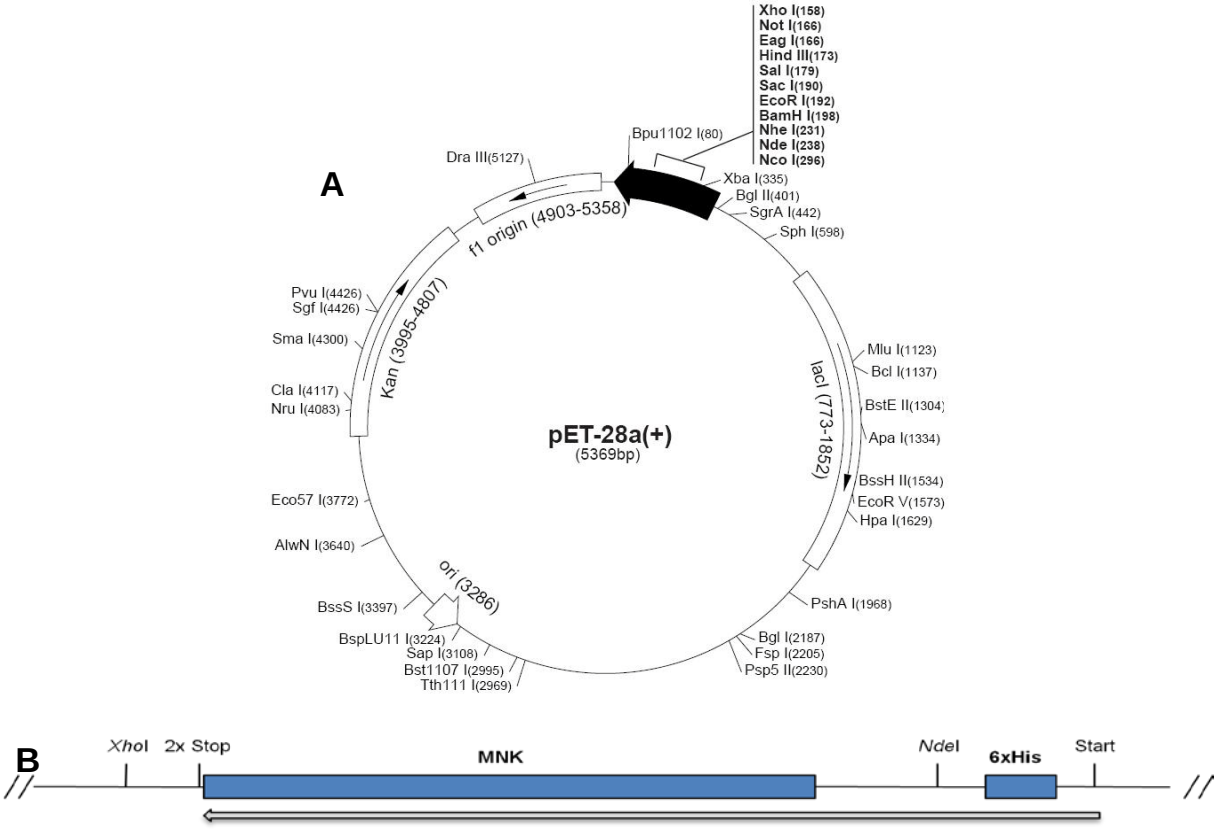

Figure 5.2: 6xHis-MNK plasmid design
A. pET28a vector map, B. DNA construct of 6xHis-MNK: arrow represents open reading frame and translational orientation

Table 5.1: Primary peptide sequences of MNK constructs

GST-MNK (aa 367-722)

MSPILGYWKIKGLVQPTRLLLEYLEEKYEEHLYERDEGDKWRNKKFELGLEFPNLPYYIDGDVKLTQSMAIIRYIADKH
NMLGGCPKERAEISMLEGAVLDIRYGVSRIAYSKDFETLKVDFLSKLPEMLKMFEDRLCHKTYLNGDHVTHPDFMLY
DALDVVLYMDPMCLDAFPKLVCFKKRIEAIPQIDKYLKSSKYIAWPLQGWQATFGGGDHPPKSDLVPRGSPGILPRI
LKFLKSIDLQEPLQKKFCFPPVKENISQDIDHILETLSALAVDLGGTNLRVAIVSMKGEIVKKYTQFNPKTYEERINLILQ
MCVEAAAEAVKLNCRILGVGISTGGRVNPREGIVLHSTKLIQEWNSVDLRTPLSDTLHLPVWVDNDGNCAALAERK
FGQGKGLENFVTLITGTGIGGGIIHQHELIHGSSFCAAELGHLVVSLDGPDCSCGSHGCIEAYASGMALQREAKKLH
DEDLLLVEGMSVPKDEAVGALHLIQAAKLGNAKAQSILRTAGTALGLGVVNILHTMNPSLVILSGVLASHYIHIVKDV
IRQQALSSVQDVDVVVSDLVDPALLGAASMVLDYTTRRIYPSTRAAAS

GST-MNK (aa 387-722)

MSPILGYWKIKGLVQPTRLLLEYLEEKYEEHLYERDEGDKWRNKKFELGLEFPNLPYYIDGDVKLTQSMAIIRYIADKH
NMLGGCPKERAEISMLEGAVLDIRYGVSRIAYSKDFETLKVDFLSKLPEMLKMFEDRLCHKTYLNGDHVTHPDFMLY
DALDVVLYMDPMCLDAFPKLVCFKKRIEAIPQIDKYLKSSKYIAWPLQGWQATFGGGDHPPKSDLVPRGSPGIQFC
FPPVKENISQDIDHILETLSALAVDLGGTNLRVAIVSMKGEIVKKYTQFNPKTYEERINLILQMCVEAAAEAVKLNCRIL
GVGISTGGRVNPREGIVLHSTKLIQEWNSVDLRTPLSDTLHLPVWVDNDGNCAALAERKFGQGKGLENFVTLITGT
GIGGGIIHQHELIHGSSFCAAELGHLVVSLDGPDCSCGSHGCIEAYASGMALQREAKKLHDEDLLLVEGMSVPKDEA
VGALHLIQAAKLGNAKAQSILRTAGTALGLGVVNILHTMNPSLVILSGVLASHYIHIVKDVIRQQALSSVQDVDVVVS
DLVDPALLGAASMVLDYTTRRIYPSTRAAAS

GST-MNK (aa 407-722)

MSPILGYWKIKGLVQPTRLLLEYLEEKYEEHLYERDEGDKWRNKKFELGLEFPNLPYYIDGDVKLTQSMAIIRYIADKH
NMLGGCPKERAEISMLEGAVLDIRYGVSRIAYSKDFETLKVDFLSKLPEMLKMFEDRLCHKTYLNGDHVTHPDFMLY
DALDVVLYMDPMCLDAFPKLVCFKKRIEAIPQIDKYLKSSKYIAWPLQGWQATFGGGDHPPKSDLVPRGSPGIPLSA
LAVDLGGTNLRVAIVSMKGEIVKKYTQFNPKTYEERINLILQMCVEAAAEAVKLNCRILGVGISTGGRVNPREGIVLH
STKLIQEWNSVDLRTPLSDTLHLPVWVDNDGNCAALAERKFGQGKGLENFVTLITGTGIGGGIIHQHELIHGSSFCA
AELGHLVVSLDGPDCSCGSHGCIEAYASGMALQREAKKLHDEDLLLVEGMSVPKDEAVGALHLIQAAKLGNAKAQ
SILRTAGTALGLGVVNILHTMNPSLVILSGVLASHYIHIVKDVIRQQALSSVQDVDVVVSDLVDPALLGAASMVLDYT
TRRIYPSTRAAAS

His-MNK (aa 406-720)

MGSSHHHHHHSSGLVPRGSHMENLYFQGTLSALAVDLGGTNLRVAIVSMKGEIVKKYTQFNPKTYEERINLILQMC
VEAAAEAVKLNCRILGVGISTGGRVNPREGIVLHSTKLIQEWNSVDLRTPLSDTLHLPVWVDNDGNCAALAERKFG
QGKGLENFVTLITGTGIGGGIIHQHELIHGSSFCAAELGHLVVSLDGPDCSCGSHGCIEAYASGMALQREAKKLHDE
DLLLVEGMSVPKDEAVGALHLIQAAKLGNAKAQSILRTAGTALGLGVVNILHTMNPSLVILSGVLASHYIHIVKDVIR
QQALSSVQDVDVVVSDLVDPALLGAASMVLDYTTRR

A – GNE sequence, A – Tag (GST or His), A – Residual amino acids, A – Thrombin, A – TEV sites

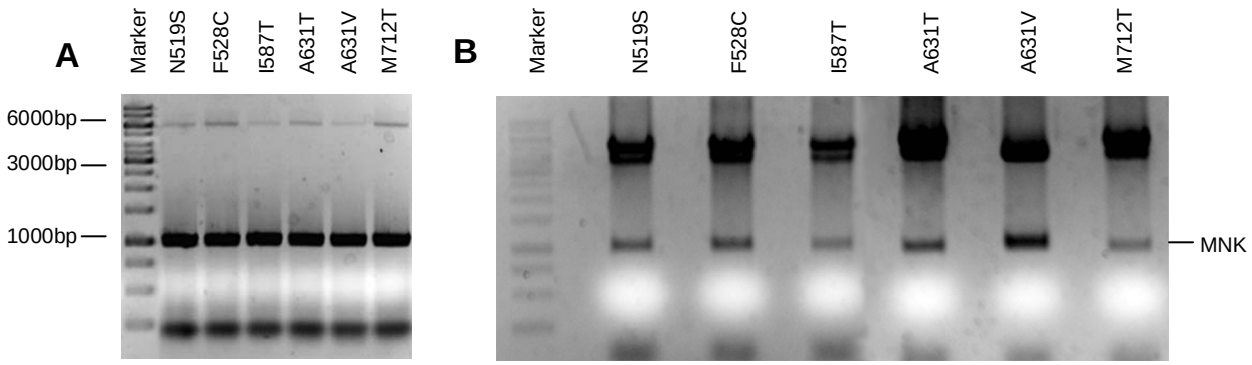

Figure 5.3: Cloning results for MNK HIBM mutants in pET28 vector
A. PCR products of MNK HIBM mutants
B. Positive pET28a-MNK mutant plasmids verified by *Nde*I/*Xho*I double digestion

After PCR a clear band at the expected size around 1000 bp is clearly visible (Figure 5.3A) as well as fragments of the vectors at 6000 bp. These PCR products were then subsequently cloned into pCR blunt vector, amplified and transfer via double ligation of the specific endonuclease site into pET28a vector (Figure 5.3B).

Table 5.2: Sequencing result of MNK mutants
Bold letters represent modifications in the DNA of this mutant

Name	MNK wild-type	MNK mutant
D517A	AAT GAT GGC	AAT G**C**T GGC
D517N	AAT GAT GGC	AAT **A**AT GGC
N519S	GGC AAC TGT	GGC A**G**C TGT
F528C	AAA TTT GGC	AAA T**G**T GGC
I587T	TGC ATT GAA	TGC A**C**T GAA
A631T	GCT GCG AAA	GCT **A**CG AAA
A631V	GCT GCG AAA	GCT G**T**G AAA
M712T	AGC ATG GTT	AGC A**C**G GTT

6. References

1. Schauer, R., *Sialic acids: fascinating sugars in higher animals and man.* Zoology (Jena), 2004. **107**(1): p. 49-64.
2. Blix, G., *Über die Kohlenhydratgruppen des Submaxillarismucins.* Hoppe-Seyler's Z Physiol Chem, 1936. **240**: p. 43-54.
3. Klenk, E., *Neuraminsäure, das Spaltprodukt eines neuen Gehirnlipoids.* Hoppe-Seyler's Z Physiol Chem, 1941. **268**: p. 50-58.
4. Blix, F.G., A. Gottschalk, and E. Klenk, *Proposed nomenclature in the field of neuraminic and sialic acids.* Nature, 1957. **179**(4569): p. 1088.
5. Varki, A., *Glycan-based interactions involving vertebrate sialic-acid-recognizing proteins.* Nature, 2007. **446**(7139): p. 1023-9.
6. Varki, A., *Diversity in the sialic acids.* Glycobiology, 1992. **2**(1): p. 25-40.
7. Angata, T. and A. Varki, *Chemical diversity in the sialic acids and related alpha-keto acids: an evolutionary perspective.* Chem Rev, 2002. **102**(2): p. 439-69.
8. Varki, A., *Loss of N-glycolylneuraminic acid in humans: Mechanisms, consequences, and implications for hominid evolution.* Am J Phys Anthropol, 2001. **Suppl 33**: p. 54-69.
9. Kolter, T. and K. Sandhoff, *Sialic acids--why always alpha-linked?* Glycobiology, 1997. **7**(7): p. vii-ix.
10. Kean, E.L., *Sialic acid activation.* Glycobiology, 1991. **1**(5): p. 441-7.
11. Malykh, Y.N., R. Schauer, and L. Shaw, *N-Glycolylneuraminic acid in human tumours.* Biochimie, 2001. **83**(7): p. 623-34.
12. Roth, J., et al., *Occurrence of sialic acids in Drosophila melanogaster.* Science, 1992. **256**(5057): p. 673-5.
13. Alviano, C.S., L.R. Travassos, and R. Schauer, *Sialic acids in fungi: a minireview.* Glycoconj J, 1999. **16**(9): p. 545-54.
14. Zeleny, R., et al., *Sialic acid concentrations in plants are in the range of inadvertent contamination.* Planta, 2006. **224**(1): p. 222-7.
15. Schachter, H., *The joys of HexNAc. The synthesis and function of N- and O-glycan branches.* Glycoconj J, 2000. **17**(7-9): p. 465-83.
16. Muhlenhoff, M., M. Eckhardt, and R. Gerardy-Schahn, *Polysialic acid: three-dimensional structure, biosynthesis and function.* Curr Opin Struct Biol, 1998. **8**(5): p. 558-64.
17. Van den Steen, P., et al., *Concepts and principles of O-linked glycosylation.* Crit Rev Biochem Mol Biol, 1998. **33**(3): p. 151-208.
18. Varki, A., *Sialic acids as ligands in recognition phenomena.* Faseb J, 1997. **11**(4): p. 248-55.
19. Schauer, R., *Sialic acids as antigenic determinants of complex carbohydrates.* Adv Exp Med Biol, 1988. **228**: p. 47-72.
20. Schauer, R., *Achievements and challenges of sialic acid research.* Glycoconj J, 2000. **17**(7-9): p. 485-99.
21. Kelm, S. and R. Schauer, *Sialic acids in molecular and cellular interactions.* Int Rev Cytol, 1997. **175**: p. 137-240.
22. Bocci, V., *The role of sialic acid in determining the life-span of circulating cells and glycoproteins.* Experientia, 1976. **32**(2): p. 135-40.
23. Varki, A.C., R.; Esko, J.:, *Essentials of Glycobiology*. 2008: Cold Spring Harbor Laboratory Press.
24. Crocker, P.R., J.C. Paulson, and A. Varki, *Siglecs and their roles in the immune system.* Nat Rev Immunol, 2007. **7**(4): p. 255-66.
25. Hartnell, A., et al., *Characterization of human sialoadhesin, a sialic acid binding receptor expressed by resident and inflammatory macrophage populations.* Blood, 2001. **97**(1): p. 288-96.

26. Tedder, T.F., et al., *CD22, a B lymphocyte-specific adhesion molecule that regulates antigen receptor signaling.* Annu Rev Immunol, 1997. **15**: p. 481-504.
27. Schachner, M. and U. Bartsch, *Multiple functions of the myelin-associated glycoprotein MAG (siglec-4a) in formation and maintenance of myelin.* Glia, 2000. **29**(2): p. 154-65.
28. Varki, A. and T. Angata, *Siglecs--the major subfamily of I-type lectins.* Glycobiology, 2006. **16**(1): p. 1R-27R.
29. Suzuki, Y., *Sialobiology of influenza: molecular mechanism of host range variation of influenza viruses.* Biol Pharm Bull, 2005. **28**(3): p. 399-408.
30. Miller-Podraza, H., et al., *Recognition of glycoconjugates by Helicobacter pylori. Comparison of two sialic acid-dependent specificities based on haemagglutination and binding to human erythrocyte glycoconjugates.* Glycoconj J, 1997. **14**(4): p. 467-71.
31. Yuyama, Y., et al., *Postnatal change of pig intestinal ganglioside bound by Escherichia coli with K99 fimbriae.* J Biochem, 1993. **113**(4): p. 488-92.
32. Schengrund, C.L., B.R. DasGupta, and N.J. Ringler, *Binding of botulinum and tetanus neurotoxins to ganglioside GT1b and derivatives thereof.* J Neurochem, 1991. **57**(3): p. 1024-32.
33. Born, G.V. and W. Palinski, *Unusually high concentrations of sialic acids on the surface of vascular endothelia.* Br J Exp Pathol, 1985. **66**(5): p. 543-9.
34. Vimr, E.R., et al., *Diversity of microbial sialic acid metabolism.* Microbiol Mol Biol Rev, 2004. **68**(1): p. 132-53.
35. Tomlinson, S., et al., *Role of sialic acid in the resistance of Trypanosoma cruzi trypomastigotes to complement.* J Immunol, 1994. **153**(7): p. 3141-7.
36. Kircheis, R., et al., *Selective lysis of early embryonic cells by the alternative pathway of complement--a possible mechanism for programmed cell death in embryogenesis.* In Vivo, 1996. **10**(4): p. 389-403.
37. Ajona, D., et al., *Expression of complement factor H by lung cancer cells: effects on the activation of the alternative pathway of complement.* Cancer Res, 2004. **64**(17): p. 6310-8.
38. Rens-Domiano, S. and T. Reisine, *Structural analysis and functional role of the carbohydrate component of somatostatin receptors.* J Biol Chem, 1991. **266**(30): p. 20094-102.
39. Emig, S., et al., *The nuclear pore complex protein p62 is one of several sialic acid-containing proteins of the nuclear envelope.* J Biol Chem, 1995. **270**(23): p. 13787-93.
40. Hu, J., et al., *Involvement of Sialic Acid in the Regulation of GABA Uptake Activity of GABA Transporter 1.* Glycobiology.
41. Egrie, J.C. and J.K. Browne, *Development and characterization of novel erythropoiesis stimulating protein (NESP).* Nephrol Dial Transplant, 2001. **16 Suppl 3**: p. 3-13.
42. Kluge, A., et al., *Interaction of rat peritoneal macrophages with homologous sialidase-treated thrombocytes in vitro: biochemical and morphological studies. Detection of N-(O-acetyl)glycoloylneuraminic acid.* Eur J Cell Biol, 1992. **59**(1): p. 12-20.
43. Ashwell, G. and J. Harford, *Carbohydrate-specific receptors of the liver.* Annu Rev Biochem, 1982. **51**: p. 531-54.
44. Stevens, J., et al., *Glycan microarray analysis of the hemagglutinins from modern and pandemic influenza viruses reveals different receptor specificities.* J Mol Biol, 2006. **355**(5): p. 1143-55.
45. Ngampasutadol, J., et al., *Human factor H interacts selectively with Neisseria gonorrhoeae and results in species-specific complement evasion.* J Immunol, 2008. **180**(5): p. 3426-35.
46. Madico, G., et al., *Factor H binding and function in sialylated pathogenic neisseriae is influenced by gonococcal, but not meningococcal, porin.* J Immunol, 2007. **178**(7): p. 4489-97.
47. Rutishauser, U., *Polysialic acid in the plasticity of the developing and adult vertebrate nervous system.* Nat Rev Neurosci, 2008. **9**(1): p. 26-35.
48. Pan, B., et al., *Myelin-associated glycoprotein and complementary axonal ligands, gangliosides, mediate axon stability in the CNS and PNS: neuropathology and behavioral deficits in single- and double-null mice.* Exp Neurol, 2005. **195**(1): p. 208-17.

49. Yang, L.J., et al., *Sialidase enhances spinal axon outgrowth in vivo.* Proc Natl Acad Sci U S A, 2006. **103**(29): p. 11057-62.
50. Hughes, R.A. and D.R. Cornblath, *Guillain-Barre syndrome.* Lancet, 2005. **366**(9497): p. 1653-66.
51. Kim, Y.J. and A. Varki, *Perspectives on the significance of altered glycosylation of glycoproteins in cancer.* Glycoconj J, 1997. **14**(5): p. 569-76.
52. Chen, S. and M. Fukuda, *Cell type-specific roles of carbohydrates in tumor metastasis.* Methods Enzymol, 2006. **416**: p. 371-80.
53. Dennis, J., et al., *Surface sialic acid reduces attachment of metastatic tumour cells to collagen type IV and fibronectin.* Nature, 1982. **300**(5889): p. 274-6.
54. Fogel, M., P. Altevogt, and V. Schirrmacher, *Metastatic potential severely altered by changes in tumor cell adhesiveness and cell-surface sialylation.* J Exp Med, 1983. **157**(1): p. 371-6.
55. Yogeeswaran, G. and P.L. Salk, *Metastatic potential is positively correlated with cell surface sialylation of cultured murine tumor cell lines.* Science, 1981. **212**(4502): p. 1514-6.
56. Bhavanandan, V.P., *Cancer-associated mucins and mucin-type glycoproteins.* Glycobiology, 1991. **1**(5): p. 493-503.
57. Rhodes, J.M., *Usefulness of novel tumour markers.* Ann Oncol, 1999. **10 Suppl 4**: p. 118-21.
58. Wahrenbrock, M.G. and A. Varki, *Multiple hepatic receptors cooperate to eliminate secretory mucins aberrantly entering the bloodstream: are circulating cancer mucins the "tip of the iceberg"?* Cancer Res, 2006. **66**(4): p. 2433-41.
59. Bresalier, R.S., et al., *Cell surface sialoprotein alterations in metastatic murine colon cancer cell lines selected in an animal model for colon cancer metastasis.* Cancer Res, 1990. **50**(4): p. 1299-307.
60. Sawada, R., S. Tsuboi, and M. Fukuda, *Differential E-selectin-dependent adhesion efficiency in sublines of a human colon cancer exhibiting distinct metastatic potentials.* J Biol Chem, 1994. **269**(2): p. 1425-31.
61. Varki, N.M. and A. Varki, *Heparin inhibition of selectin-mediated interactions during the hematogenous phase of carcinoma metastasis: rationale for clinical studies in humans.* Semin Thromb Hemost, 2002. **28**(1): p. 53-66.
62. Tangvoranuntakul, P., et al., *Human uptake and incorporation of an immunogenic nonhuman dietary sialic acid.* Proc Natl Acad Sci U S A, 2003. **100**(21): p. 12045-50.
63. Hinderlich, S., et al., *A bifunctional enzyme catalyzes the first two steps in N-acetylneuraminic acid biosynthesis of rat liver. Purification and characterization of UDP-N-acetylglucosamine 2-epimerase/N-acetylmannosamine kinase.* J Biol Chem, 1997. **272**(39): p. 24313-8.
64. Haverkamp, J., J.M. Beau, and R. Schauer, *Improved synthesis of CMP-sialates using enzymes from frog liver and equine submandibular gland.* Hoppe Seylers Z Physiol Chem, 1979. **360**(2): p. 159-66.
65. Eckhardt, M., et al., *Expression cloning of the Golgi CMP-sialic acid transporter.* Proc Natl Acad Sci U S A, 1996. **93**(15): p. 7572-6.
66. Harduin-Lepers, A., M.A. Recchi, and P. Delannoy, *1994, the year of sialyltransferases.* Glycobiology, 1995. **5**(8): p. 741-58.
67. Reinke, S.O., et al., *Regulation and pathophysiological implications of UDP-GlcNAc 2-epimerase/ManNAc kinase (GNE) as the key enzyme of sialic acid biosynthesis.* Biol Chem, 2009. **390**(7): p. 591-9.
68. Suzuki, O., et al., *UDP-GlcNAc2-epimerase regulates cell surface sialylation and ceramide-induced cell death in human malignant lymphoma.* Int J Mol Med, 2008. **22**(3): p. 339-48.
69. Keppler, O.T., et al., *UDP-GlcNAc 2-epimerase: a regulator of cell surface sialylation.* Science, 1999. **284**(5418): p. 1372-6.
70. Cardini, C.E. and L.F. Leloir, *Enzymatic formation of acetylgalactosamine.* J Biol Chem, 1957. **225**(1): p. 317-24.
71. Comb, D.G. and S. Roseman, *Enzymic synthesis of N-acetyl-D-mannosamine.* Biochim Biophys Acta, 1958. **29**(3): p. 653-4.

72. Ghosh, S. and S. Roseman, *Enzymatic phosphorylation of N-acetyl-D-mannosamine.* Proc Natl Acad Sci U S A, 1961. **47**: p. 955-8.
73. Warren, L. and H. Felsenfeld, *N-Acetylmannosamine-6-phosphate and N-acetylneuraminic acid-9-phosphate as intermediates in sialic acid biosynthesis.* Biochem Biophys Res Commun, 1961. **5**: p. 185-90.
74. Van Rinsum, J., et al., *Subcellular localization and tissue distribution of sialic acid precursor-forming enzymes.* Biochem J, 1983. **210**(1): p. 21-8.
75. Stasche, R., et al., *A bifunctional enzyme catalyzes the first two steps in N-acetylneuraminic acid biosynthesis of rat liver. Molecular cloning and functional expression of UDP-N-acetylglucosamine 2-epimerase/N-acetylmannosamine kinase.* J Biol Chem, 1997. **272**(39): p. 24319-24.
76. Effertz, K., S. Hinderlich, and W. Reutter, *Selective loss of either the epimerase or kinase activity of UDP-N-acetylglucosamine 2-epimerase/N-acetylmannosamine kinase due to site-directed mutagenesis based on sequence alignments.* J Biol Chem, 1999. **274**(40): p. 28771-8.
77. Kornfeld, S., et al., *The Feedback Control of Sugar Nucleotide Biosynthesis in Liver.* Proc Natl Acad Sci U S A, 1964. **52**: p. 371-9.
78. Kamerling, J.P., et al., *2-Acetamidoglucal, a new metabolite isolated from the urine of a patient with sialuria.* Biochim Biophys Acta, 1979. **583**(3): p. 403-8.
79. Ghaderi, D., et al., *Evidence for dynamic interplay of different oligomeric states of UDP-N-acetylglucosamine 2-epimerase/N-acetylmannosamine kinase by biophysical methods.* J Mol Biol, 2007. **369**(3): p. 746-58.
80. Horstkorte, R., et al., *Protein kinase C phosphorylates and regulates UDP-N-acetylglucosamine-2-epimerase/N-acetylmannosamine kinase.* FEBS Lett, 2000. **470**(3): p. 315-8.
81. Oetke, C., et al., *Epigenetically mediated loss of UDP-GlcNAc 2-epimerase/ManNAc kinase expression in hyposialylated cell lines.* Biochem Biophys Res Commun, 2003. **308**(4): p. 892-8.
82. Giordanengo, V., et al., *Epigenetic reprogramming of UDP-N-acetylglucosamine 2-epimerase/N-acetylmannosamine kinase (GNE) in HIV-1-infected CEM T cells.* Faseb J, 2004. **18**(15): p. 1961-3.
83. Seppala, R., V.P. Lehto, and W.A. Gahl, *Mutations in the human UDP-N-acetylglucosamine 2-epimerase gene define the disease sialuria and the allosteric site of the enzyme.* Am J Hum Genet, 1999. **64**(6): p. 1563-9.
84. Leroy, J.G., et al., *Dominant inheritance of sialuria, an inborn error of feedback inhibition.* Am J Hum Genet, 2001. **68**(6): p. 1419-27.
85. Enns, G.M., et al., *Clinical course and biochemistry of sialuria.* J Inherit Metab Dis, 2001. **24**(3): p. 328-36.
86. Sparks, S.E., et al., *Use of a cell-free system to determine UDP-N-acetylglucosamine 2-epimerase and N-acetylmannosamine kinase activities in human hereditary inclusion body myopathy.* Glycobiology, 2005. **15**(11): p. 1102-10.
87. Noguchi, S., et al., *Reduction of UDP-N-acetylglucosamine 2-epimerase/N-acetylmannosamine kinase activity and sialylation in distal myopathy with rimmed vacuoles.* J Biol Chem, 2004. **279**(12): p. 11402-7.
88. Salama, I., et al., *No overall hyposialylation in hereditary inclusion body myopathy myoblasts carrying the homozygous M712T GNE mutation.* Biochem Biophys Res Commun, 2005. **328**(1): p. 221-6.
89. Saito, F., et al., *A Japanese patient with distal myopathy with rimmed vacuoles: missense mutations in the epimerase domain of the UDP-N-acetylglucosamine 2-epimerase/N-acetylmannosamine kinase (GNE) gene accompanied by hyposialylation of skeletal muscle glycoproteins.* Neuromuscul Disord, 2004. **14**(2): p. 158-61.
90. Hinderlich, S., et al., *The homozygous M712T mutation of UDP-N-acetylglucosamine 2-epimerase/N-acetylmannosamine kinase results in reduced enzyme activities but not in*

altered overall cellular sialylation in hereditary inclusion body myopathy. FEBS Lett, 2004. **566**(1-3): p. 105-9.

91. Wang, Z., et al., *Roles for UDP-GlcNAc 2-epimerase/ManNAc 6-kinase outside of sialic acid biosynthesis: modulation of sialyltransferase and BiP expression, GM3 and GD3 biosynthesis, proliferation, and apoptosis, and ERK1/2 phosphorylation.* J Biol Chem, 2006. **281**(37): p. 27016-28.
92. Weidemann, W., et al., *The collapsin response mediator protein 1 (CRMP-1) and the promyelocytic leukemia zinc finger protein (PLZF) bind to UDP-N-acetylglucosamine 2-epimerase/N-acetylmannosamine kinase (GNE), the key enzyme of sialic acid biosynthesis.* FEBS Lett, 2006. **580**(28-29): p. 6649-54.
93. Amsili, S., et al., *UDP-N-acetylglucosamine 2-epimerase/N-acetylmannosamine kinase (GNE) binds to alpha-actinin 1: novel pathways in skeletal muscle?* PLoS One, 2008. **3**(6): p. e2477.
94. Reinke, S.O. and S. Hinderlich, *Prediction of three different isoforms of the human UDP-N-acetylglucosamine 2-epimerase/N-acetylmannosamine kinase.* FEBS Lett, 2007. **581**(17): p. 3327-31.
95. Kontou, M., et al., *The key enzyme of sialic acid biosynthesis (GNE) promotes neurite outgrowth of PC12 cells.* Neuroreport, 2008. **19**(12): p. 1239-42.
96. Leung, T., et al., *p80 ROKalpha binding protein is a novel splice variant of CRMP-1 which associates with CRMP-2 and modulates RhoA-induced neuronal morphology.* FEBS Lett, 2002. **532**(3): p. 445-9.
97. Askanas, V., R.B. Alvarez, and W.K. Engel, *beta-Amyloid precursor epitopes in muscle fibers of inclusion body myositis.* Ann Neurol, 1993. **34**(4): p. 551-60.
98. Grunholz, H.J., et al., *Inhibition of in vitro biosynthesis of N-acetylneuraminic acid by N-acyl- and N-alkyl-2-amino-2-deoxyhexoses.* Carbohydr Res, 1981. **96**(2): p. 259-70.
99. Zeitler, R., et al., *Inhibition of N-acetylglucosamine kinase and N-acetylmannosamine kinase by 3-O-methyl-N-acetyl-D-glucosamine in vitro.* Eur J Biochem, 1992. **204**(3): p. 1165-8.
100. Blume, A., et al., *Characterization of ligand binding to the bifunctional key enzyme in the sialic acid biosynthesis by NMR: I. Investigation of the UDP-GlcNAc 2-epimerase functionality.* J Biol Chem, 2004. **279**(53): p. 55715-21.
101. Benie, A.J., et al., *Characterization of ligand binding to the bifunctional key enzyme in the sialic acid biosynthesis by NMR: II. Investigation of the ManNAc kinase functionality.* J Biol Chem, 2004. **279**(53): p. 55722-7.
102. Zhu, X., F. Stolz, and R.R. Schmidt, *Synthesis of thioglycoside-based UDP-sugar analogues.* J Org Chem, 2004. **69**(21): p. 7367-70.
103. Stolz, F., et al., *Novel UDP-glycal derivatives as transition state analogue inhibitors of UDP-GlcNAc 2-epimerase.* J Org Chem, 2004. **69**(3): p. 665-79.
104. Al-Rawi, S., et al., *Synthesis and biochemical properties of reversible inhibitors of UDP-N-acetylglucosamine 2-epimerase.* Angew Chem Int Ed Engl, 2004. **43**(33): p. 4366-70.
105. Mantey, L.R., et al., *Efficient biochemical engineering of cellular sialic acids using an unphysiological sialic acid precursor in cells lacking UDP-N-acetylglucosamine 2-epimerase.* FEBS Lett, 2001. **503**(1): p. 80-4.
106. Towbin, H., T. Staehelin, and J. Gordon, *Electrophoretic transfer of proteins from polyacrylamide gels to nitrocellulose sheets: procedure and some applications. 1979.* Biotechnology, 1992. **24**: p. 145-9.
107. Jourdian, G.W., L. Dean, and S. Roseman, *The sialic acids. XI. A periodate-resorcinol method for the quantitative estimation of free sialic acids and their glycosides.* J Biol Chem, 1971. **246**(2): p. 430-5.
108. Reissig, J.L., J.L. Storminger, and L.F. Leloir, *A modified colorimetric method for the estimation of N-acetylamino sugars.* J Biol Chem, 1955. **217**(2): p. 959-66.
109. Dagert, M. and S.D. Ehrlich, *Prolonged incubation in calcium chloride improves the competence of Escherichia coli cells.* Gene, 1979. **6**(1): p. 23-8.

110. Birnboim, H.C. and J. Doly, *A rapid alkaline extraction procedure for screening recombinant plasmid DNA.* Nucleic Acids Res, 1979. **7**(6): p. 1513-23.
111. *The CCP4 suite: programs for protein crystallography.* Acta Crystallogr D Biol Crystallogr, 1994. **50**(Pt 5): p. 760-3.
112. Vagin, A. and A. Teplyakov, *Molecular replacement with MOLREP.* Acta Crystallogr D Biol Crystallogr. **66**(Pt 1): p. 22-5.
113. Tong, Y., et al., *Crystal structure of the N-acetylmannosamine kinase domain of GNE.* PLoS One, 2009. **4**(10): p. e7165.
114. Murshudov, G.N., A.A. Vagin, and E.J. Dodson, *Refinement of macromolecular structures by the maximum-likelihood method.* Acta Crystallogr D Biol Crystallogr, 1997. **53**(Pt 3): p. 240-55.
115. Emsley, P. and K. Cowtan, *Coot: model-building tools for molecular graphics.* Acta Crystallogr D Biol Crystallogr, 2004. **60**(Pt 12 Pt 1): p. 2126-32.
116. Penner, J., et al., *Influence of UDP-GlcNAc 2-epimerase/ManNAc kinase mutant proteins on hereditary inclusion body myopathy.* Biochemistry, 2006. **45**(9): p. 2968-77.
117. Holm, L. and P. Rosenstrom, *Dali server: conservation mapping in 3D.* Nucleic Acids Res. **38**(Web Server issue): p. W545-9.
118. Bork, P., C. Sander, and A. Valencia, *An ATPase domain common to prokaryotic cell cycle proteins, sugar kinases, actin, and hsp70 heat shock proteins.* Proc Natl Acad Sci U S A, 1992. **89**(16): p. 7290-4.
119. Titgemeyer, F., et al., *Evolutionary relationships between sugar kinases and transcriptional repressors in bacteria.* Microbiology, 1994. **140 (Pt 9)**: p. 2349-54.
120. Hansen, T., et al., *The first archaeal ATP-dependent glucokinase, from the hyperthermophilic crenarchaeon Aeropyrum pernix, represents a monomeric, extremely thermophilic ROK glucokinase with broad hexose specificity.* J Bacteriol, 2002. **184**(21): p. 5955-65.
121. Schiefner, A., et al., *The crystal structure of Mlc, a global regulator of sugar metabolism in Escherichia coli.* J Biol Chem, 2005. **280**(32): p. 29073-9.
122. Krissinel, E. and K. Henrick, *Inference of macromolecular assemblies from crystalline state.* J Mol Biol, 2007. **372**(3): p. 774-97.
123. Hayward, S. and R.A. Lee, *Improvements in the analysis of domain motions in proteins from conformational change: DynDom version 1.50.* J Mol Graph Model, 2002. **21**(3): p. 181-3.
124. Huizing, M. and D.M. Krasnewich, *Hereditary inclusion body myopathy: a decade of progress.* Biochim Biophys Acta, 2009. **1792**(9): p. 881-7.
125. Muller, C. and C. Sorg, *Use of formalin-fixed melanoma cells for the detection of antibodies against surface antigens by a micro-immune adherence technique.* Eur J Immunol, 1975. **5**(3): p. 175-8.
126. Du, J., et al., *Metabolic glycoengineering: sialic acid and beyond.* Glycobiology, 2009. **19**(12): p. 1382-401.
127. Ghaderi, D., *The key enzyme of the N-acetylneuraminic acid biosynthesis, UDP-GlcNAc-2-epimerase/ManNAc-kinase*, in *Biology, Chemistry, Pharmacy*. 2006, FU Berlin: Berlin.
128. Blume, A., *Expression and Functional Characterisation of the key Enzyme of the Sialic Acid Biosynthesis, UDP-GlcNAc 2-Epimerase/ManNAc Kinase*, in *Biology, Chemistry, Pharmacy*. 2003, FU Berlin: Berlin.
129. Hinderlich, S., *Charakterisierung der UDP-N-Acetylglucosamin-2-Epimerase/N-Acetylmannosaminkinase als bifunktionelles Enzym*, in *Biology, Chemistry, Pharmacy*. 1998, FU Berlin: Berlin.
130. Weihofen, W.A., et al., *Structures of human N-Acetylglucosamine kinase in two complexes with N-Acetylglucosamine and with ADP/glucose: insights into substrate specificity and regulation.* J Mol Biol, 2006. **364**(3): p. 388-99.
131. Nishimasu, H., et al., *Crystal structures of an ATP-dependent hexokinase with broad substrate specificity from the hyperthermophilic archaeon Sulfolobus tokodaii.* J Biol Chem, 2007. **282**(13): p. 9923-31.

132. Nocek, B., et al., *Structural studies of ROK fructokinase YdhR from Bacillus subtilis: insights into substrate binding and fructose specificity.* J Mol Biol. **406**(2): p. 325-42.
133. Lowe, G. and B.V. Potter, *A stereochemical investigation of phosphoryl transfer catalysed by phosphoglucomutase by the use of alpha-D-glucose 1-[(S)-16O,17O,18O]phosphate.* Biochem J, 1981. **199**(3): p. 693-8.
134. Pollard-Knight, D., et al., *The stereochemical course of phosphoryl transfer catalysed by glucokinase.* Biochem J, 1982. **201**(2): p. 421-3.
135. Krause, S., et al., *Localization of UDP-GlcNAc 2-epimerase/ManAc kinase (GNE) in the Golgi complex and the nucleus of mammalian cells.* Exp Cell Res, 2005. **304**(2): p. 365-79.
136. Galeano, B., et al., *Mutation in the key enzyme of sialic acid biosynthesis causes severe glomerular proteinuria and is rescued by N-acetylmannosamine.* J Clin Invest, 2007. **117**(6): p. 1585-94.
137. Zeidan, Q. and G.W. Hart, *The intersections between O-GlcNAcylation and phosphorylation: implications for multiple signaling pathways.* J Cell Sci. **123**(Pt 1): p. 13-22.

7. Publications

Scientific papers

Nguyen LD[#], Wratil PR[#], Fan H, Reutter W. *Novel inhibitors of the GNE decrease sialic acid expression on tumors cell lines and influence malignant biological functions.* J Biol Chem 2012 (In preparation)

Nguyen LD[#], Martinez J[#], Hinderlich S, Zimmer R, Tauberger E, Reutter W, Saenger W, Fan H*, Moniot S*. *Crystal structures of N-acetylmannosamine kinase provide insights into enzyme activity and inhibition.* J Biol Chem 2012 (In submission)

Zhang J, Tang Q, Zhou C, Jia W, Da Silva L, **Nguyen LD**, Reutter W, Fan H. *GLIS, a bioactive proteoglycan fraction from Ganoderma lucidum, displays anti-tumor activity by increasing both humoral and cellular immune response.* Life Sci. 2010 Nov 20;87(19-22):628-37.

Posters

IUCR, Madrid 2011

Structures of N-Acetylmannosamine kinase in complex with ADP/ATP for drug designs

Jacobo Martinez, Sebastien Moniot, **Long Duc Nguyen**, Hua Fan, Werner Reutter, Wolfram Saenger

Glyco 21, Wien 2011

Analyzing crystal structures of ManNAc kinase: Insights into activity and inhibition

Long Duc Nguyen, Jacobo Martinez, Stephan Hinderlich, Werner Reutter, Wolfram Saenger, Hua Fan, Sebastien Moniot

2nd HZB Joint Users, Berlin 2010

Structures of human N-Acetylmannosamine kinase in complex with substrate and cofactor

Jacobo Martinez, Sebastien Moniot, **Long Duc Nguyen**, Hua Fan, Werner Reutter, Wolfram Saenger